Atg9 and the visualisation of autophagic compartments

Christie Ann Bader
B.Ed, B.Sc. (Hons)

University of South Australia
School of Health Science
Division of Pharmacy and Medical Science
Sansom Institute

Submitted February 2015

Table of contents

Table of contents ..... **ii**

List of figures ..... **vii**

List of tables ..... **viii**

Table of abbreviations ..... **ix**

Summary ..... **xi**

Preface and Publications ..... **xiii**

Acknowledgements ..... **xviii**

Chapter 1: Introduction **2**

1.1 Introduction to autophagy 3

1.1.1 Activation of autophagy *5*

1.1.2 Events during autophagy initiation *7*

1.1.3 Autophagosome membrane nucleation *9*

1.1.4 Autophagosome isolation membrane expansion and closure *10*

1.2 Autophagosome maturation 14

1.2.1 Amphisome formation *14*

1.2.2 Autolysosome formation *17*

1.3 Autophagy functions in lipid homeostasis 20

1.3.1 Lipid droplets are involved in regulating lipid homeostasis and storage *20*

1.3.2 Lipophagy is an alternate route for lipid metabolism *22*

1.4 Imaging of autophagy.....25

1.4.1 Fluorescent proteins as tools for labelling autophagic machinery 25

1.4.2 Organic fluorescence probes can be used to monitor autophagy.....27

1.4.3 Metal based fluorescence probes as potential tools for detecting autophagy 29

1.5 Rationale.....32

1.6 Hypotheses and aims.....34

Chapter 2: Atg9 is required for amphisome and autolysosome compartmentalisation.....36

2.1 Preface.....37

2.2 Abstract.....38

2.3 Introduction.....39

2.4 Materials and methods.....43

2.4.1 Drosophila stocks.....43

2.4.2 Gene expression and protein analysis 44

2.4.3 Immunostaining and microscopy 45

2.4.4 Image Analysis.....46

2.5 Results.....48

2.5.1 Atg9 depletion reduced the number and size of autophagosomes at a time point in Drosophila development when autophagy is normally up-regulated. 48

2.5.2 Atg9 is required for Rab11 intraluminal vesicles and compartmentalised acidification in amphisomes during developmental autophagy. 53

2.5.3 Atg9 depletion reduced the size of autolysosomes and altered the compartmentalisation of LysoTracker® and Lamp1 intraluminal vesicles in fat body cells during developmental autophagy. *56*

2.5.4 Atg9 depletion abrogated Rab11 intraluminal vesicle formation and impaired midgut degradation in Drosophila during metamorphosis. *59*

2.6 Discussion 62

Chapter 3: Modulation of the cellular organelle specificity in Re(I) tetrazolato complexes leads to unprecedented phosphorescent labeling of lipid droplets 68

3.1 Preface 69

3.2 Publication details 70

3.3 Author contribution 71

3.4 Abstract 72

3.5 Introduction 73

3.6 Materials and methods 76

3.6.1 Fly stocks and cultured cells *76*

3.6.2 Tissue and cell staining *76*

3.6.3 Cytotoxicity assay *76*

3.6.4 Cell imaging using two-photon and confocal microscopy *77*

3.6.5 Image analysis *77*

3.7 Results and Discussion 79

Chapter 4: A Rhenium molecular probe detects lipid droplets and autophagosomes 92

4.1 Preface 93

4.2 Abstract 94

4.3 Introduction 95

4.4 Material and methods 99

4.4.1 Fly stocks *99*

4.4.2 Developmental staging *99*

4.4.3 Nutrient deprivation *99*

4.4.4 Tissue isolation and staining *100*

4.4.5 Imaging and analysis *100*

4.4.6 Rhenium molecular probe lipid interaction *101*

4.5 Results 103

4.5.1 The Rhenium based molecular probe detected lipid droplets in Drosophila fat body tissue, but also localised to an acidic compartment during metamorphosis. *103*

4.5.2 The spectral profile of the Rhenium molecular probe was dependent on its subcellular location. *105*

4.5.3 The Rhenium molecular probe colocalised with autophagosomes during development and following starvation. *106*

4.5.4 Genetic modulation of autophagy altered the Rhenium molecular probe distribution. *111*

4.5.5 The Rhenium molecular probe interacted with specific lipids. *116*

4.6 Discussion 117

Chapter 5: General discussion.....124

Reference.....136

List of figures

FIGURE 1.1 AUTOPHAGOSOME FORMATION AND MATURATION. 4

FIGURE 2.1 ATG9 EXPRESSION AND CELLULAR LOCALISATION IN DROSOPHILA FAT BODY DURING DEVELOPMENT. 49

FIGURE 2.2 DEPLETION OF ATG9 BY RNAI SILENCING REDUCED THE SIZE OF AUTOPHAGIC COMPARTMENTS, BUT DID NOT IMPAIR ACIDIFICATION. 51

FIGURE 2.3 QUANTIFICATION OF THE NUMBER AND SIZE OF ATG8A-GFP AUTOPHAGIC COMPARTMENTS IN CONTROL AND ATG9 RNAI SILENCED FAT BODY CELLS. 52

FIGURE 2.4 INTRALUMINAL RAB11 COMPARTMENTS WERE ABSENT FROM AUTOPHAGIC COMPARTMENTS IN ATG9 DEPLETED FAT BODY CELLS. 54

FIGURE 2.5 ATG9 DEPLETION PREVENTED THE FORMATION OF RAB11 INTRALUMINAL VESICLES AND ALTERED INTRALUMINAL ACIDIFICATION OF ATG8 COMPARTMENTS IN RESPONSE TO STARVATION. 55

FIGURE 2.6 LAMP1 AUTOPHAGIC COMPARTMENTS HAD ALTERED INTRALUMINAL ACIDIFICATION AND A REDUCED SIZE IN RESPONSE TO $ATG9^{RNAi}$. 57

FIGURE 2.7 QUANTIFICATION OF CHANGES IN SIZE AND RELATIVE ACIDIFICATION OF LAMP1 COMPARTMENTS IN RESPONSE TO $ATG9^{RNAi}$ 58

FIGURE 2.8 COMPARTMENTS CONTAINING INTRALUMINAL VESICLES WERE POSITIVE FOR RAB11 AND LAMP1 AT A TIME WHEN DEVELOPMENTAL AUTOPHAGY OCCURS. 58

FIGURE 2.9 ATG9 DEPLETION REDUCED THE SIZE OF RAB11 AND LYSOTRACKER® COMPARTMENTS IN THE MIDGUT. 60

FIGURE 2.10 ATG9 DEPLETION PREVENTED INTRALUMINAL VESICLES IN THE GASTRIC CAECA, RESULTING IN REDUCED MIDGUT DEGRADATION. 61

FIGURE 3.1 FORMULATION OF RE(I) TETRAZOLATO COMPLEXES 1 AND 2 75

FIGURE 3.2 ABSORPTION AND EMISSION PROFILES OF COMPLEXES 80

FIGURE 3.3 EX VIVO EMISSION FINGERPRINTING OF COMPLEXES 1 AND 2 AS COMPARED TO ENDOGENOUS FLUORESCENCE IN *DROSOPHILA* FAT BODY TISSUE. 84

FIGURE 3.4 RHENIUM COMPLEXES ARE NOT CYTOTOXIC TO *DROSOPHILA* TISSUE. 85

FIGURE 3.5 CELLULAR LOCALISATION OF COMPLEXES 1 AND 2 IN RELATION TO LATE ENDOSOMES. 86

FIGURE 3.6 CELLULAR LOCALISATION OF COMPLEXES 1 AND 2 IN RELATION TO MITOCHONDRIA. 87

FIGURE 3.7 CELLULAR LOCALISATION OF COMPLEXES 1 AND 2 IN RELATION TO LIPID DROPLETS. 88

FIGURE 3.8 CELLULAR LOCALISATION OF COMPLEXES 1 AND 2 IN RELATION TO FREE CHOLESTEROL. 89

FIGURE 4.1 THE RHENIUM MOLECULAR PROBE WAS DETECTED IN DROSOPHILA FAT BODY LIPID DROPLETS, BUT LOCATED TO ACIDIC COMPARTMENTS DURING METAMORPHOSIS. 104

FIGURE 4.2 SPECTRAL PROFILING OF THE RHENIUM MOLECULAR PROBE IN ACIDIC COMPARTMENTS AND LIPID DROPLETS. 105

FIGURE 4.3 THE RHENIUM MOLECULAR PROBE LOCALISED WITH ATG8AGFP UPON STARVATION AND DURING PUPAL DEVELOPMENT. 108

FIGURE 4.4 QUANTIFICATION OF ATG8AGFP POSITIVE COMPARTMENTS AND ATG8AGFP/RHENIUM MOLECULAR PROBE POSITIVE COMPARTMENTS DURING STARVATION AND DEVELOPMENT 109

FIGURE 4.5 NEUTRAL LIPID STAIN OIL RED O LOCALISED WITH ATG8AGFP DURING EITHER LARVAL STARVATION OR PUPAL DEVELOPMENT. 110

FIGURE 4.6 THE RHENIUM MOLECULAR PROBE LOCALISED TO ACIDIC COMPARTMENTS WHEN AUTOPHAGY WAS INDUCED BY THE INHIBITION OF TOR. 112

FIGURE 4.7 REDUCED AUTOPHAGY BY ATG9 RNAI SILENCING WAS DETECTED WITH THE RHENIUM MOLECULAR PROBE. 113

FIGURE 4.8 ALTERED DEVELOPMENTAL AUTOPHAGY BY ATG9 RNAI SILENCING WAS DETECTED WITH THE RHENIUM MOLECULAR PROBE. 114

FIGURE 4.9 QUANTIFICATION OF RHENIUM MOLECULAR PROBE AND LYSOTRACKER® POSITIVE COMPARTMENTS DURING STARVATION AND DEVELOPMENT. 115

FIGURE 4.10 THE RHENIUM MOLECULAR PROBE INTERACTED WITH SPECIFIC LIPIDS 116

FIGURE 5.1 THE RHENIUM TETRAZOLATE COMPLEXES 1 AND 2 HAD AN AFFINITY FOR POLAR LIPIDS 131

List of tables

TABLE 3.1 . IMAGING PARAMETERS FOR ASSESSING THE INTRACELLULAR LOCALISATION OF THE RHENIUM COMPLEXES 78

TABLE 3.2 PHOTOPHYSICAL DATA FOR COMPLEXES 1 AND 2. 80

Table of abbreviations

3-methyladenine	3-MA
Autophagy-related gene	Atg
Adaptor Protein	AP
Adenosine mono-phosphate	AMP
Adenosine mono-phosphate-activated protein kinase	AMPK
Adenosine tri-phosphate	ATP
Amino acid	AA
Analysis of variance	ANOVA
Bovine serum albumin	BSA
Charge transfer	CT
c-Jun N-terminal kinase	JNK
Deoxyribonucleic acid	DNA
Dimethyl sulfoxide	DMSO
Dulbecco's modified eagle medium	DMEM
Endosomal sorting complex required for transport	ESCRT
FAK family kinase-interacting protein of 200 kDa	FIP200
FYVE and coiled-coil domain containing 1	FYCO1
Green fluorescent protein	GFP
Guanine nucleotide exchange factor	GEF
Hydrogen nuclear magnetic resonance	H-NMR
Ligand-to-ligand charge transfer character	LLCT
Lysophosphatidic acid	LPA
Lysosome-associated membrane glycoprotein	Lamp
LysoTracker®	LysoTr
Main beam splitter	MBS
Metal-to-ligand charge transfer	MLCT
Microtubule-associated protein 1A/1B-light chain 3	LC3
Monosialoganglioside	GM1
Neutral lipid storage disease	NLSD
Nicotinamide adenine dinucleotide phosphate	NAD(P)H
Patatin-like phospholipase domain containing 5	PNPLA5

Phosphate buffered saline	PBS
Phosphatidylinositol 3-kinase	PI3K
Phosphatidylinositol 3-phosphate	PI3P
Phosphatidylethanolamine	PE
Polymerase chain reaction	PCR
Pre-autophagosome structure	PAS
Puparium formation	PF
Rat Sarcoma	Ras
Region of interest	ROI
Ribonucleic acid	RNA
RNA interference	RNAi
Room temperature	RT
Soluble NSF attachment protein receptor	SNARE
Standard error of the mean	s.e.m
Synaptosomal-associated protein	SNAP
Target of Rapamycin	TOR
Target of Rapamycin complex	TORC
TBC1 Domain Family, Member 14	TBC1D14
Tectonin domain-containing protein	TECPR1
Transmission electron microscopy	TEM
Uncoordinated-51-like kinase 1	ULK1
Upstream activating sequence	UAS
UV-irradiation-resistance-associated gene	UVRAG
Vacuolar ATPase	V-ATPase
Vesicle associated membrane proteins	VAMP
Vesicular protein sorting	Vps
WD-repeat protein interacting with phosphoinositides	WIPI

Summary

Autophagy involves the formation of a double membrane compartment, known as an autophagosome, which can encapsulate cytoplasmic content, including whole organelles, proteins and lipids, for degradation. Autophagosomes have been implicated in lipid trafficking, glycogen turnover, organelle recycling, the clearance of protein aggregates and removal of cytotoxic metabolites, and therefore play a critical role in cellular metabolism and the maintenance of homeostasis. Dysregulation of autophagy is observed in a number of important human diseases, including metabolic disorders such as diabetes, neurodegenerative diseases and cancers; and therefore an understanding of the mechanisms that govern this process and the development of novel investigative tools for autophagy will provide insight into a range of pathologies.

Autophagy-related gene 9 protein (Atg9) is the only transmembrane protein which has been identified as part of the core autophagic machinery, and is thought to be required for the formation of autophagosomes. Atg9 localises to a number of organelles and endosomal compartments, where it is speculated to recruit membrane for the formation of autophagosomes. We show that Atg9 knock-down altered the morphology of amphisomes-autolysosomes and this suggested that Atg9 has a specific function during autophagosome maturation. Atg9 depletion prevented the formation of intraluminal vesicles in amphisomes-autolysosomes, resulting in altered acidification of the lumen of these compartments. The specific changes to the compartmentalised acidification in amphisomes-autolysosomes following Atg9 depletion most likely reduced the degradative capacity of the autolysosome, which was evident by impaired degradation of larval tissues during larval to adult transition. We speculate that Atg9 localisation to endosomal compartments may relate more to its function during autophagosome maturation, and

therefore may not be an ideal indicator of membrane trafficking during autophagosomes formation.

Autophagy has recently been identified as an important pathway for lipolysis, allowing the breakdown of lipid droplets, as well as the trafficking and regulation of intracellular lipids. A Rhenium(I) based fluorescent complex was used to detected lipids, in both lipid droplets and autophagosomes. The Rhenium molecular probe was responsive to specific autophagic cues, including lipid degradation via autophagy during larval to adult development in *Drosophila*, in response to extreme starvation and the induction of autophagy by the inhibition of target of Rapomycin (TOR). Lipid sequestration by autophagosomes was modulated by Atg9 depletion and these changes were also detected by the Rhenium molecular probe. In addition, the Rhenium molecular probe was responsive to pH, with a spectral shift observed when detected in autolysosomes. These findings indicated that the Rhenium molecular probe could be used for the investigation of the interaction between lipid droplets and autophagosomes, and has potential as a pH biosensor.

Changes to the chemical structure of the Rhenium(I) based complex could alter the subcellular localisation of the complex. A second Rhenium based complex was described that showed localisation to acidic endosomes and lysosomes. Interestingly, this complex was still capable of interacting with lipids, suggesting a potential for future development of a range of organelle specific lipid dyes for live cell fluorescence's microscopy, based on these prototype Rhenium complexes. The development of fluorescent probes for the detection of intracellular lipids, would provide an exciting new tool for research and diagnostic purposes, with a range of metabolic and neurodegenerative pathologies displaying altered intracellular lipid biology.

Preface and Publications

This thesis is presented in a publication style format, with a general introduction and chapters that are structured in a manuscript format, containing a specific introduction, materials and methods, results and discussion sections. The specific references pertaining to each chapter have been compiled at the end of the thesis. This publication style format was selected as the thesis contains content from multiple published works, including a review article and several original research articles.

Chapter 1 provides an introduction to the process of autophagy and also contains background information on autophagosome maturation, the role of autophagy in lipid homeostasis, and autophagy imaging by fluorescence microscopy. Sections of this text have been taken from a published review entitled ‘At the intersection of the pathways for exocytosis and autophagy’ on which I am an author. Permission was obtained from the other authors for this inclusion and the text has been appropriately referenced.

Chapter 2 is a manuscript that has been prepared ready for submission to the Journal of Cell Science. This chapter characterizes autophagic compartments in Atg9 depleted *Drosophila* tissue and demonstrates a function for Atg9 in intraluminal vesicle formation, compartmentalised acidification and autophagosome maturation.

A version of Chapter 3 has been published in The Royal Society of Chemistry Advances [Bader, C. A., Brooks, R. D., Ng, Y. S., Sorvina, A., Werrett, M. V., Wright, P. J., Anwer, A. G., Brooks, D. A., Stagniz, S., Muzziol, S., Silberstein, M., Skelton, B. W., Goldys, E. M., Plush, S. E., Shandala, T. & Massi, M. (2014) Modulation of the organelle specificity in Re(I) tetrazolato complexes leads to labeling of lipid droplets. *Royal Society Chemistry*

Advances. 4: 16345-16351.]. The paper reports the cellular localisation of two Rhenium(I) tetrazolate complexes by fluorscence, and I performed the cellular detection and localisation studies for these Rhenium(I) tetrazolato complexes. The synthesis and chemical characterisation of Rhenium(I) tetrazolato complexes was performed by collaborators from the Department of Chemistry, Curtin University, WA, Australia; Department of Physics and Astronomy, Macquarie University, NSW, Australia; and the Department of Industrial Chemistry, University of Bologna, Bologna, Italy. The chapter contains additional cell biology data and information that I collected, pertaining to the published work.

Data from Chapter 4 has also been prepared as a publication ready for submission. This chapter reports the use of one of the Re(I) tetrazolato complexes described in Chapter 3 and its application for the detection of lipid droplets and autophagosomes. The specificity of the lipid binding properties of this molecular probe have also been defined.

A general discussion has been presented to link the findings in each of the chapters and to position these observations in terms of the wider literature in the fields of autophagy and imaging. The ground breaking findings present a logical frame work for future research to develop live cell imaging techniques and to further analyse the critical processes of autophagy and lipid metabolism.

Publications

Bader, C. A., Brooks, R. D., Ng, Y. S., Sorvina, A., Werrett, M. V., Wright, P. J., Anwer, A. G., Brooks, D. A., Stagni, S., Muzzioli, S., Silberstein, M., Skelton, B. W., Goldys, E. M., Plush, S. E., Shandala, T. & Massi, M. (2014) Modulation of the organelle specificity in re(i) tetrazolato complexes leads to labeling of lipid droplets. *The Royal Society of Chemistry Advances.* 4: 16345-16351.

Brooks, D. A., Bader, C., Ng, Y.S., Brooks, R.D., Borlace, G.N. And Shandala,T. (2012) At the intersection of the pathways for exocytosis and autophagy. *In:* Weigert, R. (Ed.) *Crosstalk and integration of membrane trafficking pathways.* Intech.

Shandala, T., Kakavanos-Plew, R., Ng, Y.S., Bader, C., Sorvina, C., Parkinson-Lawrence, E.J., Brooks, R.D., Borlace, G.N., Prodoehl, M.J. And Brooks, D.A. (2012) Molecular machinery regulating exocytosis. *In:* Weigert, R. (Ed.) *Crosstalk and integration of membrane trafficking pathways.* Intech.

Sorvina, A., Brooks, D. A., Ng, Y. S., Bader, C. A., Weigert, R. & Shandala, T. (2013) Bacterial challenge initiates endosome-lysosome response in *drosophila* immune tissues. *Intravital.* 2: E23889.

Declaration

I Christie Ann Bader declare that this thesis presents work carried out by myself and does not incorporate without acknowledgment any material previously submitted for a degree or diploma in any university; and to the best of my knowledge does not contain any materials previously published or written by another person, except where due reference is made in the text; and that all substantive contributions by others to the work presented, including jointly authored publications, is clearly acknowledged.

Acknowledgements

Many thanks to my supervisors Prof. Doug Brooks, Dr Tetyana Shandala and Dr Sally Plush for the opportunity to participate in a group that is dynamic and diverse. Their support and guidance has allowed me to expand my skills beyond my expectations and I am grateful for the time and energy that they have invested into my education and growth.

Thanks to the past and present members of the Mechanisms in Cell Biology and Disease Research Group, who have assisted me in gaining the skills and knowledge to complete this significant task. In particular, I would like to acknowledge Yeap Shen Ng, Alexandra Sorvina, Ian Johnson, Robert Brooks and John Bresland for their support in and out of the laboratory.

And finally thanks to my friends and family, particularly to my parents, Beverley and Peter Bader who have been nothing but supportive and encouraging of me. I would also like to acknowledge my writing companions Indie, Tommy Ruff and Lewis, who all worked very hard keeping my feet warm while I wrote this thesis.
Thank you.

Chapter 1: Introduction

1.1 Introduction to autophagy

Autophagy is a cellular process that is responsible for a number of critical cellular functions including; the elimination of defective proteins and organelles, the clearance of abnormal protein aggregates, the sequestering of intracellular material for energy production, the removal of intracellular pathogens and the recycling of aged organelles (Colombo and Simon, 2009; Jia and Sowers, 2014; Kundu and Thompson, 2008; Mehrpour et al., 2010). Autophagy can degrade non-essential cytoplasmic content in response to cellular stress, liberating essential macromolecules to help maintain energy balance and normal cellular function (Quan and Lee, 2013). These functions are likely to be important in the autophagy-mediated protection against ageing, cancer, neurodegenerative diseases and infection (Levine and Kroemer, 2008). Autophagy normally occurs at a basal level in most cell types, but stimuli such as; starvation, hormonal and developmental signalling, accumulation of unfolded proteins or invasion of microorganisms, can modulate the rate of autophagic activity (Meijer and Codogno, 2004).

Three types of autophagy have been described, all of which allow the delivery of cytoplasmic content to the lysosome for degradation and these include; microautopahgy, chaperone-mediated autophagy and macroautophagy. In microautophagy, cytoplasmic content is directly sequestered by the lysosome via invagination of the lysosomal membrane (De Duve and Wattiaux, 1966). Chaperone-mediated autophagy also allows direct up-take into the lysosome, but this is mediated by receptors, which only allow a subset of long lived proteins to be transferred directly into the lysosomal lumen (Chiang et al., 1989). Macroautophagy, which will be the focus of this thesis and hereafter referred to as autophagy, involves the encapsulation of cytoplasmic content into a double membrane

compartment, which is then delivered to the lysosome via a series of maturation steps (Gordon and Seglen 1989; Hoyvik et al.1991). This type of autophagy allows the delivery of large portions of the cytoplasm, including organelles, to endosomes and lysosomes for degradation and recycling.

The encapsulation of cytoplasmic content by autophagy is mediated by the recruitment of autophagy-related gene (Atg) proteins to the so-called pre-autophagosomal structure (PAS; Suzuki et al., 2001; Suzuki et al., 2007). At the PAS, Atg proteins co-ordinate the generation of an isolation membrane, which forms a structure termed the phagophore. The expansion of the isolation membrane then encapsulates cytoplasmic content or organelles in a double membrane compartment called an autophagosome. Cytoplasmic content that is sequestered by the autophagosome can be broken down by hydrolytic enzymes, which are delivered to the autophagosome by endosomes and lysosomes; in a process called autophagosome maturation. This involves the fusion of autophagosomes with late endosomes, forming a compartment termed the amphisome, and is followed by fusion with lysosomes to form mature autolysosomes (Figure 1.1).

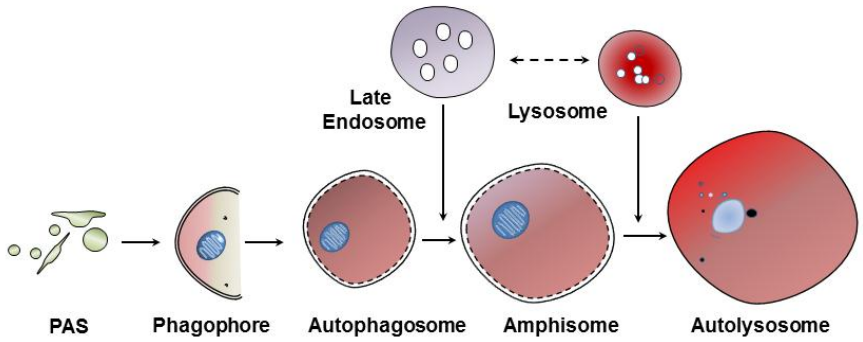


Figure 1.1 Autophagosome formation and maturation.

Autophagosomes form de-novo in a step-wise process beginning at the pre-autophagosomal structure (PAS) a cellular location were the phagophore forms to encapsulate the cytoplasmic content intended for degradations. The complete closure of this compartment forms the autophagosome which then fuses with a late endosome to form an amphisome, followed by fusion with a lysosome to form the final mature compartments named the autolysosome.

1.1.1 Activation of autophagy

Multiple nutrient sensing pathways converge at the target of Rapamycin (TOR), which is a master regulator of cellular growth and protein synthesis, as well as a negative regulator of autophagy (Takahara and Maeda, 2013). TOR is present as a member of two complexes, TOR complex 1 (TORC1) and TOR complex 2 (TORC2), of which TORC1 has a more well defined role in the regulation of autophagy (Takahara and Maeda, 2013; Vlahakis et al., 2014). In the presence of amino acids TORC1 is normally localised to the lysosome via a Rat sarcoma (Ras) related GTP-binding protein GTPase and Ragulator protein complex (Bar-Peled et al., 2012; Sancak et al., 2010). The Ragulator complex binds the lysosome via the vacuolar ATPase (V-ATPase) complex, which is directly involved in sensing amino acids inside the lysosomal lumen (Shen and Mizushima, 2014; Zoncu et al., 2011). Though the mechanism has not been fully elucidated, current evidence suggests that the interaction between the Ragulator complex and the V-ATPase complex regulates the activation of TORC1 to inhibit autophagy (Bar-Peled et al., 2012; Zoncu et al., 2011; Sancak et al., 2010). Reduced amino acid availability supresses this interaction and reduces the activation of TORC1 in cells, allowing autophagy initiation (Meijer and Dubbelhuis, 2004; Nobukuni et al., 2005; Nicklin et al., 2009). The interaction between TORC1 and the lysosomal Ragulator is also influenced by the cellular location of lysosomes (Korolchuk et al., 2011). Under nutrient rich conditions, lysosomes are peripherally located and TORC1 is activated via its interaction with the lysosome. However, starvation increases lysosomal pH and causes the perinuclear clustering of lysosomes and this reduces the interaction of the lysosome with TORC1, promoting autophagy (Korolchuk et al., 2011). The regulation of TOR via the lysosome provides a cellular feedback mechanism enabling the control of autophagic activity in direct response to nutrient conditions.

Hormones, which respond to whole organism energy and growth status, also act as upstream regulators of TORC1. Growth-factors such as insulin, regulate TORC1 via the Ras and class III phosphatidylinositol 3-kinase (PI3K) pathways, which induce for example tuberous sclerosis 1 or tuberous sclerosis 2 phosphorylation to activate TORC1 (Laplante and Sabatini, 2012). During metamorphosis in *Drosophila*, the steroid hormone ecdysone suppresses insulin signalling via PI3K and this allows autophagic up-regulation in the fat body (Rusten et al., 2004). This up-regulation of autophagy is essential for energy supply to the developing tissue during transition to the adult stage (Rusten et al., 2004). Cellular energy levels can also regulate TORC1 via adenosine mono-phosphate-activated protein kinase (AMPK), which is activated in response to an increase in the AMP:ATP ratio (Inoki et al., 2003; Shaw et al., 2004; Nobukuni et al., 2005; Tee et al., 2005; Sun et al., 2008). Active AMPK inhibits TORC1, by preventing its interaction with the activator proteins Rheb and Raptor (Inoki et al., 2003; Shaw et al., 2004; Nobukuni et al., 2005; Tee et al., 2005; Sun et al., 2008). Thus, autophagy can proceed to degrade cellular components that can then enter β-oxidation pathways and consequently generate ATP.

Autophagy is also able to be induced in response to increased cellular lipid content, which may be sequestered by autophagosomes to prevent lipotoxicity or to fuel β-oxidation pathways and provide energy. For example, in mouse hepatocytes, excess lipids were shown to induce autophagy by increasing transforming growth factor β-activated kinase 1, which activates AMPK leading to TORC1 inhibition (Inokuchi-Shimizu et al., 2014). Free fatty acids have also been shown to induce autophagy via the protein kinase C pathway, which appears to be independent of TORC1, however, the exact mechanism is yet to be

clearly established (Cai et al., 2014; Tan et al., 2012). Sphingolipid and ceramide, can also activate c-Jun N-terminal kinase (JNK), resulting in the transcription of autophagy genes, leading to autophagy initiation (Alexaki et al., 2014; Pattingre et al., 2009; Scarlatti et al., 2004). Thus, unlike amino acids and glucose that suppress autophagy, increased amounts of cellular lipids lead to increased autophagic activity and this is used to maintain lipid homeostasis.

1.1.2 Events during autophagy initiation

Autophagy induction via TORC1 or AMPK, activates an autophagy initiation complex called uncoordinated-51-like kinase 1 or ULK1 (mammalian homolog of Atg1), which directs the assembly of other autophagic machinery at the PAS. Under nutrient rich conditions the ULK1 complex, which contains ULK1:Atg13:FIP200 (FAK family kinase-interacting protein of 200 kDa), interacts with TORC1 or AMPK, and this supresses autophagy (Hosokawa et al., 2009; Kim et al., 2011a; Lee et al., 2010). However, the inhibition of TORC1 leads to the activation of ULK1 and the phosphorylation of Atg13 and FIP200 (Chang and Neufeld 2009: Hosokawa et al. 2009; Jung et al. 2009). Alternatively ULK1 can be directly phosphorylated by AMPK, independently of TORC1, to initiate autophagy (Egan et al., 2011; Kim et al., 2011a). Activated ULK1 complex acts as a protein kinase, phosphorylating Beclin1, which is present in a complex with vesicular protein sorting 34 (Vps34; Nazarko and Zhong, 2013; Russell et al., 2013). Phosphorylated Beclin1 recruits Atg14 to this protein complex, activating Vps34 to promote autophagosome formation and the recruitment of other Atg proteins (Nazarko and Zhong, 2013; Russell et al., 2013).

Both ULK1 and Beclin1 are involved in the recruitment of the transmembrane protein Atg9 from peripheral cellular locations, including from the Golgi and the plasma membrane, to the PAS. The phosphorylation of the motor protein myosin II, by ULK1 facilitates the redistribution of Atg9 from the Golgi to the PAS (Mack et al., 2012; Tang et al., 2011; Young et al., 2006). Consequently, the depletion of ULK1 leads to Atg9 accumulation at the Golgi and this reduces autophagosome formation (Young et al., 2006). The Beclin1 complex also facilitates trafficking of Atg9 from the Golgi via an interaction with the UV-irradiation-resistance-associated gene UVRAG (He et al., 2013; Takahashi et al., 2011). Autophagy induction causes the dissociation of UVRAG from the ER tethering complex RAD50 interactor 1, to allow an interaction with the Belcin1 complex, and this interaction is critical for the translocation of Atg9 to the PAS (He et al., 2013; Takahashi et al., 2011). The recruitment of Atg9 from the plasma membrane also involves the Beclin1 complex, which appears to be regulated through the membrane protein connexin (Bejarano et al., 2014). Under nutrient rich conditions Beclin1 associates with connexin at the plasma membrane (Bejarano et al., 2014). The induction of autophagy causes Atg9 and Atg14 to localise with connexin, allowing the activation of the Beclin1 complex by Atg14 (Bejarano et al., 2014). The activated Beclin1 complex is then able to phosphorylate membrane lipids in proximity to the connexin–Atg complex, inducing internalization of Atg9, along with connexin and Atg14 (Bejarano et al., 2014).

In yeast, Atg9 is phosphorylated by Atg1, facilitating the further recruitment of autophagic machinery to the PAS; including the microtubule-associated protein 1A/1B-light chain 3 LC3/Atg8, which is involved in isolation membrane expansion; and Atg18, which is required for membrane nucleation (Papinski and Kraft, 2014; Papinski et al., 2014). Atg9 also directly interacts with the tethering protein Trs85 to recruit Ypt1, a Rab protein

required for autophagosome formation (Kakuta et al., 2012; Wang et al., 2013). However, it is not known if, in higher eukaryotes, Atg9 phosphorylation is required for the recruitment of autophagic proteins.

1.1.3 Autophagosome membrane nucleation

The nucleation of the autophagosome limiting membrane is controlled by the Beclin1 complex, which phosphorylates phosphatidylinositol to phosphatidylinositol 3-phosphate (PI3P) in order to interact with Atg18 (mammalian homolog WD-repeat protein Interacting with Phosphoinositides (WIPI) 1 and WIPI2; (Wirth et al., 2013). An autophagy specific PI3P pool of lipid appears to form on a membrane structure termed an omegasome, which is thought to originate from the endoplasmic reticulum (Simonsen and Tooze, 2009). It is likely that Atg18 acts as a scaffold protein at this site, aiding in the assembly of multi-protein complexes that are required for membrane expansion (Koyama-Honda et al., 2013; Kundu and Thompson, 2008; Polson et al., 2010).

Atg9 is also implicated in autophagosome nucleation (Suzuki et al., 2007), although it is unclear if this occurs in conjunction with the Beclin1 complex. In yeast, Atg9 is present on vesicles, which originate from the Golgi and cluster near mitochondria (Mari et al., 2010). The initiation of autophagy increases the number of Atg9 vesicles at the mitochondria (Yamamoto et al., 2012), which then translocate to the PAS (Mari et al., 2010). At the PAS, Atg9 vesicles have been observed to fuse (Gao et al., 2010; Yamamoto et al., 2012), possibly facilitated by the scaffold protein Atg17 and Atg1 as a tethering complex (Ragusa et al., 2012; Stanley et al., 2014). The ability of Atg9 to self-interact via its C-terminus is essential for its function in autophagy initiation, and may also facilitate vesicular fusion at the PAS (Cao et al., 2009; He et al., 2008). Following this initial event, Atg9 remains with

the phagophore, but does not appear to be involved in the expansion of the isolation membrane (Yamamoto et al., 2012). Atg9 vesicular fusion is therefore suggested to provide a platform for isolation membrane expansion and the recruitment of other molecular machinery (Jin and Klionsky, 2014).

In mammalian cells, Atg9 is also detected on vesicles in close proximity to the recycling endosome (Orsi et al., 2012), which may originate from the plasma membrane (Puri et al., 2013) or Golgi (Takahashi et al., 2011). Upon autophagy induction, Atg9 vesicles fuse with Atg16L vesicles, which are derived from the plasma membrane (Puri et al., 2013). This fusion is regulated by the soluble NSF attachment protein receptor (SNARE) protein, Vesicle associated membrane proteins (VAMP) 3 (Puri et al., 2013). Inhibition of this event by the knock-down of VAMP3 reduces autophagosome formation (Puri et al., 2013). In higher eukaryotes, unlike yeast, Atg9 does not remain at the isolation membrane, suggesting that it has a more transient interaction with the phagophore (Longatti et al., 2012; Orsi et al., 2012). Furthermore, Atg9 moves away from the PAS following autophagy initiation (Longatti et al., 2012; Orsi et al., 2012), coincident with an increase in Atg9 localisation to other cellular compartments, such as late endosomes (Young et al., 2006). This redistribution of Atg9 appears to be dependent on other Atg proteins, including Atg18 and has been suggested to be involved in facilitating further membrane recruitment to the phagophore (Longatti et al., 2012; Orsi et al., 2012; Young et al., 2006).

1.1.4 Autophagosome isolation membrane expansion and closure

The autophagosome isolation membrane is thought to be derived from a number of pre-existing membrane compartments. Early observations by transmission electron microscopy indicated that the endoplasmic reticulum may be a membrane source for the

formation of autophagosomes (Arstila and Trump, 1968). More recent studies have shown membrane bridges connecting phagophores and the endoplasmic reticulum in a range of cell types, supporting these initial observations (Fujita et al., 2008a; Hayashi-Nishino et al., 2009; Yla-Anttila et al., 2009). Electron microscopy has also shown a close association between autophagosomes and lipid droplets, with membranes appearing to form within this lipid storage organelle (Yla-Anttila et al., 2009). Lipids mobilized from lipid droplets have been shown to contribute to the expanding phagophore, in a process that is dependent upon Patatin-like phospholipase domain containing 5 (PNPLA5), a lipid droplet associated lipase (Dupont et al., 2014). Lipid transfer has also been observed from mitochondria to autophagic structures, using the fluorescent lipid NBD-PS (Hailey et al., 2010). Additionally, early autophagic proteins were shown to localise to mitochondria, and the mitochondria protein Fis1 has been detected on autophagosomes following nutrient depravation (Hailey et al., 2010). In addition to these organelles, vesicles trafficked from the Golgi and the plasma membrane via endosomes, may also act as critical membrane sources for autophagosomes (Longatti and Tooze, 2009; Mari et al., 2011). Impaired vesicular trafficking, by the silencing of trafficking machinery, reduces autophagosome formation, supporting the notion of a vesicular trafficking model for membrane recruitment (Bejarano et al., 2014; Lynch-Day et al., 2010; Moreau et al., 2011; Orsi et al., 2012; Puri et al., 2013; Puri et al., 2014; Ravikumar et al., 2010; Yen et al., 2010).

Atg9 trafficking from the Golgi and plasma membrane, is required for the recruitment of molecular machinery to the PAS and autophagosome nucleation, as described above; but may also allow the trafficking of membrane to the expanding phagophore. The localisation of Atg9 vesicles to the PAS has been shown to involve vesicular trafficking machinery, as

well as autophagy initiation machinery (Longatti and Tooze, 2009). Atg9 translocation from the Golgi requires the vesicular trafficking machinery UVRAG (He et al., 2013; Takahashi et al., 2011), motor protein myosin II and the zipper-interacting protein kinase ZIPK (Tang et al., 2011). Clathrin-dependent endocytosis is required for Atg9 trafficking from the plasma membrane, with the inhibition of key regulators, dynamin or clathrin adaptor protein AP2, reducing Atg9 association with the PAS (Popovic and Dikic, 2014; Puri et al., 2013). Endosome trafficking machinery, such as Rab11 and its effector TBC1D14 have also been shown to function in Atg9 relocation to the PAS (Longatti et al., 2012). Retrograde trafficking of Atg9 from the PAS is also required for autophagosome formation. This involves the Atg18 homolog WIPI2, with its depletion resulting in increased Atg9 localisation to autophagic precursors, which accumulated and are unable to acquire LC3/Atg8 (Orsi et al., 2012). The movement of Atg9 has therefore been suggested to play a critical role in the recruitment of membrane from peripheral pools to the expanding phagophore (Reggiori and Tooze, 2012).

Two ubiquitin-like conjugation systems have been identified to function in the expansion and closure of autophagosomes, the Atg12-Atg5 conjugation system and the LC3/Atg8-phosphotidylethanolamine (PE) complex (Ichimura et al., 2000; Klionsky and Schulman, 2014; Mizushima et al., 1998). Atg12 is conjugated to Atg5 by Atg7, which acts as an E1-like protein ligase and Atg10, which functions as a E2-like protein ligase (Geng and Klionsky, 2008). The conjugated form of Atg12-Atg5 associates with Atg16 dimers at the PAS to become a multimeric complex (Klionsky and Schulman, 2014; Kuma et al., 2002). This multimeric complex has been shown to act *in vitro* as a membrane tether and it has been suggested that this function may assist in membrane expansion at the phagophore (Romanov et al., 2012). The Atg12-Atg5-Atg16 complex is also required for the

association of the second LC3/Atg8 related conjugation system (Fujita et al., 2008b; Hanada et al., 2007). Following the cleavage of LC3/Atg8 C-terminal arginine by Atg4, Atg7 acts as a E1-like protein ligase, and Atg3 as an E2-like protein ligase, to mediate the conjugation of LC3/Atg8 to PE (Geng and Klionsky, 2008; Kirisako et al., 2000; Li et al., 2011). This step results in the localisation of LC3/Atg8-PE to the phagophore (McPhee and Baehrecke, 2009; Nakatogawa et al., 2007). LC3/Atg8-PE is able to specifically target autophagic cargo via its interaction with receptor proteins, tethering the isolation membrane to the target content (Klionsky and Schulman, 2014; Shintani et al., 2002). It has also been suggested that Atg8 can facilitate vesicular fusion, which may allow phagophore expansion and the eventual closure to form the complete autophagosome (Weidberg et al., 2011).

Autophagosome closure remains one of the less well characterised events in autophagosome formation. One mechanism proposed for autophagosome closure involves the endosomal sorting complex required for transport, or ESCRT machinery. ESCRT-mutants are reported to have impaired autophagy progression (Rusten and Stenmark, 2009), and form abnormal autophagosomes (Rusten et al., 2007). The ESCRT machinery appears to be involved in abscission events, which involve the fission of narrow membrane tubules, including intraluminal vesicle formation in endosomes and at the final stages of cytokinesis (Raiborg and Stenmark, 2009). As the phagophore is a double membrane structure, autophagosome closure resembles the narrowing of a membrane tubule (Rusten and Stenmark, 2009). It has therefore been suggested that ESCRT machinery may also facilitate this final step in autophagosome formation, but this model is yet to be tested (Rusten and Stenmark, 2009). Following closure of the autophagosome,

the double membrane compartment enters the maturation process, by interaction with endosomes and then lysosomes.

1.2 Autophagosome maturation

1.2.1 Amphisome formation

An early step in autophagosome maturation involves the fusion of autophagosomes with late endosomes or multivesicular endosomes, to form amphisomes (Berg et al., 1998; Fader and Colombo, 2009; Gordon and Seglen, 1988). Multivesicular endosomes form from late endosomes, and this involves the internalisation of some of the endocytic membrane into the endosome lumen to form intraluminal vesicles (Hanson and Cashikar, 2012). This is important for endosome sorting and membrane receptor degradation and recycling (Hanson and Cashikar, 2012). Similar to autophagosome nucleation, PI3K and Vps34, phosphorylate phosphatidylinositol on endosomes to generate PI3P, which is then able to interact with the molecular machinery required for intraluminal vesicle formation (Hanson and Cashikar, 2012). This includes the ESCRT machinery, involving the four ESCRT complexes (0-III) to co-ordinate intraluminal vesicle formation (Wollert and Hurley, 2010). The depletion of subunits of these complexes impairs multivesicular endosome formation to varying degrees, often resulting in impaired endosome sorting and the formation of enlarged ‘E-Type’ vesicles (Fader and Colombo, 2009). In *Drosophila*, mouse and human cell lines, mutations in ESCRT proteins also result in the accumulation of autophagosomes and reduced autolysosome formation (Manil-Segalen et al., 2012; Rusten and Stenmark, 2009). This suggests that functional multivesicular endosomes are required for autophagosome maturation (Filimonenko et al., 2007). However, the ESCRT machinery has also been proposed to function directly in the fusion between

autophagosomes and endosomes or lysosomes, although the mechanism by which they may function in the fusion step remains unclear (Fader and Colombo, 2009; Filimonenko et al., 2007; Manil-Segalen et al., 2012; Rusten and Stenmark, 2009). It is possible that incomplete closure of the autophagosome could result in impaired maturation, supporting the suggested role for ESCRT complexes in the final step of autophagosome formation (Rusten and Stenmark, 2009). The close association between autophagosome maturation and endosome maturation, has made it difficult to clearly define the function of the ESCRT machinery in autophagy and its involvement is a continued area of debate (Rusten and Stenmark, 2009).

The GTPase, Rab11, is one of the few potential regulators that has been identified in amphisome formation (Fader et al., 2008; Szatmari et al., 2014). Rab11 localises to multivesicular endosomes and upon autophagic induction, Rab11 compartments have been shown to fuse with autophagosomes (Fader et al., 2008; Richards et al., 2011). Silencing of Rab11 or expression of a dominant negative form of Rab11, impairs endosome-autophagosome fusion, indicating that Rab11 is required for amphisome formation (Fader et al., 2008; Szatmari et al., 2014). In *Drosophila*, Rab11 is proposed to facilitate autophagosome to endosome fusion by interaction with Hook, which is a negative regulator of endosome maturation (Szatmari et al., 2014). This interaction may redirect endosomes into the autophagic pathway by preventing homotypic fusion between endosomes (Szatmari et al., 2014). The SNARE fusion protein VAMP3, has also been shown to function in amphisome formation, and its depletion resulted in impaired autophagosome to multivesicular endosome fusion (Fader et al., 2009). SNARE proteins direct vesicular fusion by assembling into trans-SNARE complexes, which contain one vesicle-SNARE on the donor membrane and three target-SNAREs on the acceptor

membrane (Barth and Kohler, 2014). VAMP3 is likely to function as a vesicle-SNARE on autophagosomes, however its corresponding target-SNAREs have yet to be identified (Fader et al., 2009).

The function of amphisome formation is unclear and there is conflicting evidence regarding the requirement for endosome fusion with the autophagosome prior to autolysosome formation (Fader and Colombo, 2009; Rusten and Stenmark, 2009). The observation that autophagic induction redirects multivesicular endosomes into the autophagic pathway and reduces exocytosis of intraluminal vesicles as exosomes (Fader et al., 2008), may indicate a need for the cell to retain content during times of stress. Changes in lysosome distribution, following autophagy induction (Bagshaw et al., 2006; Korolchuk et al., 2011; Matsushita et al., 2004), may also make it necessary for endosomes to utilise the autophagic pathway to enable cargo delivery to the lysosome. It has also been suggested that amphisome formation primes the autophagosome for fusion with a lysosome (Gordon and Seglen, 1988). Amphisomes have a lower pH than the original autophagosome, due to H^+ATPase pumps acquired from endosome fusion (Stromhaug and Seglen, 1993). During endosome maturation, pH governs late endosome fusion with lysosomes (van Weert et al., 1995), and we can speculate that reduced autophagosome pH may also be obligatory for autophagosome and lysosome fusion. Additionally, endosome fusion with the autophagosome may be required for the assembly of the molecular machinery required to initiate autolysosome formation (Gordon and Seglen, 1988; Lamb et al., 2013a). The molecular machinery required for autolysosome formation, for example Rab7, is localised on late endosomes, and thus endosomes could allow the relocation of this machinery to autophagic compartments (Gordon and Seglen, 1988; Lamb et al., 2013a).

1.2.2 Autolysosome formation

Autolysosome formation is the final step in autophagosome maturation and involves fusion with lysosomes to deliver a critical concentration of hydrolytic enzymes to the autophagosome (Shen and Mizushima, 2014). Lysosomes contain more than 60 acidic hydrolyases, including: proteases, peptidases, nucleases, glycosidases, sulfatases and lipases, allowing the breakdown of many different types of macromolecules (Schroder et al., 2010). Lysosomes also have a highly acidified lumen to maintain optimal conditions for the activity of these hydrolyases (Schroder et al., 2010). Upon autophagy activation, lysosomal pH is decreased, and this change ensures that the acidic environment is maintained upon fusion with less acidic autophagosomes (Korolchuk et al., 2011). The hydrolytic enzymes are then able act on the cytoplasmic content in the autophagosome to liberate important macromolecules back into the cell (Shen and Mizushima, 2014).

Endosomal trafficking machinery may have a functionally conserved role in both endosome maturation and autolysosome formation (Brooks, 2012; Lamb et al., 2013a). The late endosome to lysosome trafficking protein, Rab7, localises to amphisomes and is believed to facilitate the trafficking of this compartments to lysosomes for fusion (Hyttinen et al., 2013; Jäger et al., 2004). The inhibition of Rab7 function, via RNAi silencing or the expression of a dominant negative form of Rab7, resulted in the accumulation of autophagosomes or amphisomes and an absences of autolysosomes, supporting that Rab7 has a function in autolysosome formation (Fader et al., 2008; Gutierrez et al., 2004; Hyttinen et al., 2013; Jäger et al., 2004). The tethering complex, Class-c vesicular sorting protein (C-Vps) complex, is also involved in the final stages of endosome maturation (Rink et al., 2005; Solinger and Spang, 2013) and facilitates amphisome-lysosome fusion (Liang et al., 2008; Lindmo et al., 2006; Sato et al., 2000). In

yeast and *Drosophila* the C-Vps complex has been shown to be required for docking and fusion of autophagosomes or amphisomes with the vacuole/lysosomes (Lindmo et al., 2006; Sato et al., 2000). Similarly in human cells, C-Vps complex is required for autophagosome to lysosome fusion, suggesting that it does have a conserved role in autophagosome maturation and endosome maturation (Liang et al., 2008).

The fusion between autophagosomes or amphisomes and lysosomes is mediated by SNARE proteins. The SNARE protein, syntaxin17 is recruited to the fully formed autophagosome, and this can then direct fusion with endosomes or lysosomes via synaptosomal-association protein 29 and VAMP8 (Itakura et al., 2012; Itakura and Mizushima, 2013; Takats et al., 2013). In *Drosophila*, syntaxin17 has been shown to interact with VAMP7, as there is no *Drosophila* homolog for VAMP8 (Takats et al., 2013). Similar to VAMP8 in mammalian systems, VAMP7 is presumed to be present on endosomes or lysosomes, where it may act as a target-SNARE to facilitate fusion with autophagosomes (Takats et al., 2013). In mammalian cells, VAMP7 has also been detected on autophagosomes, where it is required for autophagosome maturation, however its interacting partner remains to be identified (Fader et al., 2009). Many of these studies have failed to distinguish between amphisome and autolysosome formation, but it is likely that similar molecular machinery functions at both maturation steps.

PI3P is an important regulator during autophagosome maturation, as it can interact with a number of effectors to direct autophagosomes and allow fusion with endosomes and lysosomes (Dall'Armi et al., 2013). Tectonin domain-containing protein, TECPR1 and FYVE and coiled-coil domain containing 1 (FYCO1), are PI3P effectors which have been shown to facilitate autophagosome tethering and trafficking (Chen et al., 2012; Ogawa et

al., 2011; Pankiv et al., 2010). TECPR1 forms a complex with the Atg12-Atg5 complex, which is known to participate in autophagosome formation as part of an Atg12-Atg5-Atg16 complex, however its function in autophagosome maturation appears to be independent of this interaction with Atg16 (Chen et al., 2012). The tethering protein TECRP1 in complex with Atg12-Atg5 is able to interact with PI3P and this interaction is critical for autolysosome formation (Chen et al., 2012). The PI3P effector, FYCO1 is also required for this step of maturation and has been shown to be involved in trafficking of autophagosomes along microtubules to facilitate autophagosome maturation (Pankiv et al., 2010). Additionally, the phosphorylation of PI3P to form $PI(3,5)P_2$ is hypothesised to function in the efficient trafficking of autophagosomes, endosomes and lysosomes (Dall'Armi et al., 2013). Though the effects of $PI(3,5)P_2$ on autophagy have not been fully explored, the inhibition of PI3P phosphorylation has been shown to impair autophagosome maturation, indicating that $PI(3,5)P_2$ probably has a role in regulating this process (Ferguson et al., 2009; Lenk and Meisler, 2014; Rusten et al., 2006; Rusten et al., 2007)

Cholesterol/sphingolipid-rich micro-domains are also critical for autophagosome maturation. Micro-domains, also referred to as lipid rafts, are regions of ordered lipid membrane, which are enriched with cholesterol and sphingolipids, and these facilitate protein interactions with the membrane (Delmas et al., 2013). Lysosomes are especially enriched with micro-domains, which provide interaction sites for lysosome associated membrane proteins (LAMPs; Kaushik et al., 2006), and assembly sites for SNAREs (Chintagari et al., 2006; Lang, 2007); both of which function in lysosome fusion with autophagosomes or amphisomes (Shen and Mizushima, 2014). Changes in cellular lipid levels have been shown to interfere with micro-domains and can reduce the assembly of

these lysosomal proteins (Lingwood and Simons, 2010; Zhang et al., 2009a). Therefore changes in membrane lipid content can result in the loss of autolysosome formation and accumulation of autophagosomes in the cytosol, as seen in metabolic disorders such as diabetes and lysosomal storage disorders (Fraldi et al., 2010; Parkinson-Lawrence et al., 2010; Son et al., 2012).

1.3 Autophagy functions in lipid homeostasis

Lipids are essential cellular components that supply energy, contribute to membranes and mediate cellular signalling (Liu et al., 2013). Free lipids are, however, highly toxic and cells therefore tightly regulate lipid storage and release, to maintain intracellular lipid homeostasis (Kohlwein et al., 2013). Autophagy has been strongly implicated in the maintenance of lipid homeostasis, lipid efflux and in lipid metabolism (Koga et al., 2010; Singh et al., 2009a; van Zutphen et al., 2014).

1.3.1 Lipid droplets are involved in regulating lipid homeostasis and storage

Cells contain a diverse range of lipids, most of which belong to one of three classes; glycerolipids, sphingolipids and sterols (Haberkant and Holthuis, 2014). Glycerolipids include the phospholipids, which are the main component of biological membranes (Baenke et al., 2013). Sphingolipids and sterols are also integral membrane components, primarily functioning in micro-domains (Chiantia and London, 2013; Dirkx and Solimena, 2012; Lang, 2007; Lingwood and Simons, 2010), and function in cellular and organism signalling (Hannich et al., 2011). The *de novo* synthesis of lipids begins with acetyl-CoA, generated by the citric acid cycle, which is then converted to fatty acids via a series of enzymatic reactions (Baenke et al., 2013). Fatty acids can then be converted to neutral

lipids, which can be stored for later use, in energy production, or the synthesis of structural or signalling lipids (Baenke et al., 2013).

Lipid droplets are the main site of lipid storage in cells, and contain neutral lipids in the form of triacylglycerol and esterified sterols, which are surrounded by an outer phospholipid monolayer (Melo et al., 2011a). Neutral lipids are synthesised from fatty acids, glycerol-3-phosphate or dihydroxyacetone phosphate, and sterols, by four acyltransferases in the endoplasmic reticulum (Kohlwein et al., 2013). The biogenesis of lipid droplets involves the accumulation of these neutral lipids between the cytoplasmic and luminal leaflet of the endoplasmic reticulum membrane, from which the lipid droplet is thought to bud off, and be surrounded by the phospholipid monolayer (Melo et al., 2011a; Ruggles et al., 2013).

Lipids stored within lipid droplets can be mobilized in response to cellular demand and this involves specific lipases, which can be found in the lipid droplets, the cytoplasm and lysosomes; indicating lipid metabolism can be mediated via a number of pathways (Ouimet et al., 2011). In the lipid droplet, adipose triglyceride lipase, hormone-sensitive lipase and monoacylglycerol lipase, function sequentially to hydrolyse triacylglycerol to fatty acids and glycerol (Thiam et al., 2013). Sterol esters are also hydrolysed by hormone-sensitive lipases in lipid droplets, but additional lipases may be involved (Thiam et al., 2013). Sterol ester and triacylglycerol can also be hydrolysed in the lysosome by lysosomal acid lipase (Ouimet et al., 2011) and this type of lipolysis is primarily involved in the hydrolysis of endocytosed sterol esters and triacylglyerols (Ouimet et al., 2011). Recently, however lipids stored in lipid droplets have also been shown to be delivered to

the lysosome, via autophagosomes (Ouimet et al., 2011), suggesting that autophagy may also have a function in acidic lipolysis of stored lipids.

1.3.2 Lipophagy is an alternate route for lipid metabolism

Lipid metabolism that is mediated by autophagy is termed lipophagy, and has been demonstrated in a number of cell types (Koga et al., 2010; Singh et al., 2009a; van Zutphen et al., 2014). In yeast the incorporation of lipid droplets into the vacuole (the equivalent of mammalian lysosomes) was shown to be dependent on core autophagic machinery, under both nutrient rich and nutrient restricted conditions (van Zutphen et al., 2014). In mammalian cells, lipid droplets have an increased association with autophagosomes in response to starvation and particularly prolonged exposure to starvation (Singh et al., 2009a). Lipophagy also appears to function under basal conditions, with the genetic or pharmaceutical inhibition of autophagy, resulting in the accumulation of lipid droplets and reduced triacylglyerol hydrolysis (Singh et al., 2009a). This may suggest that autophagy is able to mobilize lipid stores, most likely as an energy source under basal conditions and in response to energy deprivation (Liu and Czaja, 2013).

Changes in cellular lipids have also been shown to induce autophagy. Exposure to excess fatty acids can increase autophagic activity, with no change to the lipid accumulation in lipid droplets (Singh et al., 2009a). Cholesterol loading also induces autophagic activity, and furthermore Atg5 knock-out in macrophages impaired the hydrolysis of cholesterol esters and reduced the cellular efflux of cholesterol (Ouimet et al., 2011). Similarly, increased amounts of sphingolipid levels in cells induced autophagy and the inhibition of autophagy by Atg7 knock-down caused an accumulation of sphingolipid metabolites such

as ceramide (Alexaki et al., 2014). This suggests that excess lipids and lipid metabolites maybe sequestered by autophagosomes, which may allow the hydrolysis of these lipids or facilitate their efflux from the cell. Since lipids have been shown to regulate the induction of autophagy, via interactions with TOR (Cai et al., 2014; Inokuchi-Shimizu et al., 2014; Tan et al., 2012), autophagy is likely to function as a key regulator in cellular lipid homeostasis and to protect the cell from lipotoxicity.

Autophagy appears to function in lipid efflux to maintain intracellular lipid content, but prolonged exposure to acute lipid loading conditions can impair autophagy (Koga et al., 2010; Singh et al., 2009a). The reduced rate of autophagic clearance observed as a result of acute lipid loading, may be linked to alterations in cellular lipid profiles (Koga et al., 2010; Singh and Cuervo, 2011). For example, mice exposed to high fat diets had reduced cholesterol content in lysosomal membranes and showed a 40% decrease in autolysosome formation, when compared to their counterparts fed on regular diets (Koga et al., 2010). Cholesterol is an important membrane component of lysosomes (Schoer et al., 2000) and decreased cholesterol can cause a reduction in the micro-domains, which are important for the protein interactions involved in vesicle fusion (Lingwood and Simons, 2010; Zhang et al., 2009a). A similar defect has been seen in the lysosomal storage disorder Niemann-Pick type C, where cholesterol efflux was inhibited, resulting in the accumulation of esterified cholesterol in late endosomes and lysosomes (Peake and Vance, 2010). Altered cholesterol balance has been shown to induce autophagosome accumulation, due to a lack of autophagosome to lysosome fusion (Koga et al., 2010; Lieberman et al., 2012). Thus autophagy may not only function in the regulation of lipids, but is in turn reliant on the maintenance of lipid homeostasis.

An inverse relationship has been reported between autophagy and lipolysis, with the inhibition of autophagy reducing the lipids that are stored in lipid droplets. In *Drosophila*, impaired autophagy resulted in reduced lipid storage in both the fat body and salivary glands of larvae (Wang et al., 2012). Reduced lipid storage did not result from impaired lipid droplet biogenesis, indicating that lipolysis may be up-regulated in the absence of autophagy, possibly as a way of meeting cellular energy demands (Wang et al., 2012). Similarly, tissue specific knock-down of Atg7 in mouse liver and cardiac muscle, resulted in a reduction in lipid droplet size, following 12h to 48h of starvation (Shibata et al., 2009). In the same mouse model, however, a reduction in lipolysis and an accumulation of lipid droplets was observed when autophagy was inhibited by Atg7 knock-down (Singh et al., 2009a). This discrepancy may be due to the age of the mice with Shibata *et al.* (2009) testing younger mice than Singh *et al.* (2009a) and this could suggest that the relationship between autophagy and lipid droplets differs dependent on the developmental stage.

Autophagy has been implicated in adipocyte differentiation, and autophagy knock-down in 3T3-L1 preadipocytes inhibited lipid accumulation and decreased the amount of adipocyte differentiation factors (Singh et al., 2009b). *In vivo*, adipocyte-specific knock-down of Atg7 generated lean mice with decreased white adipose mass, and this tissue also displayed features of brown adipocytes with reduced lipid storage and elevated lipid metabolism (Singh et al., 2009b; Zhang et al., 2009b). These mice also exhibited an increase in normal brown adipose tissue, conferring a higher tolerance to obesity and improved insulin sensitivity (Singh et al., 2009b; Zhang et al., 2009b). Autophagy therefore functions to regulate body lipid accumulation by controlling adipocyte differentiation and determining the balance between white and brown fat (Liu and Czaja, 2013). It is evident that a complex interaction exists between lipid homeostasis and

autophagy, which may provide a critical insight into many lifestyle related metabolic diseases.

1.4 Imaging of autophagy

Fluorescence microscopy has been used to visualise autophagic processes (Juhasz and Neufeld, 2008; Klionsky et al., 2008; Neufeld, 2008b). The ability to visualise specific organelles, proteins and lipids, offers a greater understanding of biological processes, by providing spatiotemporal information. Fluorescent proteins and organic fluorescence probes can allow the detection of specific proteins or cellular compartments in live or fixed cells. There are however, a number of drawbacks associated with many of the currently used imaging tools. Therefore, alternative fluorescence compounds such as metal base fluorophores are being explored for use in biological settings (Parker, 2011).

1.4.1 Fluorescent proteins as tools for labelling autophagic machinery

Fluorescent proteins allow the detection of a protein of interest, by the introduction of recombinant DNA encoding the protein fused to a fluorescent protein, such as green fluorescent protein (GFP; Zhang et al., 2002). An array of naturally occurring fluorescent proteins has allowed the development of molecular probes with a range of photophysical properties, making them ideal for multicolour fluorescence microscopy in cellular biology (Idrees et al., 2014; Kogure et al., 2006; Ong et al., 2011; Stepanenko et al., 2011). Fluorescent proteins are widely used for biological imaging as they are highly specific and allow live cell imaging, which can provide information about protein dynamics and interactions in real time (Jung et al., 2013).

Drosophila have been used extensively in the investigation of autophagy, as the molecular machinery is highly conserved in mammals (Chang and Neufeld, 2010; Juhasz and Neufeld, 2008; Neufeld, 2008a; Neufeld, 2008b). With this model system, fluorescent proteins are extensively used for reporting protein localisation and dynamics (Fritsch et al., 2006; Hazelrigg and Mansfield, 2006). Fluorescent labelled proteins are often expressed using the GAL4/UAS system, which was originally derived from yeast (Duffy, 2002). A protein encoded for by GAL4 is able to bind to an Upstream Activating Sequence (UAS) enabling the induction of transcription for the genetic element (Duffy, 2002). The development of specific GAL4 drivers, has allowed spatiotemporal control over UAS genetic element expression (Duffy, 2002). As this is a widely used system for genetic manipulation in *Drosophila*, a large number of genetic variants have been developed and are often publicly available, including fluorescently tagged protein lines (Hazelrigg and Mansfield, 2006; St Pierre et al., 2014).

Fluorescent protein labelling of core autophagic machinery can be used to monitor autophagic progression in *Drosophila* (Chang and Neufeld, 2010; Neufeld, 2008b; Zirin and Perrimon, 2010). In particular Atg8a-GFP (Scott et al., 2004) and more recently Atg8a-mCherry (Chang and Neufeld, 2009), have been widely used to monitor autophagosomes (Chang and Neufeld, 2009; Chang and Neufeld, 2010; Juhasz et al., 2008; Juhasz and Neufeld, 2006; Juhasz et al., 2007; Kim et al., 2013a; Lindmo et al., 2006; Ling et al., 2014; Nagy et al., 2014c; Nagy et al., 2013; Neufeld, 2008b; Rusten et al., 2004b; Rusten et al., 2007; Scott et al., 2004). Fluorescently labelled lysosomal proteins, such as Lamp1 are also available, which can be used in combination with fluorescently labelled Atg8a to detect the late stages of autophagy (Low et al., 2013; Takats et al., 2013; Yu et al., 2010). Proteins, such as Rab11, which has been detected on

amphisomes in cell culture (Fader et al., 2008; Savina et al., 2005), can also be detected in *Drosophila* using GFP labelling (Chang, 2004; Denef et al., 2008; Jiang et al., 2007; Shandala et al., 2011; Steinert et al., 2012). Therefore multiple fluorescent proteins may be used in combination to assess each stage of autophagic maturation.

Despite the successful use of fluorescent proteins in a range of biological systems, these probes do have a number of drawbacks. Most fluorescent proteins are large molecules, for example GFP consisting of 238 amino acids; and therefore the addition of GFP to proteins may alter protein interactions and trafficking in the cell (Jung et al., 2013; Lisenbee et al., 2003). Some fluorescent proteins are also prone to form dimers, which can also interfere with normal protein function (Jung et al., 2013; Lisenbee et al., 2003). Additionally, over-expression of proteins by the insertion of recombinant DNA can lead to aggregation of protein in unrelated organelles, potentially misleading the investigator as to the real function of the protein (Lisenbee et al., 2003). In some systems, such as *Drosophila*, these effects can be reduced by the use of P-elements, which allow the expression of fluorescent proteins under the control of the gene's endogenous driver (Hazelrigg and Mansfield, 2006). The generation of transgenic animals can be time consuming and costly (Satori et al., 2013), and it is therefore important for investigators to have a range of alternative tools for cellular fluorescent imaging.

1.4.2 Organic fluorescence probes can be used to monitor autophagy

Acidotrophic dyes are the most commonly used organic fluorescence probes for the investigation of autophagy, as they can detect acidic compartments, including autolysosomes (Klionsky et al., 2012; Neufeld, 2008a). Most acidotrophic dyes are basic organic molecules which are able to be protonated on entry into acidic compartments

(Pierzynska-Mach et al., 2014). This protonation prevents the dye from moving out of the compartment causing an accumulation, which can then be detected by fluorescence microscopy (Pierzynska-Mach et al., 2014). This, however, results in the detection of these dyes in all acidified compartments, not only autolysosomes (Neufeld, 2008a; Vázquez and Colombo, 2009). Despite this draw-back, acidotrophic dyes, such as LysoTraker® are still used extensively in the study of autophagy, often in combination with other markers such as Atg8a-GFP, for more dependable reporting of autophagy and to assess autophagic maturation (Neufeld, 2008a). In some tissues, such as *Drosophila* fat body, there is low basal lysosomal activity, therefore LysoTracker® is reasonably reliable in monitoring changes in autophagic activity (Neufeld, 2008a). Since acidotrophic dyes rely on a pH gradient, most of these probes are unable to be used in fixed cells (Vázquez and Colombo, 2009) and are therefore unsuitable for use in combination with antibody staining. Acidotrophic dyes are also prone to photobleaching and can become phototoxic following excitation, making them less compatible with time lapse live cell imaging (Pierzynska-Mach et al., 2014). These dyes should therefore be used with caution in the assessment of autophagy and are best utilized in combination with other techniques (Klionsky et al., 2008).

Fluorescence probes that target the potential content of autophagosomes have also proven to be useful tools in the investigation of autophagy. Some common targets of autophagy, such as mitochondria, are easily detected by a range of commercially available molecular probes (Dolman et al., 2013), while organelles such as lipid droplets are more difficult to detect (van Meer, 2005). The chemical nature of neutral lipids makes them difficult to stain (van Meer, 2005). Most commonly used neutral lipids stains, such as, Oil-Red-O and Nile Red, are insoluble in hydrophilic solutions making them difficult to work with, and

can only be used on fixed samples (Maxfield and Wüstner, 2012; Spangenburg et al., 2011). The need for fixation of samples to image lipids, not only prevents the investigation of organelle dynamics, but can also dramatically alter protein distribution and ultra-structures within cells (Schnell et al., 2012). Lipid fixation is particularly problematic with many alcohol-based solvents and fixatives causing either fusion of lipid droplets or the extraction of lipids from samples (Fujimoto and Parton, 2011; Fukumoto and Fujimoto, 2002; Melo et al., 2011b). However, BODIPY®(493/503) is another neutral lipid dye that can be used in live or fixed samples, providing some scope for live cell imaging (Spangenburg et al., 2011). BODIPY®(493/503), as well as Oil-Red-O and Nile-Red, all have broad excitation and emission profiles, and small Stoke's shifts, making it difficult to use these probes for multi-coloured labelling (Ohsaki et al., 2010; Spandl et al., 2009; Yang et al., 2012). Thus, the investigation of lipids in cellular process including autophagy has been hindered by a lack of appropriate imaging tools (van Meer, 2005).

1.4.3 Metal based fluorescence probes as potential tools for detecting autophagy

Metal complexes have recently emerged as a promising alternative to conventional organic fluorescent probes (Fernandez-Moreira et al., 2010; Lo et al., 2012; Parker, 2011; Vaughan et al., 2013; Zhao et al., 2011). Metal complexes are able to overcome a number of the shortcomings associated with fluorescent proteins and organic fluorescence probes; including problems with self-quenching, photobleaching, a small Stoke shift, broad and formless emission profiles and poor signal discrimination versus endogenous auto-fluorescence (New et al., 2010). In addition, metal complexes also have properties that make them ideal for use as biosensors, which are able to convey information about the cellular environment, such as pH or oxidation state, as well as giving spatiotemporal information (Chan et al., 2012; New et al., 2010).

Around 80% of the metal complexes described thus far show lysosomal localisation in cells (Parker, 2011). Probes of this nature may be useful for the study of autophagosome maturation, potentially providing a more photo-stable option to traditionally used lysosomal probes (Pierzynska-Mach et al., 2014). Metal based probes that specifically localise to autophagosomes in live cells have also been described (Chen et al., 2013; He et al., 2014). One such probe is a pH sensitive zinc based probe, which was detected in autophagosomes following acidification by fusion with lysosomes (Chen et al., 2013). This probe could not be detected in HeLa cells under normal conditions and was only detected following autophagy induction by starvation and the intensity of fluorescence was sensitive to autophagic modulation (Chen et al., 2013). Two iridium based complexes have also been characterised for monitoring autophagy (He et al., 2014). These probes were shown to induce autophagy, whilst also detecting lysosomes (He et al., 2014). These complexes provide investigative tools to monitor lysosomal activity in response to autophagy induction, without the need for the treatment of cells with drugs such as Rapamycin or exposure to long starvation protocols (He et al., 2014). Metal based fluorescence probes therefore show promise for use in the investigation of autophagy, and further development and characterisation of new molecular probes may lead to the development of more specific tools.

One of the major challenges in designing metal complexes for fluorescence imaging is a lack of information about the structure-activity relationship that links the chemical nature of a complex with its biological activity (Balasingham et al., 2011; New et al., 2010). Metal complexes usually consist of a sensitising chromophore, pendant arms which can contain carboxylates, amides or phosphinates and the metal ion. Attempts to characterise

biological activity of these metal complexes have mostly focused on lanthanide(III) based complexes, from which some general observation have been made (Montgomery et al., 2009; New et al., 2010). Cellular up-take in a number of systems was primarily determined by the nature and mode of the linkage to the sensitising chromophore and this also appeared to affect protein interaction, which may in-turn facilitate certain modes of cellular up-take (Montgomery et al., 2009). Four cellular localisations are generally observed for metal complexes: lysosomes, mitochondria, protein enriched ribosomes and the nucleolus (Montgomery et al., 2009; New et al., 2010). The localisation of complexes to these cellular compartments appeared to be linked to the sensitising chromophore and to a lesser extent the number of pendant arms present (Montgomery et al., 2009). Though studies such as these provide some information about the cellular behaviour of certain metal complexes, many types of metal complexes are yet to be investigated.

Rhenium(I) tetrazolato complexes are a group of complexes that show intense luminescence, which is ideal for use in fluorescence imaging. The origin of this luminescence has been attributed to the metal-to-ligand charge transfer between the Rhenium(I) to diimine ligand (Vaughan et al., 2013; Werrett et al., 2011; Wright et al., 2012; Yam and Wong, 2011). Moreover, the phosphorescent nature of their emission is characterized by a large Stokes shift and longer excited state lifetime (Werrett et al., 2011). These properties help in preventing self-quenching and reduce autofluorescence (Werrett et al., 2011), making these attractive compounds for live cell imaging. Additionally, the possibility of fine-tuning both the chemical and the photophysical properties of these compounds has made them attractive for specific imaging applications (Wright et al., 2012). The biological activity of Rhenium(I) tetrazolato compounds had not previously been investigated, but are explored here as potential reporters for autophagy.

1.5 Rationale

Autophagy is involved in the regulation of cellular homeostasis and dysfunction of this process has been observed in a number of human diseases. A better understanding of the underlying mechanisms that orchestrate autophagy is relevant for the pathogenesis in a number of major diseases like diabetes, obesity and cancer. Though much of the core autophagic machinery has been elucidated, the function of many of these core proteins has not been fully resolved. In addition, while fluorescence imaging has been utilized for the investigation of autophagy, one of the difficulties for investigators in this field has been a lack of molecular probes for imaging specific autophagic events.

As the only transmembrane protein in the core autophagic machinery, Atg9 is purported to function in autophagosome formation, where it is suggest to have a role in membrane recruitment. In yeast, Atg9 appears to function in the generation of a membrane platform, to which other autophagic machinery can be recruited, allowing autophagosome formation (Papinski et al., 2014; Stanley et al., 2014; Yamamoto et al., 2012). In higher eukaryotes, however, Atg9 appears to enhance autophagosome formation, but is not strictly required for this initial step of autophagy (Orsi et al., 2012; Saitoh et al., 2009). In mammalian and *Drosophila* cells, Atg9 resides on several cellular compartments including late endosomes, which participate in autophagy maturation (Orsi et al., 2012; Young et al., 2006). The association of Atg9 with late endosomes is seemingly unaffected by autophagic activity (Orsi et al., 2012) and some reports have even indicated that there is an increase in Atg9 at this location following autophagy induction (Young et al., 2006). Both autophagosome formation and maturation require membrane trafficking and fusion machinery and a number of proteins that function in autophagosome formation, have also been identified to function in autophagosome maturation (Lamb et al., 2013a). Therefore we proposed that

Atg9 may also function during autophagosome maturation, possible at the stage of amphisome formation which involves autophagosome fusion with late endosomes.

For the investigation of Atg9 function we employed conventional imaging techniques, which rely heavily on the use of fluorescent proteins. However, we also identified a need for improved tools that enable the investigation of autophagy by fluorescence imaging. Commonly used acidotrophic dyes are widely used in the field, but these can generally only detect late autophagic compartments, which cannot always be distinguished from endosomal compartments. Additionally, these dyes are generally based on organic molecules, which are not ideal for live cell imaging. Metal base complexes have already shown some promise in the detection of autophagic compartments (Chen et al., 2013; He et al., 2014), but only a limited number of complexes have been assessed in cells. Rhenium(I) tetrazolato complexes are a group of complexes, which have photophysical properties that are ideal for live cell imaging (Werrett et al., 2011; Werrett et al., 2013), and their cellular distribution has not previously been investigated. Thus we have investigated this class of metal base fluorescents complexes for the imaging of autophagy.

Drosophila were employed as a model system for the investigation of autophagy, as the molecular machinery is highly conserved in mammals (Chang and Neufeld, 2010; Juhasz and Neufeld, 2008; Neufeld, 2008a; Neufeld, 2008b). In addition, a wide range of genetic variants have been developed and are publicly available for *Drosophila*, including fluorescently tagged protein lines (Hazelrigg and Mansfield, 2006; St Pierre et al., 2014). The availability of fluorescent protein labelled autophagic machinery allows the monitoring of autophagic progression, making *Drosophila* a desirable system for the investigation of this process (Chang and Neufeld, 2010; Neufeld, 2008b; Zirin and Perrimon, 2010).

1.6 Hypotheses and aims

Hypothesis 1:

Atg9 has a function during autophagosome maturation involving autophagosome fusion with late endosomes. The silencing of Atg9 will alter the formation of amphisomes and autolysosomes.

Hypothesis 2:

Rhenium(I) tetrazolato complexes can be used for live cell imaging of autophagic processes.

Aim 1:

To characterise autophagic maturation in the absence of Atg9.

Aim 2:

To identify and characterise Rhenium(I) tetrazolato complexes that have potential for fluorescence imaging of autophagy.

Chapter 2: Atg9 is required for amphisome and autolysosome compartmentalisation

2.1 Preface

The core autophagic protein Atg9 is the only transmembrane protein that has been identified in the autophagy molecular machinery. It is suspected to have a role in membrane recruitment to form autophagosomes, and therefore the trafficking of Atg9 has previously been studied in an attempt to delineate the source of autophagosome membrane. There is however, a lack of understanding of the exact role of Atg9 and very few studies have reported on the effect of Atg9 knock-down on autophagy, particularly in relation to autophagosome maturation. In this chapter we have used *Drosophila* as a model system to investigate autophagic progression in Atg9 knock-down tissue and demonstrated a role for Atg9 in autophagosome maturation. Here autophagy was investigated during *Drosophila* development, at the onset of metamorphosis, to visualise autophagy in response to natural development signals, unlike previous studies which focussed on starvation induced autophagy.

2.2 Abstract

Autophagy is an intracellular recycling and degradation process, which is important for energy metabolism, lipid metabolism, physiological stress response and organism development. During *Drosophila* development, autophagy is up-regulated in fat body and midgut cells, to control metabolic function and to enable tissue remodelling. Atg9 is the only transmembrane protein involved in the core autophagy machinery and is known to have a role in autophagosome formation. During *Drosophila* development, Atg9 co-located with Atg8 autophagosomes, the endosome marker Rab11 and endosome-lysosome marker Lamp1. RNAi silencing of *Atg9* reduced both the number and the size of autophagosomes during development and caused morphological changes to amphisomes/autolysosomes with a specific loss of intraluminal vesicles. In control cells there was compartmentalised acidification corresponding to intraluminal Rab11/Lamp-1 vesicles, but in Atg9 depleted cells there were no intraluminal vesicles and the acidification was not compartmentalised. Consequently while amphisomes and autolysosomes were formed in Atg9 depleted cells, there were no detectable intraluminal vesicles and a reduced capacity to degrade and remodel gut tissue. These results demonstrated that Atg9 is required for the presence of intraluminal vesicles and to generate localised acidification within amphisomes/autolysosomes.

2.3 Introduction

Macroautophagy or autophagy is an intracellular process that is highly conserved from yeast through to mammals, and involves the encapsulation of cytoplasmic components into a double membrane structure called an autophagosome (Ohsumi, 2014). Autophagosomes can then undergo a sequential maturation process by interacting with endosomes to form amphisomes and then lysosomes to generate autolysosomes; which eventually results in the degradation of engulfed cytoplasmic material (Berg et al., 1998; Gordon and Seglen, 1988; Lamb et al., 2013a; Shen and Mizushima, 2014). This catabolic process is an important mechanism for the bulk degradation of cytoplasmic constituents, the clearance of protein aggregates, the recycling of aged or defective organelles and for combatting intracellular pathogens (Mizushima et al., 2008). Autophagosomes also have critical functional roles in cellular homeostasis, being specifically involved in energy/nutrient sensing, glucose/glycogen metabolism, and lipid transport, storage and metabolism (Singh and Cuervo, 2011; Singh et al., 2009a). Autophagy operates at a basal level in most cell types, but can be specifically induced in response to hormonal and developmental signalling, nutrient restriction, aberrant protein folding, altered homeostasis/physiological stress, and various pathological conditions including neurodegenerative disease, infection, aging and cancer (Deretic, 2009; Kroemer et al., 2010; Kundu and Thompson, 2008; Liu and Ryan, 2012). While the core molecular machinery involved in autophagy has been identified (Harding et al., 1995; Thumm et al., 1994; Tsukada and Ohsumi, 1993), the mechanisms orchestrating this critical intracellular process and the precise role for each component of the molecular machinery are yet to be fully defined.

Over 30 autophagy-related genes (Atg) have been discovered, mainly from studies in yeast (Nakatogawa et al., 2009; Tsukada and Ohsumi, 1993). Upon the induction of autophagy, by for example starvation, most of these Atg proteins are localised to a perivacuolar structure called the pre-autophagosome structure (PAS; Suzuki et al., 2001; Suzuki et al., 2007). The PAS is a precursor for autophagosome formation and involves the recruitment of the kinase complexes Atg1/ULK1 and Atg6/Beclin1 to a structure that generates an autophagosome-specific pool of phosphatidylinositiol-3-phosphate (Rubinsztein et al., 2012). This lipid pool drives the nucleation of the phagophore and recruitment of other autophagy-related proteins to the isolation membrane (Lamb et al., 2013b; Wirth et al., 2013). Membrane expansion and closure of the phagophore involves the Atg5-Atg12 complex, which acts as an E-3 ligase to mediate the lipidation of Atg8/LC3, and the latter remains associated with the outer autophagosome membrane during maturation (Klionsky and Schulman, 2014). The multiple-spanning integral membrane protein Atg9 is an early target of the Atg1/ULK1 kinase complex and Atg9 phosphorylation is required for the efficient recruitment of Atg8 and Atg18 to the site of autophagosome formation (Papinski et al., 2014); making it an essential component of the autophagic molecular machinery.

The integral membrane properties of Atg9 and its detection in different membrane compartments, including small vesicles that reside in close proximity to the Golgi, mitochondria and the PAS, have led to the suggestion that Atg9 is involved in membrane delivery to the expanding phagophore (Lamb et al., 2013b; Mari et al., 2010). In yeast, for example, Atg9 can be detected on small 30-60 nm vesicles at the PAS (Yamamoto et al., 2012) and may interact with the Atg17 scaffolding complex assembled by Atg1/ULK1 to facilitate Atg9 vesicle fusion (Ragusa et al., 2012; Sekito et al., 2009). This vesicular fusion may provide a membrane platform on which the isolation membrane can then be

formed (Shibutani and Yoshimori, 2014; Yamamoto et al., 2012). In mammalian cells, Atg9 also localises with Atg1/ULK1 and Atg16L at recycling endosomes (Longatti et al., 2012; Puri et al., 2013) and is trafficked to the recycling endosome from the plasma membrane, possibly through the early endosome via Rab11 positive vesicles (Longatti et al., 2012; Puri et al., 2013; Ravikumar et al., 2010). While Atg9 might have a role in the formation of membrane platforms, it is sequestered to but not integrated into autophagosomes (Orsi et al., 2012), raising concerns over the ideas on membrane recruitment and suggesting that it has an alternate functional role.

Atg9 co-locates with endosomes following the induction of autophagy (Tang et al., 2011; Young et al., 2006), adding confusion about the precise role of Atg9 and leading to speculation about its involvement in autophagosome maturation. Amphisome formation, involving the heterotypic fusion of autophagosomes and endosomes, is known to utilise a range of vesicular machinery including, Rab11 (Fader et al., 2008; Savina et al., 2005), the SNARE protein VAMP3 (Fader et al., 2009) and the ESCRT proteins Vps 28, Vps25, Vps32 and Deep Orange (Lindmo et al., 2006; Rusten et al., 2007; Spowart and Lum, 2010; Vaccari et al., 2009); but the regulatory mechanism is not clear. Lysosomal fusion with the maturing autophagosome, to form autolysosomes, also involves specific vesicular machinery, including Rab7 and the SNARE protein Syntaxin 17, which binds to SNAP-29 and VAMP7 to form a ternary complex (Fader et al., 2009; Itakura et al., 2012; Takats et al., 2013). As the only integral membrane protein in the core autophagy machinery, Atg9 may play a role in endosome and lysosome recruitment acting to facilitate vesicular fusion in manner similar to that proposed for its role in membrane recruitment to the phagophore (Takahashi et al., 2011).

Drosophila provides an ideal model system to investigate the role of Atg9 in autophagy; as in the fly, autophagy is induced in response to physiological stresses, such as nutrient restriction (Mulakkal et al., 2014) and Atg9 RNAi silencing can reduce this autophagic response (Low et al., 2013; Nagy et al., 2014b; Nagy et al., 2013; Pircs et al., 2012). Autophagy is also up-regulated during *Drosophila* metamorphosis from larvae to adult-hood (Butterworth et al., 1988; Denton et al., 2013; Denton et al., 2009; Lindmo et al., 2006; Rusten et al., 2004a) and autophagosomes increase in abundance in the fat body tissue as the larvae approach puparation (Lindmo et al., 2006; Rusten et al., 2004b); enabling the investigation of autophagy under natural conditions without an exogenous stimulus. Here we have used the large size of *Drosophila* fat body cells and organelles, and the capacity for genetic manipulation in the fly, to further investigate the role of Atg9 in autophagy.

2.4 Materials and methods

2.4.1 Drosophila stocks.

Drosophila stocks were maintained in standard medium at 25°C, with a 12:12 hours light to dark schedule. Bromophenol-blue was added to the fly media and used to define different developmental time points (Andres and Thummel, 1994). Third instar larvae at minus four hours of puparium formation (-4h PF) where identified by a lack of blue dye in their gut, indicating gut clearance for in preparation for puparation, while newly formed white pupae (0h PF), were easily identified by their shape and white appearance. The yeast *GAL4-UAS* system was used for targeted gene expression (Brand and Perrimon, 1993). Fat body specific expression of transgenes from the UAS was driven by *CG-GAL4* (Asha et al., 2003) and gut specific expression of transgenes from the UAS was driven by *NP1-GAL4* (*Drosophila* genetic resource center, Kyoto). Wild-type and transgenic stock *UAS-Atg9*^{RNAi} (stock #34901) were obtained from the Bloomington *Drosophila* Stock Center (Indiana University, Indiana, USA). RNAi silencing stocks *UAS-Atg9*^{RNAi} (stock #v10045) and *UAS-Vps20*^{RNAi} (stock #v26388) were obtained from the Vienna *Drosophila* RNAi Centre (Vienna, Austria). *UAS-Lamp1-GFP* was obtained from Helmut Kramer (Center for Basic Neuroscience, Dallas, USA; Pulipparacharuvil et al., 2005). The autophagy markers *Atg8a-GFP* and *Atg8a-Cherry* were driven by an endogenous promoter and kindly provided prior to publication by Erik Baehrecke (University of Massachusetts, Medical School, MA, USA). *UAS-Rab11-GFP* was obtained from Markos González-Gaitán (University of Geneva, Geneva, Switzerland; Entchev et al., 2000; Wucherpfennig et al., 2003) and Donald F. Ready (Purdue University, West Lafayette, Indiana, USA; Satoh et al., 2005).

2.4.2 Gene expression and protein analysis

For quantitative real-time PCR (qRT-PCR) analysis fat body was explanted and pooled from 20 larvae. RNA was isolated from the fat body tissue using an RNAqueous® kit (Ambion, Auston, USA) according to the manufacturer's protocol. cDNA was synthesized using a High Capacity RNA-to-cDNA kit (Applied Biosystems, Waltham, USA). Quantitative RT-PCR was performed using a 7500 Fast Real-Time PCR System using a Fast SYBR Green Master Mix kit (Applied Biosystems, Waltham, USA). PCR primers were obtained from GeneWorks (Adelaide, Australia). The following primers were used to assay the *in vivo* efficiency of *UAS-RNAi* transgenes: *Atg9* (CG 3615) forward, 5'-AGC AGA AGC ACG GAT TCA CA-3', and reverse, 5'-GCA GTG CAT CAC AAA GGC AA-3'and *rp49* (CG7939, used as an endogenous control) forward, 5'-CGAGTTGAACTGCCTTCAAGATGA CCA-3', reverse 5'-GCTTGGTGCGCTTCTTCACGATCT-3'. Three independent biological samples were analysed for each genotype, and the mRNA expression levels were normalized against the endogenous control gene *rp49*, using the $\Delta\Delta C_T$ method.

Western blotting was performed in triplicate on three biological repeats, each repeat contained *Drosophila* fat body tissue from 10-15 either late 3rd larval instars (-4h PF) or newly formed white pupae (0h PF) using a previously described method (Shandala et al., 2011). Larval development was determined according to the method described by Andres and Thummel (1994) and described in brief above. For immunoblotting, protein was separated by SDS-PAGE (30 μg protein load) and then transferred to nitrocellulose membranes (Shandala et al., 2011). The membranes were probed with either rabbit anti-Atg9 antibody at 1/200 (Novus Biologicals, Littleton, USA, cat # NB100-98679) or for a loading control goat anti-GAPDH at 1/1000 (Imgenex, Littleton, USA) primary antibodies

and a horseradish-posixidate conjugate secondary antibody. Proteins were visualised using Novex® electro chemiluminescent substrate reagent kit (Life Technology, Carlsbad, USA) and imaged using a ImageQuant™ LAS 400 imager, software version 1.2.0.101 (GE Healthcare Bioscience, Parramatta, Australia). Quantification was performed using AlphaViewSA™ software version 3.0 (ProteinSimple, Santa Clara, USA).

2.4.3 Immunostaining and microscopy

For immunostaining, *Drosophila* fat body tissue was mounted on a microscope slide and fixed by in 2% (v/v) paraformaldehyde in PBS, for one hour on ice. The slides were then washed in 0.1% (v/v) Tween 20 (Sigma-Aldrich, St Louis, USA) in PBS for 30 minutes. Non-specific interactions were blocked by incubating the tissues with 5% (v/v) BSA (Sigma-Aldrich, St Louis, USA) and 0.1% (v/v) Tween 20 in PBS for 30 minutes, before incubation with rabbit anti-Atg9 antibody (1/50; Novus Biologicals, Littleton, USA) or donkey anti-Rab11 antibodies (1/100; obtained from Robert S. Cohen, University of Kansas; Dollar et al., 2002), diluted in 0.1% (v/v) Tween 20 and 5% (v/v) BSA in PBS for two hours at RT and then overnight at 4˚C. The tissues/slides were washed in 0.1% (v/v) Tween in PBS for 40 minutes and then incubated with either goat anti-rabbit IgG or donkey anti-goat IgG Cy5-labelled secondary antibodies (Jackson ImmunoResearch Laboratories, USA), for two hours at RT. The slides were washed in 0.1% (v/v) Tween 20 in PBS for 40 minutes and then mounted in 80% (v/v) glycerol in PBS. For live cell imaging *Drosophila* fat body and gut tissues were stained with LysoTracker® Red (1/200; Life Technology, Carlsbad, USA) for two minutes, then mounted in carbomer-940 (Snowdrift farm, Tucson, USA) based optical coupling gel (Rothstein et al., 2006). Imaging was performed using a Zeiss, LSM710 NLO confocal microscope equipped with Argon-gas and 543 nm and 633 nm solid-state lasers (Zeiss, Oberkochen, Germany) and

a two-photon Mai-Tai®, tuneable Ti:Sapphire femtosecond pulse laser (Spectra-Physics, Santa Clara, USA). Images were captured using a 63x oil immersion lens. Each confocal micrograph represented 1.5 μm thin optical sections.

For gut length analysis, the midguts were dissected from +4h PF larvae into PBS and fixed in 4% (v/v) paraformaldehyde (Denton et al., 2009). Tissues were stained with Hoechst 33258 (Invitrogen, Waltham, USA) and imaged with an Olympus IX71 epifluorescence microscope (Olympus, Shinjuku, Japan). Tissues for transmission electron microscopy (TEM) analysis were prepared as described previously (Kohler et al., 2009) and viewed with an FEI Tecnai G2 Spirit TEM (FEI, Hillsboro, USA).

2.4.4 Image Analysis

Analysis of compartment number and size was performed using Volocity® 3D Imaging Software (PerkinElmer, Waltham, USA). For each genotype and marker combination, micrographs from a minimum of 10 biological replicates were each analysed over an area of 2025 μm^2. For the analysis of the number and size of Atg8a-GFP compartments an object finder function was used, allowing automated detection based on compartment intensity at a specific threshold. Lamp1-GFP compartments were measured manually as the sub-compartmentalisation did not allow for automated detection. To assess the changes in Lamp1-GFP intraluminal compartments, a region of interest or ROI was drawn around the Lamp1-GFP compartment, and object finder was used to measure the area of the intraluminal compartments filled with LysoTracker®. An average number of 13 Lamp1-GFP compartments were measured per micrograph (range 8-38). The data was presented as a mean ± s.e.m, and the treatment groups compared by ANOVA analysis in GraphPad Prism with Dunnett post-hoc analysis (Prism software, version 6.01, USA).

The length around the perimeter of the midgut (from the foregut/midgut to midgut/foregut junction) was used to define midgut length and analysed using AnalySIS Software (Olympus, Shinjuku, Japan). At least 12 midguts from each genotype were examined. The data was presented as a mean ± s.e.m. and the different genotypes compared by a student's t-test using GraphPad Prism (Prism software, version 6.01, USA). The number of multivesicular structures (intracellular compartments that contained smaller intraluminal vesicles) in each midgut was determined manually from a total of 13 TEM images, from three independent biological replicates for each genotype, and involved a capture field view of 8.5 μm x 8.5 μm, at 11500 x magnification.

2.5 Results

2.5.1 Atg9 depletion reduced the number and size of autophagosomes at a time point in *Drosophila* development when autophagy is normally up-regulated.

Drosophila Atg9 has previously been investigated in the autophagic response to starvation and hypoxia (Low et al., 2013; Pircs et al., 2012; Tang et al., 2013), but its involvement in developmental autophagy has yet to be defined. Here we investigated Atg9 in relation to either Atg8 (another autophagy marker), Rab11 (an endosomal marker) or Lamp1 (an endosomal-lysosomal marker), in fat body tissue at 0h PF, when autophagy is known to be up-regulated (Lindmo et al., 2006; Rusten et al., 2004). There was an increased amount of the Atg9 protein in wild-type fat body tissue at 0h PF when compared to -4h PF (Figure 2.1A). In response to Atg9 RNAi silencing, the amount of *Atg9* mRNA was significantly depleted in fat body tissue at both -4h PF (Figure 2.1B) and 0h PF (Figure 2.1C); as defined by two independent RNAi lines; BL34901, hereafter referred to as $Atg9^{RNAi\ Line1}$; and v10045, $Atg9^{RNAi\ Line2}$. $Atg9^{RNAi\ Line2}$ depletion also resulted in a significant reduction in the amount of Atg9 protein detected in the fat body at both -4h PF and 0h PF (Figure 2.1A). At 0h PF, Atg9 co-located with Atg8a-GFP in fat body tissue, but not all Atg8a-GFP compartments were positive for Atg9 (Figure 2.1D-2.1D^{II}). At this time point Atg9 was also detected in association with large Rab11-GFP compartments that in most cases contained intraluminal Rab11-GFP positive vesicles (Figure 2.1E-2.1E^{II}). Atg9 was also detected in association with Lamp1-GFP compartments that contained intraluminal Lamp1-GFP positive vesicles (Figure 2.1F-2.1F^{II}). Atg9 was mainly detected as discrete punctate staining when associated with Atg8, Rab11 and Lamp1 compartments (Figure 2.1).

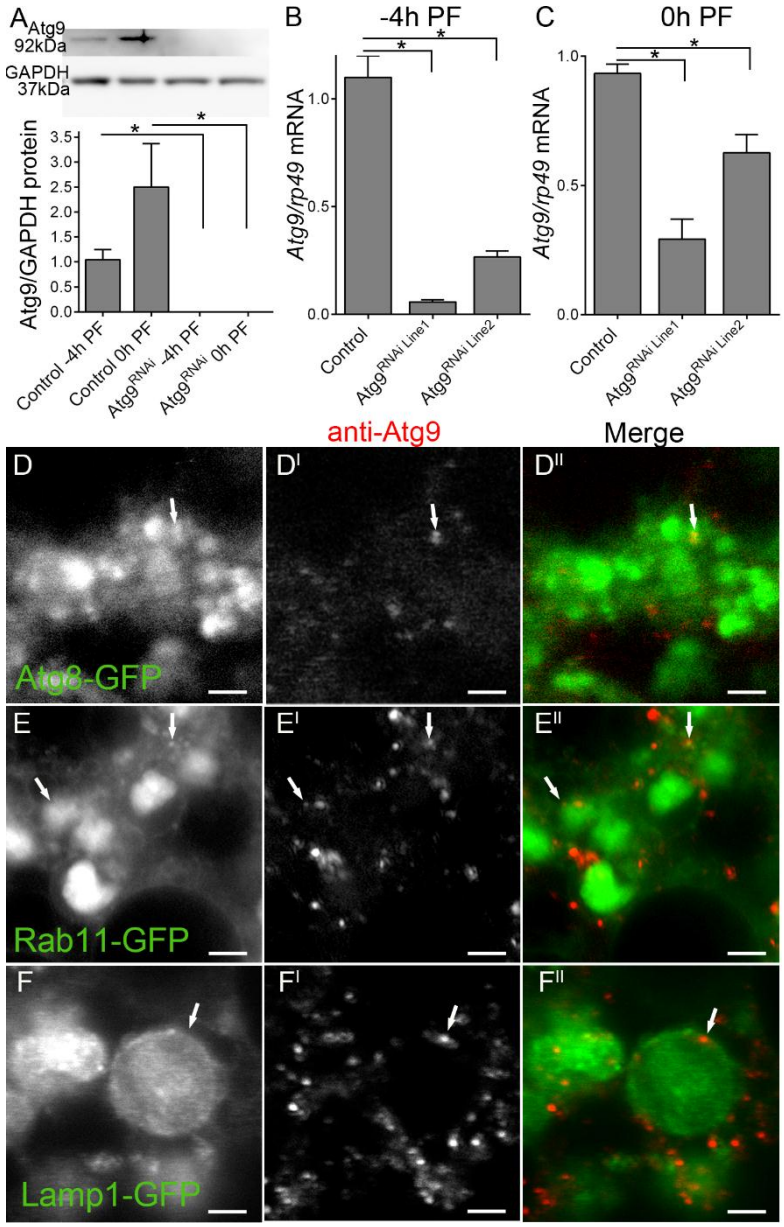


Figure 2.1 Atg9 expression and cellular localisation in Drosophila fat body during development.

(A) Western blot analysis showing Atg9 protein expression in fat body tissue of heterozygous CG-GAL4 (control) and CG-GAL4>UAS-Atg9$^{RNAi\ Line2}$. Histograms represent the relative amount of Atg9 protein in reference to GAPDH, defined by western blotting at two developmental time points (-4h PF and 0h PF). Data represented as mean ± s.e.m (n = 3). Asterisks indicate significant differences between genotype as calculated by student T-test ($p < 0.01$). (B, C) Histograms showing relative amount of *Atg9* mRNA in relation to *rp49* mRNA in fat body from controls compared to CG-GAL4>UAS-Atg9^{RNAi} (for two independent RNAi lines), at two developmental time points -4h PF (B) and 0h PF (C). Results are presented as mean ± s.e.m. (n =3). Asterisks indicate significant differences between genotype as calculated by ANOVA with Dunnett post hoc test ($p < 0.05$). (D-F^{II}) Confocal micrographs showing the localisation of Atg9 at 0h PF in W1118 fat body, detected with an anti-Atg9 antibody (greyscale in D^{I}, E^{I} and F^{I}; red in D^{II}, E^{II} and F^{II}), in relation to Atg8a-GFP (D), Rab11-GFP (E) and Lamp1-GFP (F). The arrows depict the Atg9-positive signal in close proximity to GFP-positive vesicles (D-F^{II}). Scale bars = 2 μm.

The formation of Atg8a-autophagosomes was investigated following the depletion of Atg9 by RNAi silencing. In control *Drosophila* fat body cells at 0h PF an average number of 14.92 ± 0.91 Atg8a-GFP positive compartments were detected per 1000μm^2 of cell area (visualised in Figure 2.2A, 2.2A^{ll} and quantified in Figure 2.3A) and 69.75 ± 3.26% of these Atg8a-GFP positive compartments were LysoTracker® positive (visualised in Figure 2.2A^{l}, 2.2A^{ll}). These Atg8a-GFP/LysoTracker® positive compartments had an average diameter of 3.22 ± 0.14 μm (Figure 2.3B), compared to 1.87 ± 0.06 μm for non-LysoTracker® Atg8a-GFP positive compartments. Atg9 depletion significantly reduced the number of Atg8a-GFP compartments in *Drosophila* fat body cells at 0h PF, when compared to the controls ($P < 0.05$; Figure 2.3A; 10.38 ± 0.73 and 9.39 ± 0.49 compartments per 1000 μm^2 respectively for Atg9$^{RNAi\ Line1}$ and Atg9$^{RNAi\ Line2}$). While there was a reduction in the number of Atg8a-GFP compartments following Atg9 depletion (Figure 2.3A), 61.43 ± 4.41% (Atg9$^{RNAi\ Line1}$) and 78.15 ± 3.89% (Atg9$^{RNAi\ Line2}$) of these autophagosome compartments were still positive for LysoTracker® (i.e. a similar percentage to controls; visualised in Figure 2.2B^{l}, 2.2B^{ll}, 2.2C^{l}, 2.2C^{ll}). However, the diameter of these Atg8a-GFP/LysoTracker® compartments was significantly reduced by Atg9 depletion (Figure 2.3B; average diameter of 2.77 ± 0.09 μm in Atg9$^{RNAi\ Line1}$and 2.57 ± 0.10 μm in Atg9$^{RNAi\ Line2}$; no significant difference between Atg9^{RNAi} lines). The size of Atg8a-GFP only compartments was also significantly reduced in Atg9$^{RNAi\ Line2}$ when compared to the controls (average diameter of 1.65 ± 0.04 μm, 1.87 ± 0.37 μm respectively; $P < 0.05$), but this was not significant for Atg9$^{RNAi\ Line1}$ (average diameter of 1.88 ± 0.08 μm; this was also significantly different to Atg9$^{RNAi\ Line2}$).

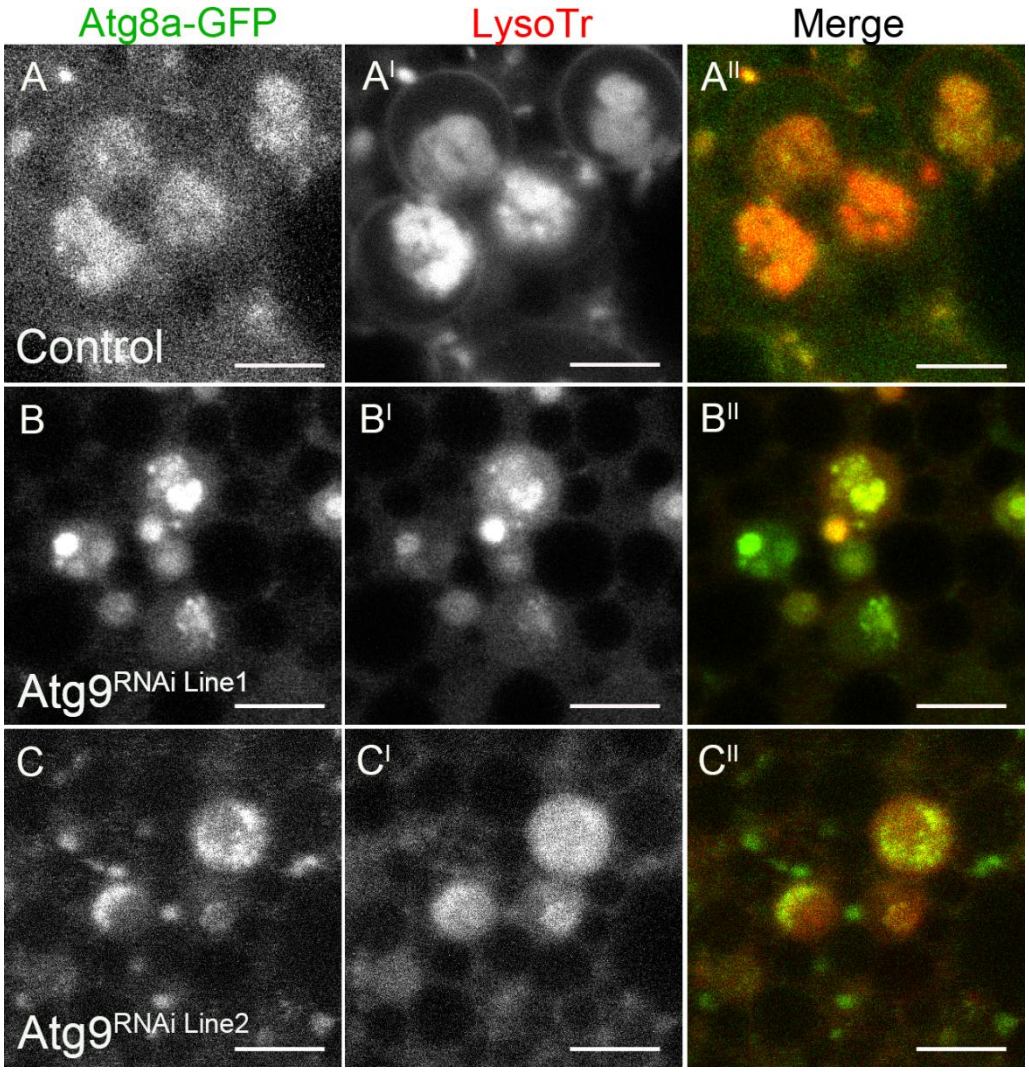


Figure 2.2 Depletion of Atg9 by RNAi silencing reduced the size of autophagic compartments, but did not impair acidification.

Confocal micrographs showing *Drosophila* fat body cells at 0h PF labelled with Atg8a-GFP (greyscale in A, B and C; green in A^{II}, B^{II} and C^{II}) and LysoTracker® (greyscale in A^{I}, B^{I} and C^{I}; red in A^{II}, B^{II} and C^{II}). Representative images from; heterozygous CG-GAL4, controls (A), CG-GAL4>UAS-Atg9$^{RNAi\ Line1}$ (B) and CG-GAL4>UAS-Atg9$^{RNAi\ Line2}$ (C). Scale bars = 5 μm.

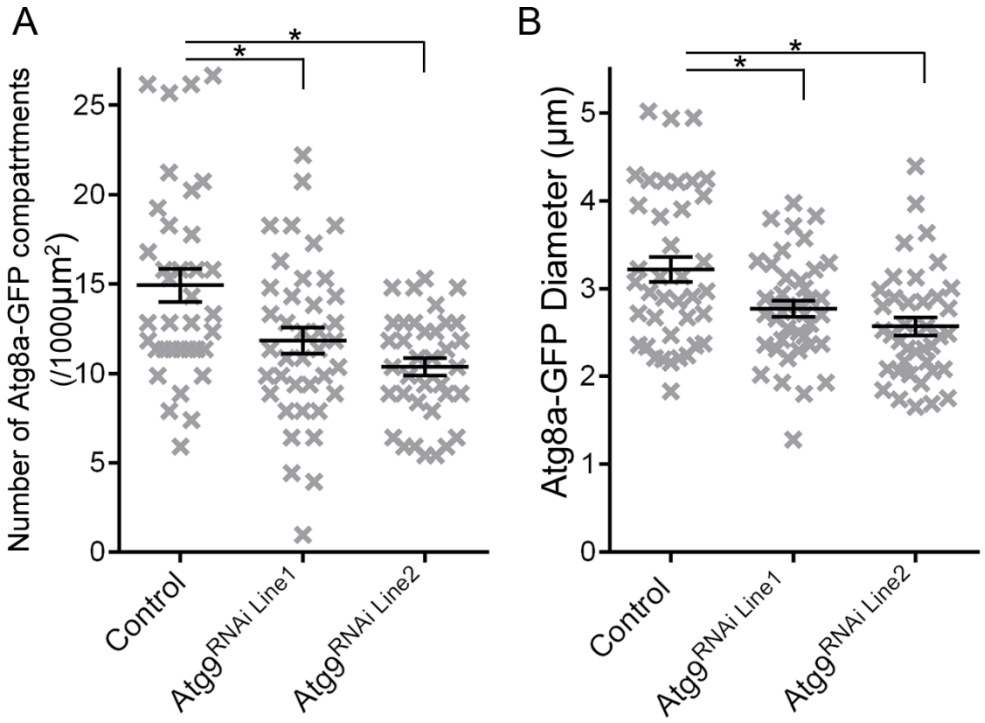


Figure 2.3 Quantification of the number and size of Atg8a-GFP autophagic compartments in control and Atg9 RNAi silenced fat body cells.

(A) Scatter plot showing the number of Atg8a-GFP compartments per 1000 µm^2. (B) Scatter plot showing the average size of Atg8aGFP/LysoTracker® positive compartments. (A and B) Data is represented as mean ± s.e.m. for each genotype; each cross represents quantification from one image (n=30). Asterisks indicate significant differences between genotype as calculated by ANOVA with Dunnett post hoc test ($p < 0.05$).

2.5.2 Atg9 is required for Rab11 intraluminal vesicles and compartmentalised acidification in amphisomes during developmental autophagy.

In control *Drosophila* fat body cells at 0h PF, Atg8a-mCherry co-located to 74.69 ± 7.76% of large Rab11-GFP compartments (> 5 μm^2; Figure 2.4A-2.4A^{ll}), which contained intraluminal Rab11-GFP vesicles (Figure 2.4A^{l}, 2.4A^{ll}). In Atg9 depleted *Drosophila* fat body cells at 0h PF, there was evidence of Atg8a-mCherry compartments (Figure 2.4B-2.4B^{ll}), though Rab11-GFP vesicles interacted with these compartments, there were no detectable intraluminal Rab11-GFP vesicles in these compartments (Figure 2.4B^{l}, 2.4B^{ll}). In control *Drosophila* fat body cells, the Rab11-GFP intraluminal vesicles were LysoTracker® positive (co-localised with Rab11; Figure 2.4C^{l}, 2.4C^{ll}), whereas in Atg9 depleted *Drosophila* fat body cells the entire lumen appeared to be acidified/ LysoTracker® positive (no Rab11 co-localisation; Figure 2.4D^{l}, 2.4D^{ll}). Interestingly, at an earlier developmental time point when there is normally minimal autophagy, starvation induced autophagy resulted in similar changes to Rab11 intraluminal compartment morphology and acidification in fat body cells from *Drosophila* with Atg9^{RNAi} silencing (Figure 2.5); indicating that the changes to Rab11 intraluminal vesicles and acidification were not just the result of a developmental phenomenon. Depletion of the endosomal ESCRT-III protein Vps20 by RNAi silencing also resulted in a loss of Rab11-GFP intraluminal vesicles, but the LysoTracker® then had a cytoplasmic distribution (Figure 2.4E-2.4E^{ll}).

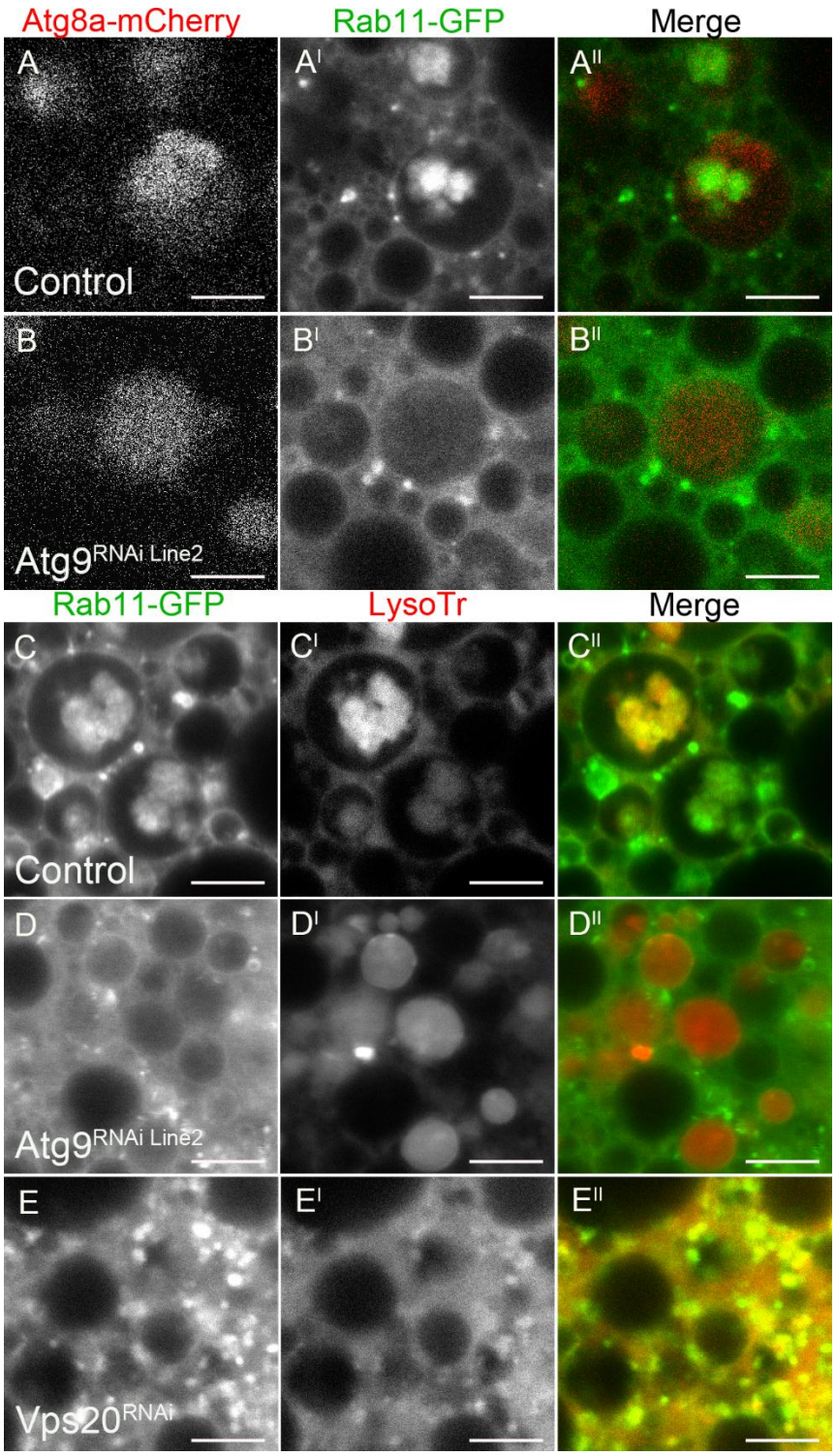


Figure 2.4 Intraluminal Rab11 compartments were absent from autophagic compartments in Atg9 depleted fat body cells.

(A-E^{II}) Confocal micrographs of *Drosophila* fat body cells at 0h PF labelled with Atg8a-mCherry (greyscale in A and B; red in A^{II} and B^{II}) and Rab11-GFP (greyscale in A^{I} and B^{I}; green in A^{II} and B^{II}); or Rab11-GFP (greyscale in C, D and E; green in C^{II}, D^{II} and E^{II}) and LysoTracker® (greyscale in C^{I}, D^{I} and E^{I}; red in C^{II}, D^{II} and E^{II}). Representative images from heterozygous CG-GAL4, controls (A and C), CG-GAL4>UAS-Atg9$^{RNAi\ Line2}$ (B and D) and CG-GAL4>UAS-Vps20^{RNAi} (E). Scale bars = 5 μm.

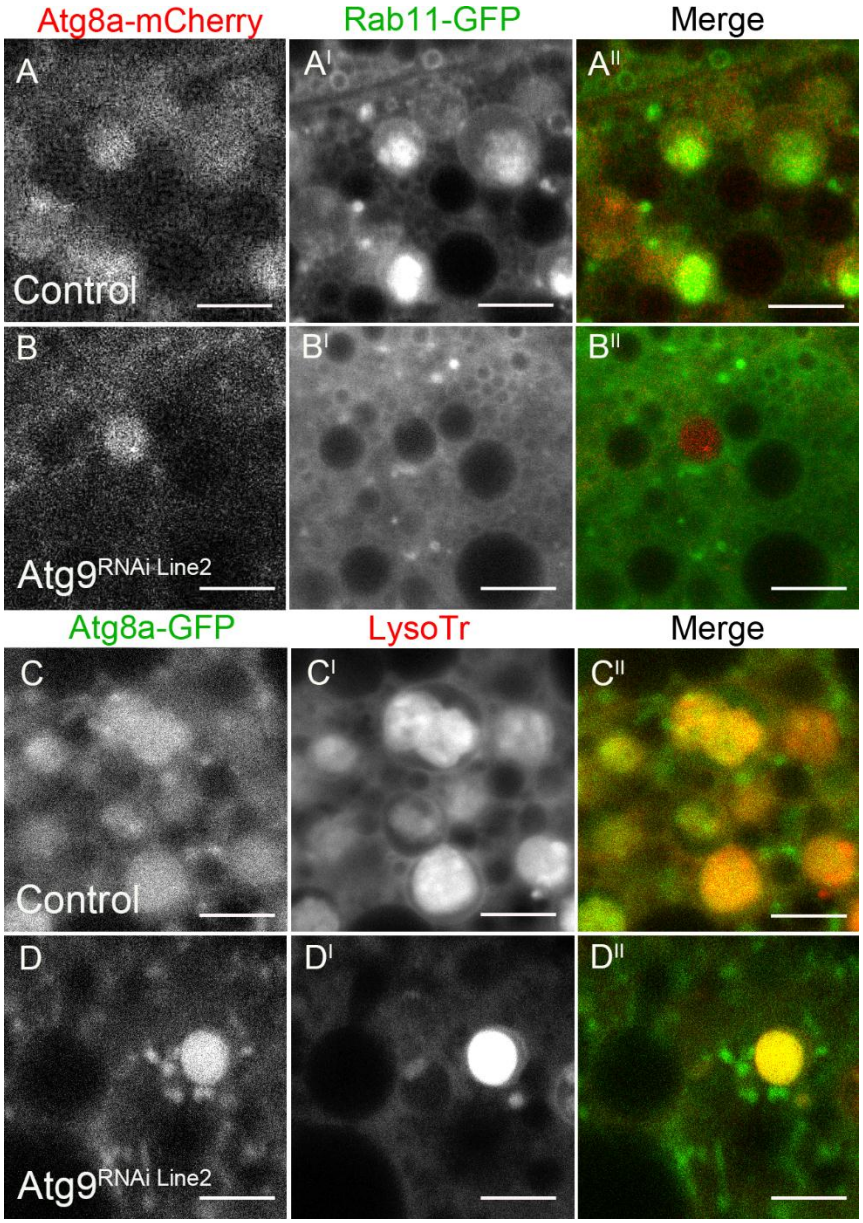


Figure 2.5 Atg9 depletion prevented the formation of Rab11 intraluminal vesicles and altered intraluminal acidification of Atg8 compartments in response to starvation.

(A-D^{II}) Confocal micrographs showing *Drosophila* fat body cells at -4h PF, following 4h of starvation, labelled with Atg8a-mCherry (greyscale in A and B; red in A^{II} and B^{II}) and Rab11-GFP (greyscale in A^{I} and B^{I}; green in A^{II} and B^{II}); or Atg8a-GFP (greyscale in C and D; green in C^{II} and D^{II}) and LysoTracker® (greyscale in C^{I} and D^{I}; red in C^{II} and D^{II}). Representative images from heterozygous CG-GAL4, controls (A and C) and CG-GAL4>UAS-Atg9$^{RNAi\ Line2}$ (B and D). Scale bars = 5 μm.

2.5.3 Atg9 depletion reduced the size of autolysosomes and altered the compartmentalisation of LysoTracker® and Lamp1 intraluminal vesicles in fat body cells during developmental autophagy.

In control *Drosophila* fat body cells at 0h PF, Atg8a-mCherry co-located with Lamp1-GFP compartments and many of these Lamp1-GFP/Atg8a-mCherry positive compartments contained intraluminal Lamp1-GFP vesicles (Figure 2.6A-2.6A^{ll}). Co-location of Atg8a-mCherry with Lamp1-GFP was also detected in Atg9 depleted *Drosophila* fat body cells, but there was a more uniform distribution of Lamp1-GFP in these compartments (Figure 2.6B^{l}, 2.6B^{ll}, 2.6D, 2.6D^{ll}). In addition, in the Atg9 depleted *Drosophila* fat body cells the Lamp1-GFP positive compartments were significantly smaller ($P < 0.05$; Figure 2.7A; 3.89 ± 0.11 µm in Atg9$^{RNAi\ Line1}$ and 2.85 ± 0.13 µm in Atg9$^{RNAi\ Line2}$) than the controls (4.73 ± 0.18 µm). In control *Drosophila* fat body cells LysoTracker® was compartmentalised into intraluminal vesicles within Lamp1-GFP compartments (Figure 2.6C^{l}, 2.6C^{ll}), while for the Atg9 depleted *Drosophila* fat body cells there was a more uniform distribution of LysoTracker® in the Lamp1-GFP compartments (Figure 2.6D^{l}, 2.6D^{ll}). Consequently, the area of the Lamp1-GFP compartments that was acidified in Atg9 depleted *Drosophila* fat body cells was greater than that in the control cells ($P < 0.05$; Figure 2.7B). In control *Drosophila* fat body cells the intraluminal vesicles within Lamp1-GFP compartments were also positive for intraluminal Rab11 (Figure 2.8).

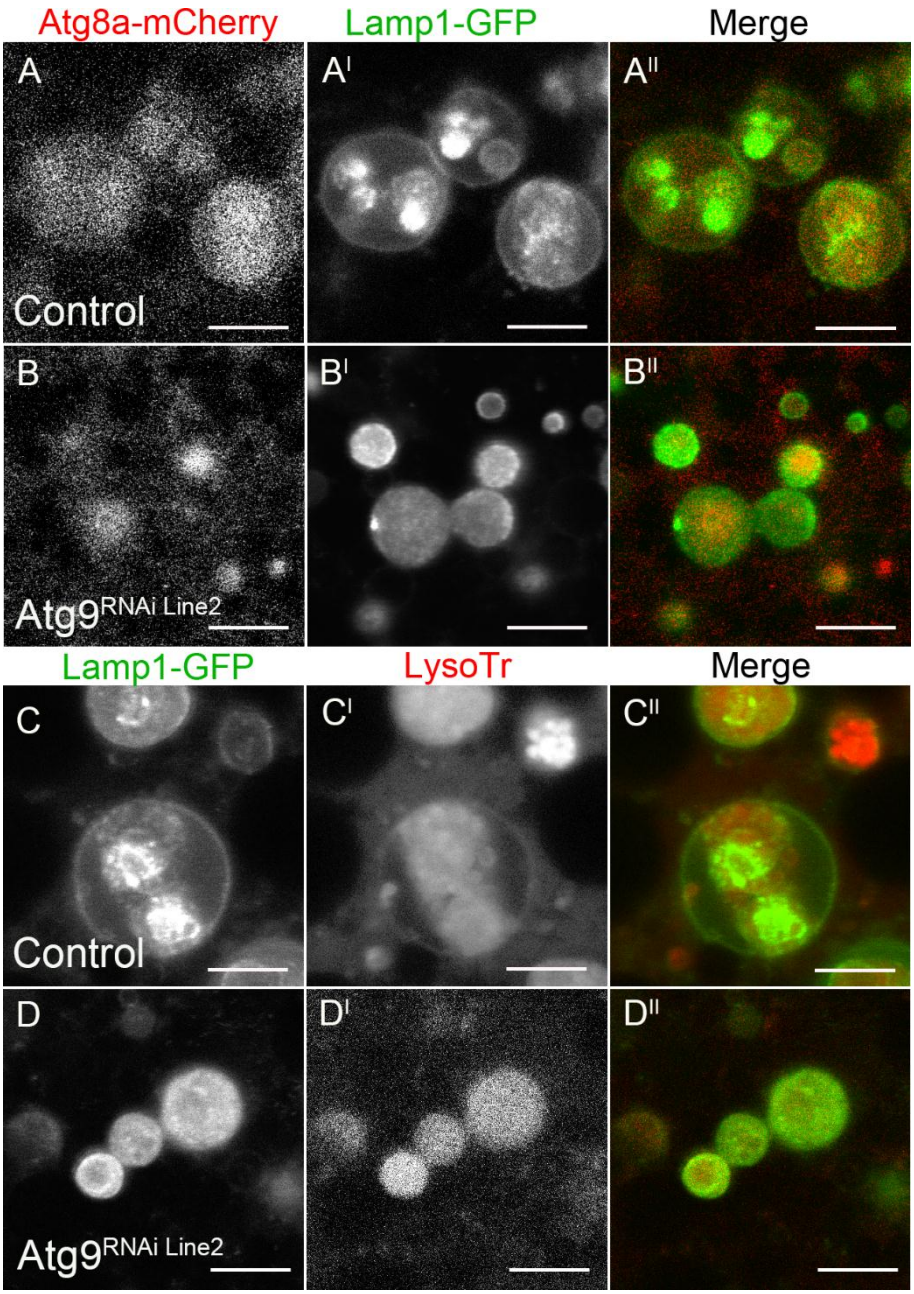


Figure 2.6 Lamp1 autophagic compartments had altered intraluminal acidification and a reduced size in response to Atg9^{RNAi}.

Confocal micrographs showing *Drosophila* fat body cells at 0h PF labelled with Atg8a-mCherry (greyscale in A and B; red in A^{II} and B^{II}) and Lamp1-GFP (greyscale in A^{I} and B^{I}; green in A^{II} and B^{II}); or Lamp1-GFP (greyscale in C and D; green in C^{II} and D^{II}) and LysoTracker® (greyscale in C^{I} and D^{I}; red in C^{II} and D^{II}). Representative images from heterozygous CG-GAL4, controls (A and C) and CG-GAL4>UAS-Atg9$^{RNAi\ Line2}$ (B and D). Scale bars = 5 μm.

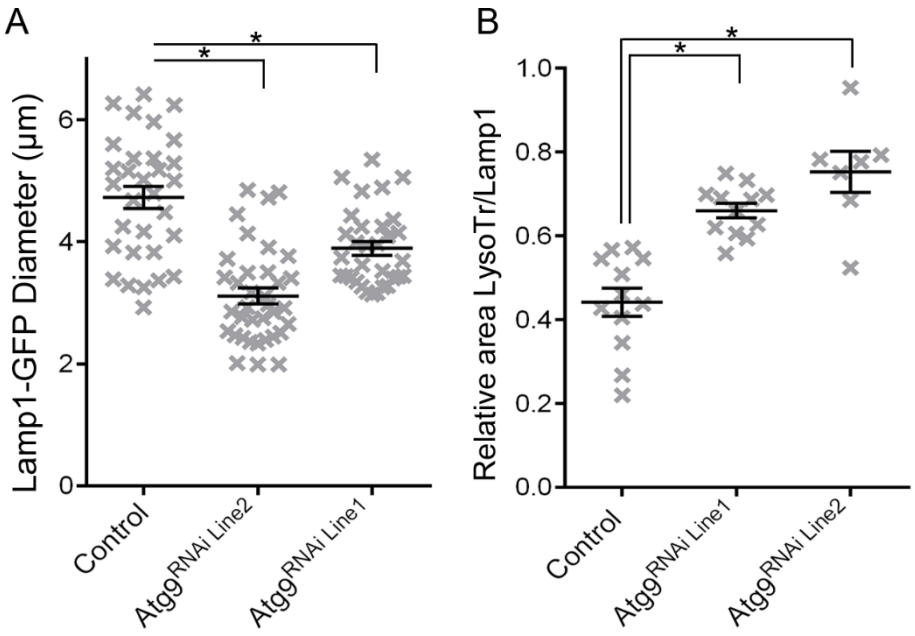


Figure 2.7 Quantification of changes in size and relative acidification of Lamp1 compartments in response to Atg9^{RNAi}.

(A) Scatter plot showing size of Lamp1-GFP positive compartments (n=30). (B) Scatter plot showing the size of LysoTracker® intraluminal compartments relative to Lamp1-GFP compartment (n=10). (A and B) Data is represented as mean ± s.e.m. for each genotype; each cross represents quantification from one image. Asterisks indicates significant differences between genotype as calculated by ANOVA with Dunnett post hoc test ($p < 0.05$).

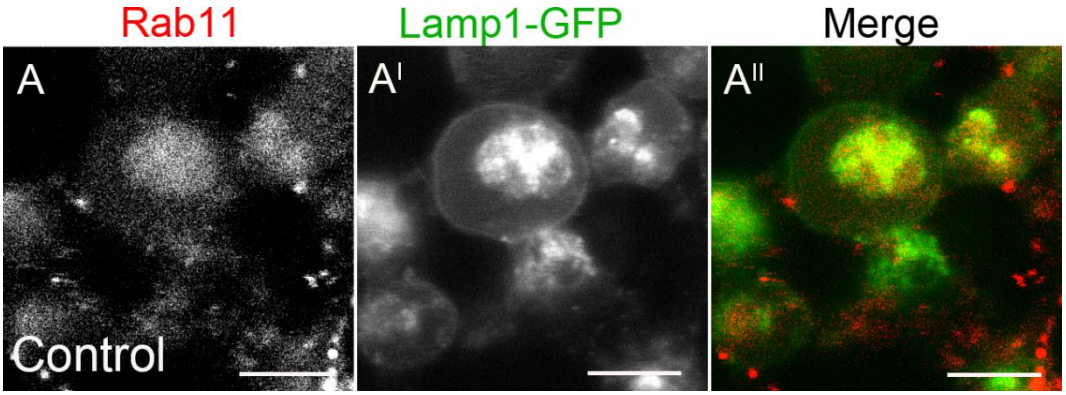


Figure 2.8 Compartments containing intraluminal vesicles were positive for Rab11 and Lamp1 at a time when developmental autophagy occurs.

(A) Confocal micrograph showing *Drosophila* fat body cells at 0h PF labelled with anti-Rab11 (greyscale in A; red in A^{II}) and Lamp1-GFP (greyscale in A^{I}; green in A^{II}). Scale bars = 5 µm.

2.5.4 Atg9 depletion abrogated Rab11 intraluminal vesicle formation and impaired midgut degradation in *Drosophila* during metamorphosis.

The *Drosophila* larval midgut is degraded by autophagy during metamorphosis (Denton et al., 2009; Lee et al., 2002). In Atg9 depleted *Drosophila* midgut cells at 0h PF, the Rab11-GFP and LysoTracker® compartments were small and the morphology was altered when compared to control midgut cells (Figure 2.9A-2.9B^{II}). This difference in compartment morphology was particularly evident for LysoTracker®, with control midgut cells having larger compartments that contained intraluminal vesicles (Figure 2.9A^{I}, 2.9A^{II}) and Atg9 depleted midgut cells having smaller compartments with little evidence of compartmentalisation (Figure 2.9B^{I}, 2.9B^{II}). TEM analysis of *Drosophila* midgut cells at 0h PF supported this altered compartment morphology, with control midgut cells having larger vesicles with multiple intraluminal vesicles (Figure 2.10A, 2.10B), whereas the compartments in Atg9 depleted midgut cells had either a uniform granular appearance or only limited evidence of intraluminal vesicles (Figure 2.10C, 2.10D). Consequently, there were significantly more multivesicular structures ($P < 0.03$) identified in control midgut cells (12.20 ± 1.90) than Atg9$^{RNAi\ Line2}$ midgut cells (6.91 ± 1.27). This appeared to affect autophagic degradation as at +4h PF the control *Drosophila* pupae had shorter midguts with an average perimeter of 2273 ± 57 µm and gastric caeca that were almost completely degraded (Figure 2.10E), whereas the midguts from Atg9$^{RNAi\ Line2}$ pupae were significantly longer than controls ($P < 0.05$) with an average perimeter of 6363 ± 368 µm and gastric caeca that remained intact (Figure 2.10F).

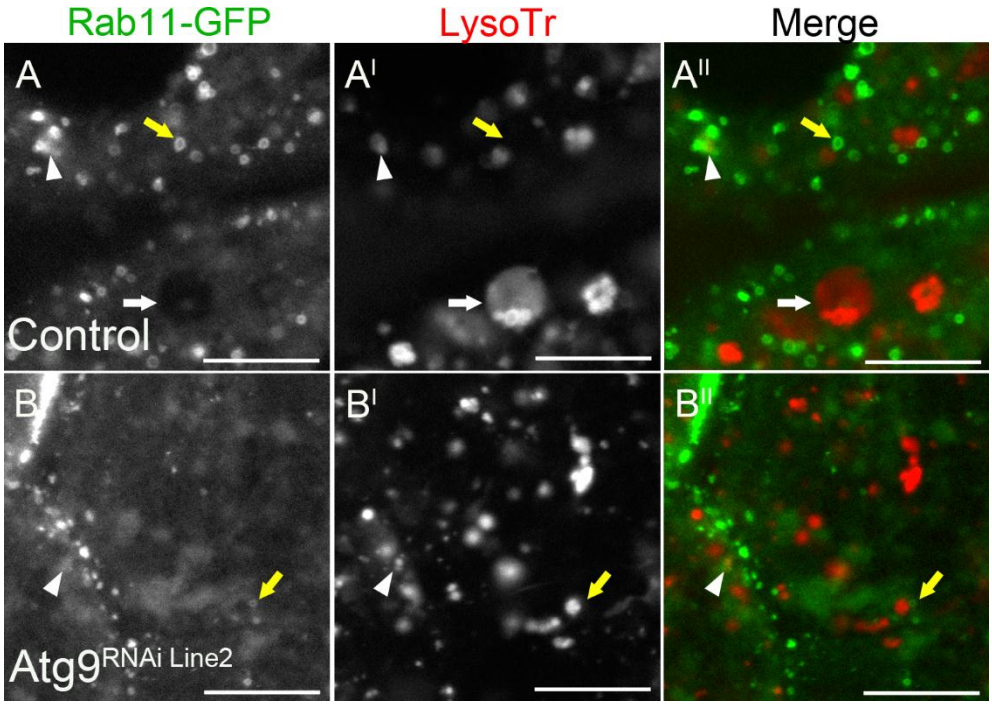


Figure 2.9 Atg9 depletion reduced the size of Rab11 and LysoTracker® compartments in the midgut.

Confocal micrograph of *Drosophila* midgut cells at 0h PF labelled with Rab11-GFP (greyscale in A and B; green in A^{II} and B^{II}), and LysoTracker® (greyscale in A^{I} and B^{I}; red in A^{II} and B^{II}). Representative images from heterozygous NP1-GAL4, control (A) and NP1-GAL4>UAS-Atg9$^{RNAi\ Line2}$ (B). Arrow heads indicate Rab11-GFP in close proximity to LysoTracker® (A and B), white arrows indicate enlarged LysoTracker® compartments (A), yellow arrows depicted Rab11-GFP as large rings (A and B). Scale bars = 10 µm.

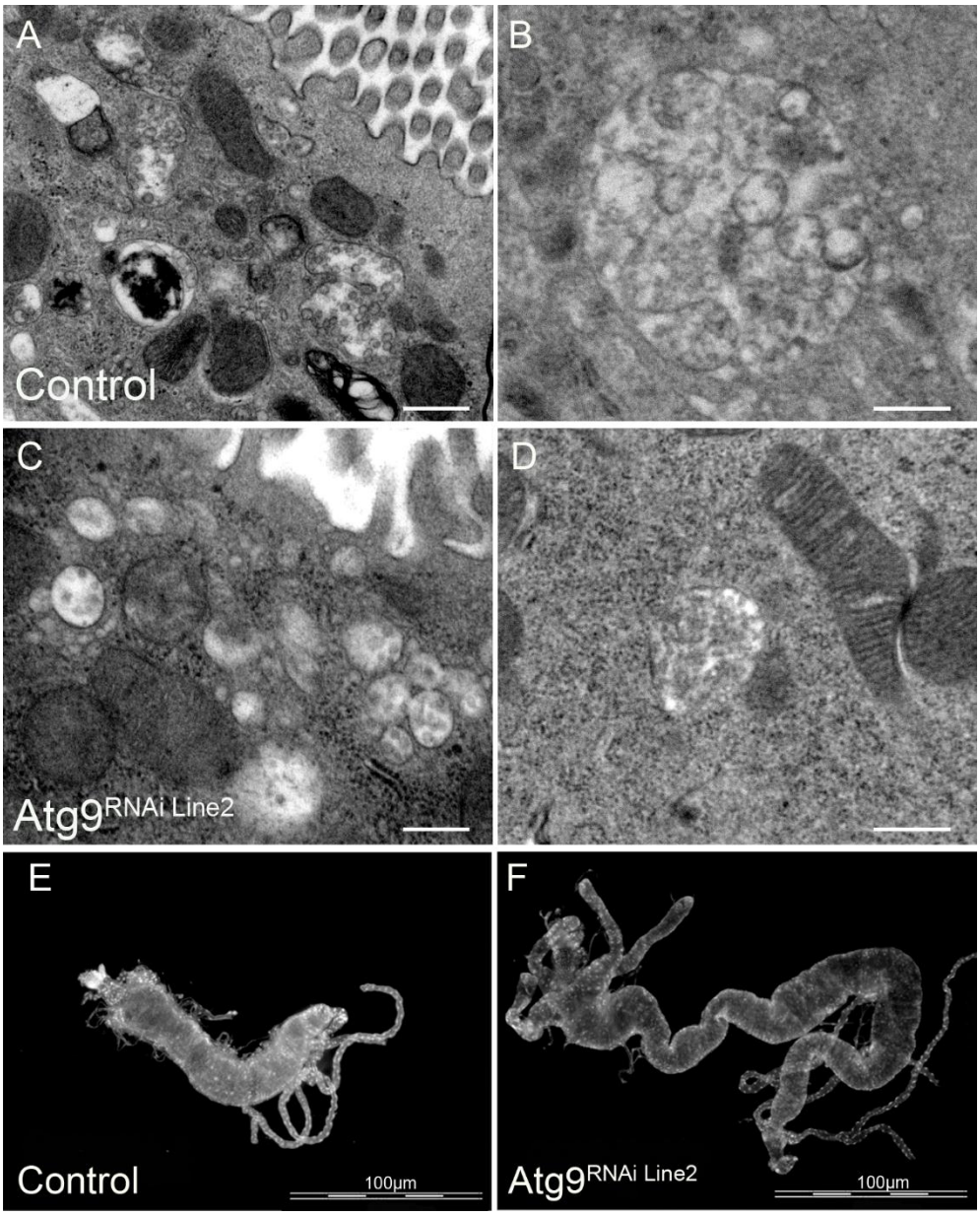


Figure 2.10 Atg9 depletion prevented intraluminal vesicles in the gastric caeca, resulting in reduced midgut degradation.

(A-D) TEM micrograph of *Drosophila* midgut cells at 0h PF, illustrating subcellular compartments containing intraluminal vesicles. Scale bars = 500 nm. (E-F) Fluorescence image of Hoechst stained midguts from +4h PF pupae. Scale bars = 100 µm. Representative images from heterozygous NP1-GAL4, control (A, B and E) and NP1-GAL4>UAS-Atg9$^{RNAi\ Line2}$ (C, D and F).

2.6 Discussion

Autophagy is a cellular degradation and recycling process that is important during energy metabolism, lipid metabolism, physiological stress, tissue remodelling and organism development (Singh and Cuervo, 2011). Changes in autophagy progression have been shown to be important in numerous human pathologies including neurological disorders, cancer and infectious diseases (Choi et al., 2013). Defining the mechanism and regulation of autophagy is essential to fully understand the pathophysiology of these diseases and this may lead to the design of new targeted therapies. Atg9 is the only transmembrane protein known to be involved in autophagy and it is thought to function in early autophagosome formation, however, it localises to multiple cellular locations (Orsi et al., 2012; Puri et al., 2013; Young et al., 2006) and is not thought to be integrated into autophagosome membranes (Orsi et al., 2012). In this study, we have demonstrated that Atg9 has a function relating to intraluminal vesicles and is required for compartmentalised acidification within amphisomes and autolysosomes.

In yeast, Atg9 is required for autophagy and its depletion prevents the formation of autophagosomes that are induced by rapamycin treatment or through nitrogen/amino acid starvation (Suzuki et al., 2001). In mammals, the depletion of Atg9 also reduces autophagic activity, limiting LC3-I to LC3-II lipidation, reducing the number of early autophagic structures or LC3 puncta formed, and decreasing the turnover of long lived proteins (Orsi et al., 2012; Saitoh et al., 2009; Yamada et al., 2005; Young et al., 2006). Similarly, in *Drosophila*, the depletion of Atg9 by RNAi silencing reduced the number of autophagic structures detected in fat body cells following starvation of third instar larvae and also reduced protein clearance (Low et al., 2013; Nagy et al., 2014b; Tang et al., 2013). The reduction in both the number and the size of autophagosomes during

development, which were observed upon RNAi silencing of *Atg9* in the fat body, would be compatible with previous reports for roles of Atg9 in membrane recruitment to the phagophore and for membrane expansion (Lamb et al., 2013b; Low et al., 2013; Nagy et al., 2014b; Orsi et al., 2012; Saitoh et al., 2009; Suzuki et al., 2001; Tang et al., 2013; Yamada et al., 2005; Young et al., 2006).

Autophagosomes interact with endosomes and lysosomes in a maturation process that sequentially generates amphisomes and then autolysosomes. This autophagosome maturation process is essential for the delivery of endolytic and exolytic acid hydrolases, as well as the generation of the acidic conditions, which enable the degradation of the luminal content of autophagosomes (Dunn, 1990; Fengsrud et al., 1995; Gordon and Seglen, 1988). In mammalian cells, Atg9 has been observed to be trafficked via the endosomal network and under normal nutrient conditions is often associated with recycling endosomes (Longatti et al., 2012; Orsi et al., 2012; Puri et al., 2013). The induction of autophagy by starvation decreases the association of Atg9 with recycling endosomes (Longatti et al., 2012; Orsi et al., 2012), but increases Atg9 localisation with late endosomes (Tang et al., 2011; Young et al., 2006). We also observed the localisation of Atg9 to compartments that were positive for the endosome and lysosome markers Rab11 and Lamp1, respectively. These observations have led to the hypothesis that Atg9 might have a role in autophagosome maturation (Takahashi et al., 2011). We observed, however, both amphisome and autolysosome formation following Atg9 depletion, indicating that the process of autophagosome maturation was not abrogated. This implied that the recruitment of endosomes and lysosomes, and the vesicular fusion machinery that mediates the fusion of these degradative organelles to form respectively amphisomes and autolysosomes, was not impaired by Atg9 depletion. Despite the capacity to form

amphisomes and autolysosomes, there appeared to be a disruption to developmental autophagy and the reduced turnover of midgut tissue, suggesting that the degradative properties of these compartments might still be impaired.

Impaired autophagic degradation generally results in either, the accumulation of autophagosomes, which can be caused by abrogated fusion with endosome and lysosome compartments (Eskelinen, 2006; Fader and Colombo, 2009; Fader et al., 2009; Lee et al., 2007); or the enlargement of autolysosomes (Settembre et al., 2008a; Settembre et al., 2008b). Atg9 depletion resulted in smaller amphisomes/autolysosomes and no obvious accumulation of autophagosomes. There were, however, significant morphological changes to amphisomes-autolysosomes, with a loss of intraluminal vesicles. In late endosomes, intraluminal vesicles are formed to allow the internalisation of ubiquitinated proteins, membrane rafts, other specific lipid domains and membrane receptors/cargo (Babst, 2011). Amphisomes result from the fusion of autophagosomes with these multivesicular endosomes (Fader et al., 2008; Fader et al., 2009; Tamai et al., 2007) and Rab11 multivesicular structures normally increase in size and co-localise with autophagosomal markers following the induction of autophagy (Fader et al., 2008). The ECSRT machinery that is required for intraluminal vesicle formation is also required for autophagosome maturation; as RNAi depletion or mutations in ECSRT machinery can cause the accumulation of autophagosomes (Filimonenko et al., 2007; Lee et al., 2007; Manil-Segalen et al., 2012; Rusten et al., 2007). Here, RNAi depletion of the ESCRT-III subunit Vps20, prevented the formation of Rab11 amphisomes and autolysosomes, instead generating compartments similar to class E-compartments (Doyotte et al., 2005). Paradoxically, while Atg9 RNAi affected intraluminal vesicle formation it did not impair

the formation of amphisomes and autolysosomes, suggesting that Atg9 might be required to initiate the formation of intraluminal vesicles.

Atg9 localises with a number of endosomal markers that are associated with late endosomes and multivesicular endosomes, including Rab11 and Rab7 (Denzer et al., 2000; Fader et al., 2008; Satoh et al., 2005; Savina et al., 2005; Vanlandingham and Ceresa, 2009); and clusters of Atg9 positive tubules/vesicles have been shown to emanate from these multivesicular endosomes (Orsi et al., 2012). This could suggest that Atg9 functions in intraluminal vesicle formation in endosomes, prior to amphisome formation. The intraluminal vesicles observed in amphisomes and autolysosomes, were however positive for Lamp1 and Atg8, proteins thought to associate with the membranes of lysosomes and autophagosomes, respectively. Though Lamp1 protein has been detected on both endosomes and lysosomes it is enriched in lysosomal compartments and consequently preferentially associated with autolysosomes rather than amphisomes (Schroder et al., 2010). In *Drosophila* wing discs, Lamp1 has also been detected on the intraluminal vesicles in multivesicular compartments (Rusten et al., 2006) and in larval fat body Lamp1 intraluminal vesicles have been observed within Lamp1/Atg8 positive compartments following starvation (Kim et al., 2012). These intraluminal vesicles could be formed by the fusion of autophagosomes with multivesicular endosomes (Bright et al., 2005; Chen and Yu, 2013; Yu et al., 2010), but from our data we could not exclude that amphisomes or autolysosomes directly form intraluminal vesicles.

The hydrolytic enzymes delivered by endosomes and lysosomes to autophagosomes require an acidic environment to function effectively (Mindell, 2012) and increased lysosome pH is known to decrease protein degradation in autolysosomes (Hosogi et al.,

2014; Mousavi et al., 2001; Zhang et al., 2013). The low pH environment of endosomes, lysosomes and maturate autophagosomes is controlled by vesicular H^+ATPase complexes, which act as a proton pump to facilitate acidification (Forgac, 2007). We observed compartmentalisation of LysoTracker® in control, but not Atg9 depleted cells which may explain the reduced degradative capacity and inability to degrade midgut tissue when Atg9 is depleted in this tissue. Inability to distribute the H^+ATPase complex to the lumen of degradative vesicles might be central to this impaired degradative capacity (Shen and Mizushima, 2014) and be required to generate a localised low pH environment.

Atg9 appears to have an important functional role in intraluminal vesicle formation and it is clear that this compartmentalisation is required to develop an appropriately localised acidic environment within degradative compartments. While Atg9 has a role in intraluminal vesicle formation in endosomes, it remains to be established whether these intraluminal vesicles can be formed directly in amphisomes and autolysosomes. Previous studies have implied that Atg9 has a role in autophagosome maturation, but from this study it was evident that this role might not involve vesicular fusion with endosomes and lysosomes as previously suggested. Rather, Atg9 may function in the formation of intraluminal vesicles that are required for correct amphisome and autolysosome function. This effectively adds to the potential role of Atg9 in intracellular trafficking (Popovic and Dikic, 2014; Saitoh et al., 2009), the induction of autophagy and PAS coordination (Orsi et al., 2012), as well as the purported roles in vesicular interaction and vesicle fusion. It remains to be established how Atg9 facilitates intraluminal vesicle formation and compartmentalised acidification.

Chapter 3: Modulation of the cellular organelle specificity in Re(I) tetrazolato complexes leads to unprecedented phosphorescent labeling of lipid droplets

3.1 Preface

The investigation of autophagy has relied heavily on the use of protein markers, which have specific functions and localisation. Atg9 for example, has been used to ascertain the trafficking and source of autophagic membrane, based on the assumption that Atg9 functions primarily in the recruitment of membrane to the forming autophagosomes. However, in the previous chapter evidence was provided that Atg9 also functions in autophagosome maturation, highlighting one of the drawbacks of protein centred approaches for the investigation of autophagic events. Fluorescent molecular probes may provide alternative tools for monitoring autophagic processes and to address this need, we assessed a panel of six Rhenium(I) based metal ion complexes (developed by collaborators at Curtin University, Western Australia). Two complexes were identified as having potential for cellular imaging, with rapid up-take and distinct sub-cellular localisation. This chapter, has been adjusted from the publication 'Modulation of the cellular organelle specificity in Re(I) tetrazolato complexes leads to unprecedented phosphorescent labelling of lipid droplets' (published in ***RSC Adv.***, 2014), which reports the initial characterisation of these two Rhenium based complexes. One of the complexes showed a localisation to lipid droplets, while the other complex localised to acidic compartments. Lipophilic dyes are less common than acidotrophic dyes and lipid droplets have recently been shown to interact with autophagosomes, therefore the lipophilic complex was ultimately selected for additional investigation in the next chapter (Chapter 4), in the context of autophagy and the focus of this thesis.

3.2 Publication details

RSC Adv., 2014, **4**, 16345-16351

DOI: 10.1039/C4RA00050A

Received 03 Jan 2014, Accepted 20 Mar 2014

First published online 20 Mar 2014

Modulation of the cellular organelle specificity in Re(I) tetrazolato complexes leads to unprecedented phosphorescent labelling of lipid droplets

Christie A. Bader,[a] Robert D. Brooks,[a] Yeap S. Ng,[a] Alexandra Sorvina,[a] Melissa V. Werrett,[b] Phillip J. Wright,[b] Ayad G. Anwer,[c] Douglas A. Brooks,[a] Stefano Stagni,[d] Sara Muzzioli,[d] Morry Silberstein,[b] Brian W. Skelton,[e] Ewa M. Goldys,[c] Sally E. Plush,[a] Tetyana Shandala,*[,a] Massimiliano Massi*[,b]

[a] School of Pharmacy and Medical Science, University of South Australia, Adelaide 5001 SA, Australia

[b] Department of Chemistry, Curtin University, Bentley 6102 WA, Australia

[c] Department of Physics and Astronomy, Macquarie University, North Ryde 2109 NSW, Australia

[d] Department of Industrial Chemistry, University of Bologna, Bologna 40126, Italy

[e] Centre for Microscopy, Characterisation and Analysis, University of Western Australia, Crawley 6009 WA, Australia

Corresponding author Email: Tetyana.Shandala@unisa.edu.au; M.Massi@curtin.edu.au.

3.3 Author contribution

Name of principle author Christie A. Bader

Contribution to the manuscript Performed cell imaging and co-localisation studies; analysed and interpreted data; collated figures for cell biology studies; wrote biological sections of the manuscript.

Name of co-author Robert D. Brooks

Contribution to the manuscript Performed spectral analysis of compounds ex vivo; edited manuscript

Names of co-authors Yeap S. Ng and Alexandra Sorvina

Contribution to the manuscript Assisted in cell biology studies; edited manuscript

Names of co-authors Melissa V. Werrett, Phillip J. Wright, Ayad G. Anwer, Ewa M. Goldys, Stefano Stagni, Sara Muzzioli, Morry Silberstein

Contribution to the manuscript Synthesis of complexes; photophysical characterisation of complexes; interpretation and collation of photophysical data

Name of co-author Brian W. Skelton

Contribution to the manuscript Time gated imaging

Names of co-authors Douglas A. Brooks, Sally E. Plush, Tetyana Shandala, Massimiliano Massi

Contribution to the manuscript Experimental design; data interpretation; manuscript preparation and editing.

3.4 Abstract

The biological behaviour in terms of cellular incubation and organelle specificity for two complexes of the type *fac*-[Re(CO)$_3$(**phen**)**L**], where **phen** is 1,10-phenanthroline and **L** is either 3-pyridyltetrazolate or 4-cyanophenyltetrazolate, are herein investigated. The emission signal detected from live insect *Drosophila* and human cell lines, generated by exploiting two-photon excitation at 830 nm to reduce cellular damage and autofluorescence, suggests photophysical properties that are analogous to those measured from dilute solutions, meaning that the complexes remain intact within the cellular environment. Moreover, the Rhenium complex linked to 4-cyanophenyltetrazolate shows high specificity for the lipid droplets, whereas the complex bound to 3-pyridyltetrazolate tends to localise within the lysosomes. This differential localisation implies that in these complexes, organelle specificity can be achieved and manipulated by simple functional group transformations thus avoiding more complex bioconjugation strategies. More importantly, these results highlight the first example of phosphorescent labelling of the lipid droplets, whose important cellular functions have been recently highlighted along with the fact that their role in the metabolism of healthy and diseased cells has not been fully elucidated.

3.5 Introduction

The development of organelle-specific dyes for biomedical research has become an area of increasing interest. Metal complexes emitting from triplet metal-to-ligand charge transfer states (^{3}MLCT) have recently emerged as a promising alternative to conventional fluorescent probes (Fernandez-Moreira et al., 2010; Lo et al., 2012; Parker, 2011; Zhao et al., 2011). The goal is to overcome the apparent shortcomings of organic-based fluorophores such as self-quenching, photobleaching and signal discrimination versus endogenous autofluorescence (e.g. emission from species such as flavins). Families of luminescent Re(I) (Amoroso et al., 2008; Balasingham et al., 2012a; Viola-Villegas et al., 2008), Ru(II) (Lo et al., 2008; Maggioni et al., 2012), Ir(III) (Lo et al., 2005; Lo et al., 2013; Murphy et al., 2010), Pt(II) (Chung et al., 2013), Au(I) (Balasingham et al., 2012b), Au(III) (Zou et al., 2013) and trivalent lanthanoid (Smith et al., 2012; Thielemann et al., 2013; Walton et al., 2013) complexes have potentially shown significant advantages as cellular labels. A challenge in the field, however, is to define a structure-activity relationship that will allow a direct link between the chemical nature of a complex and its biological activity in terms of cellular permeability and organelle targeting (Balasingham et al., 2011; New et al., 2010). An understanding of this relationship is of critical importance for the rational design of a chemical structure that encompasses and optimises chemical properties (e.g. solubility and lipophilicity), photophysical characteristics (absorption/emission energy and photoluminescent quantum yield) and biological behaviour (targeting to specific cellular compartments, cell types or discrimination between healthy and diseased cells). While some aspects of this rationalisation have been pursued by covalently linking non-specific phosphorescent metal complexes to biological vectors such as sugars or oligopeptides (Fernández-Moreira et al., 2012; Ferri et al., 2010; Louie et al., 2011; Maggioni et al., 2012; Mari et al., 2012; Viola-Villegas et al., 2008;

Yin Zhang et al., 2013), comparably less information is available for non-bioconjugated metal complexes (Puckett et al., 2010).

Preliminary guidelines to govern the cellular uptake and specificity of tricarbonyl diimine Re(I) complexes through modification of their chemical nature have started to emerge (Balasingham et al., 2011). The majority of the studies, however, have been carried out on cationic complexes. Meanwhile, the behaviour of analogous neutral non-bioconjugated complexes has received scarce attention. Hence, the structure-activity relationship for neutral complexes of the type *fac*-[$Re(CO)_3$(**diim**)**L**], where **diim** is a bidentate ligand and **L** represents an anionic donor species, requires further investigation. Aiming to extend the structure-activity studies to neutral Re(I) complexes, we have recently investigated cellular uptake and organelle targeting of neutral Re(I) tetrazolato complexes, the structures of which are shown in Figure 3.1.

The complexes **1** and **2** are reported, with the difference being that in complex **2** the pyridine ring is capable of undergoing protonation equilibrium at physiological pH. Our results show that the two complexes have well differentiated organelle targeting. Remarkably, complex **1** was found to exhibit high specificity for the lipid droplets of live human and *Drosophila* adipose cells. These spherical organelles store neutral triglycerides and while in the past they were simplistically considered to function as lipid storage, it is now established that they have fundamental roles in the regulation of cellular metabolism (Brasaemle and Hansen, 2006; Cermelli et al., 2006) and in the development of a number of key human diseases, including diabetes, neutral lipid storage disease (NLSD) as well as associated cardiomyopathies (Digel et al., 2010; Farese and Walther, 2009; Greenberg et al., 2011; Greenberg and Obin, 2008; Krahmer et al., 2013b; Thiele and Spandl, 2008).

However, a comprehensive understanding of the cellular function of the lipid droplets is yet to be uncovered. The need to improve our understanding of the function of this organelle makes an efficient stain for lipid droplets a highly desirable tool. In this respect and to the best of our knowledge, our result represents the first example of a metal-based phosphorescent probe specifically recognising this vital organelle in live mammalian and insect cells. This is significant because staining of adipose cells is currently achieved with the exclusive use of fluorescent labels, consequently suffering from the previously listed drawbacks (Kuerschner et al., 2008).

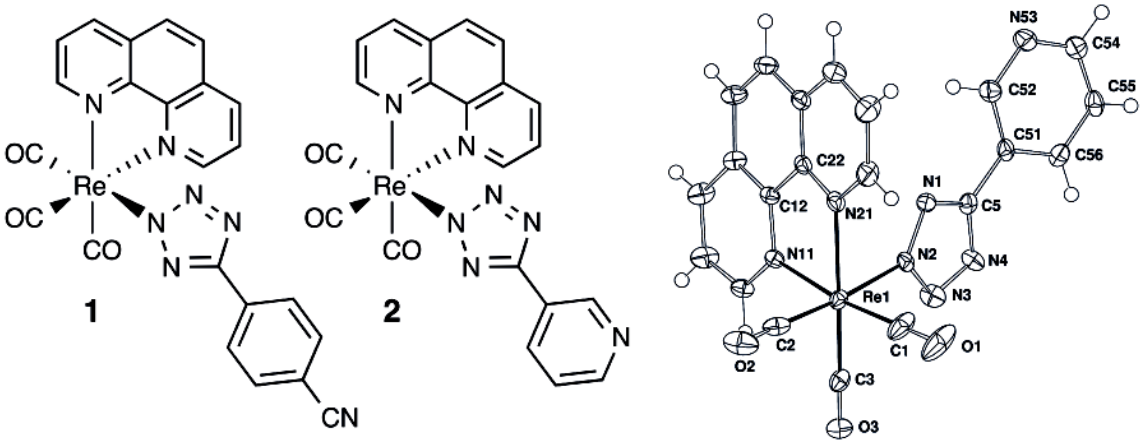


Figure 3.1 Formulation of Re(I) tetrazolato complexes 1 and 2 used as phosphorescent labels and X-ray crystal structure of 2, with thermal ellipsoids at the 50% probability level.

3.6 Materials and methods

3.6.1 Fly stocks and cultured cells

Drosophila wild-type stock w^{1118} was obtained from the Bloomington *Drosophila* Stock Center (Indiana University, Indiana, USA). Stocks were maintained on standard medium at 25˚C. Differentiated murine adipose 3T3-L1 cells were kindly provided by Dr Y. Khew-Goodall (SA Pathology, Adelaide, Australia). 3T3-L1 pre-adipocyte cells were propagated and differentiated as previously described in Zhang et al. (2011).

3.6.2 Tissue and cell staining

Fat body tissue from *Drosophila* 3rd larval instars was dissected in PBS, and immediately mounted on poly-L-lysine (Sigma-Aldrich, St Louis, USA). Prior to staining 3T3-L1 cells were cultured for 24-48 hours to facilitate adherence on fibronectin-coated coverslips. Live tissues and cells were stained with Rhenium complexes, by incubating with a 10 μM solution of each complex in PBS for 10 minutes at room temperature, followed by 2-5 minutes of washing in PBS. Staining with LysoTracker®Green, MitoTracker®Red, (Invitrogen, Waltham, USA), Filipin (Sigma-Aldrich, St. Louis, USA) and Oil Red (Sigma-Aldrich, St. Louis, USA), was performed according to manufacturers instructions. To visualise and prevent dehydration, the samples were mounted to slides with a carbomer-940 (Snowdrift farm, Tucson, USA) based optical coupling gel.[8]

3.6.3 Cytotoxicity assay

To assess cytotoxicity of the complexes, cellular NAD(P)H-dependent redox activity was measured using CellTiter 96® AQueous Non-Radioactive Cell Proliferation Assay (MTS) according to the manufacturer instruction (Promega, Fitchburg, USA). Briefly, fat body tissues were dissected from wild-type larvae in PBS. Tissue was then incubated with 20

μM of complex **1** or **2** for fifteen minutes**,** then immediately transferred to 120 μL of MTS and PMS in DMEM medium in 96 well plate. The tissues were allowed to incubate at room temperature for 3 hours. The absorbance was then measured at 490 nm by VICTOR X™ Multilabel Plate Readers (PerkinElmer, Wltham, USA).

3.6.4 Cell imaging using two-photon and confocal microscopy

A Ziess LSM710 META NLO inverted microscope (Zeiss, Oberkochen, Germany) was supplemented with a two-photon Mai-Tai® (tunable Ti:Sapphire femtosecond pulse laser; Spectra-Physics, Santa Clara, USA). The images were acquired using a Plan-APOCHROMAT 63X/ NA1.4 oil immersion objective. Spectral fingerprinting for fat body tissue was acquired in lambda stack mode (770-860 nm continuum of excitation range, main beam splitter (MBS) 690+, spectral emission range 416-727 nm, with 38.9 nm intervals), and saved as a Rhenium complex reference spectrum. Imaging parameters for assessing the intracellular localisation are shown in Table 3.1.

3.6.5 Image analysis

The emission intensity of spectral lambda stacks was assessed in ImageJ (National Institute of Health, USA) using mean grey levels in five region of interest with area of 16px. Graphs were prepared using Microsoft Excel (2010). The composite figures were prepared using ImageJ (National Institute of Health, USA) and Adobe Photoshop CS4 software (Adobe Systems Inc, USA).

Table 3.1 . Imaging parameters for assessing the intracellular localisation of the Rhenium complexes.

PARAMETERS	**ENDOSOME/LYSOSOME**		**MITOCHONDRIA**		**LIPID DROPLET**			**CHOLESTEROL**	
PROBES	Re	LysoTracker® Green	Re	MitoTracker® Red	Re	Oil Red	Phase contrast	Re	Filipin
EXCITATION λ (nm)	2P 830	488	2P 830	543	2P 830	543	543	2P 830	2P 830
DETECTION λ (nm)	600-654	497-558	480-550	556-658	600-654	582-754	T-PMP	416-272	416-727
MBS	690+	488/543/633	690+	488/543/633	690+	488/543		690+	690+
CAPTURE MODE	sequential		sequential		independent			spectral unmixing	
REPRESENTATIVE IMAGE	Figure 4		ESI Figure S10		Figure 4			ESI Figure S10	

***2P=Two-Photon**

3.7 Results and Discussion

Complexes **1** and **2** were prepared according to a previously published procedure (Wright et al., 2012), via direct exchange of the chloro ligand in *fac*-[Re(CO)$_3$(**phen**)Cl], where **phen** = 1,10-phenanthroline, with the corresponding tetrazolato species. The complexes were satisfactorily characterised via IR and NMR spectroscopy as well as elemental analysis. Complex **2** crystallizes in the monoclinic $P2_1/c$ space group and shows the typical *facial* arrangement of the three CO ligands. The tetrazolato ligand coordinates via its N2 atom. In the crystal packing, neighbouring tetrazolato ligands engage in π-stacking interaction with a plane-to-plane distance of *ca.* 3.4 Å, whereas the lone pair of the pyridine ring locks in a vertex-to-face arrangement with the **phen** ligand (N **phen** ≈ 3.0 Å). The X-ray structure of **1** has been reported elsewhere (Wright et al., 2012).

The photophysical properties of **1** and **2** were measured in air-equilibrated aqueous solutions (*ca.* 10^{-5} M), containing 1% DMSO to facilitate solubilisation. The combined data are reported in Table 3.2 and Figure 3.2, respectively. Both complexes show absorption profiles with intense ligand centred π-π* transitions around 266 nm and charge transfer bands in the 370-380 nm region. The charge transfer transition was ascribed to a metal-to-ligand charge transfer (MLCT; Re → **phen**), mixed with ligand-to-ligand charge transfer character (LLCT; tetrazole → **phen**) (Werrett et al., 2011). Upon excitation to the lowest singlet ^{1}MLCT manifold, a typical broad and structureless emission band, characteristic of the CT nature of the excited state, was observed between 570 and 585 nm for each complex. The excited state is characterised by a relatively long lifetime (τ), suggesting phosphorescent decay from the triplet ^{3}MLCT state. Indeed, this prolonged excited state lifetime with respect to faster fluorescence makes these complexes also amenable for time-gated detection techniques to eliminate background endogenous

autofluorescence (Botchway et al., 2008; Murphy et al., 2010). Notably, the lifetime decay of **1** appears to be bi-exponential, with a major component at 2.373 μs and a minor component (14%) at 575 ns. These values are both longer than the lifetime of complex **2**, which is 277 ns and mono-exponential. The same trend is observed for the values of quantum yields (Φ), 10.3% and 1.8% for complexes **1** and **2**, respectively. This difference was interpreted as potential aggregation of complex **1** in the aqueous medium, possibly resulting in less efficient quenching of the ^{3}MLCT excited states by molecules of water and oxygen.

Table 3.2 Photophysical data for complexes 1 and 2.

	Absorption	**Emission (10^{-5} M; H_2O/DMSO 99:1; RT)**		
Complex	λ_{max}[nm] ($10^4\varepsilon$ [$Lmol^{-1}cm^{-1}$])	λ [nm]	τ [ns][a]	Φ
1	266 (8.60) 378 (0.54)	569	575 (14%) 2,373 (86%)	0.103
2	266 (8.37) 370 (0.34)	582	277	0.018

[a] From air-equilibrated solutions at room temperature.

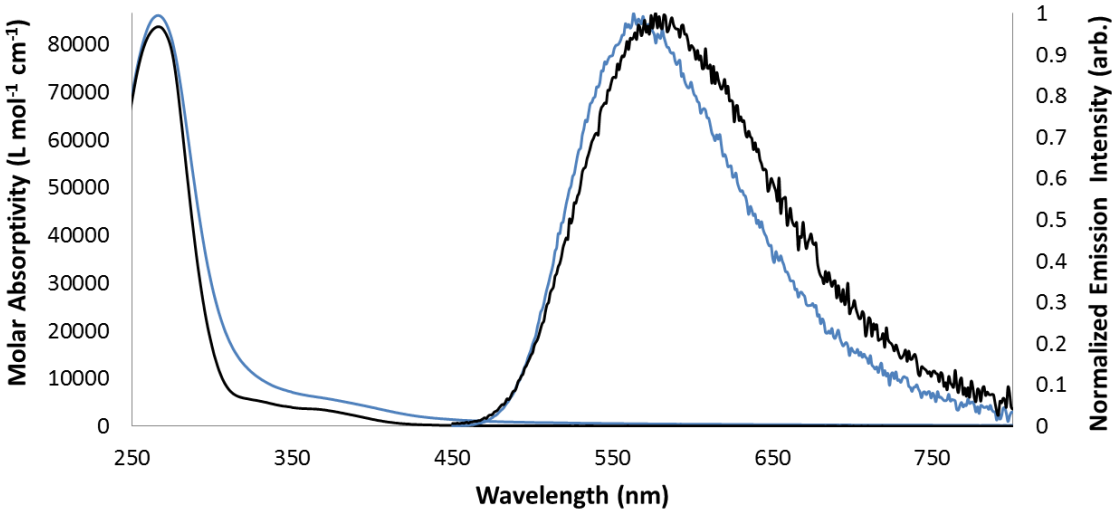


Figure 3.2 Absorption and emission profiles of complexes 1 (blue line) and 2 (black line) from a diluted (*ca.* 10^{-5} M) air-equilibrated H_2O/DMSO 99:1 solution at room temperature.

To investigate the cellular penetration of the complexes **1** and **2**, we employed *Drosophila* larval adipose tissues, which offer distinct advantage for cell biological analysis as it consists of proportionally enlarged cytoplasmic and nuclear areas. The distribution of the complexes was also analysed in human adipose 3T3-L1 cells, with the aim to define the cross-species similarity in their intracellular penetration and distribution. The cells were incubated with 10 μM of each complex for 10 minutes at respective permissive temperatures, 25 °C for insect tissue and 37 °C for human cells. The intracellular localisation of the complexes was then detected with the use of two-photon excitation, which offers significant advantages for biomedical imaging, given that infrared excitation has a better tissue penetration, reduced out-of-focus photo-bleaching and minimised cellular damage (Botchway et al., 2008; Ferri et al., 2010; Ho et al., 2012; Lo et al., 2011; Masanta et al., 2011).

As a first step, we optimised excitation wavelength and emission intervals to specifically detect the signal of the Re complexes above the background level. Live unstained tissues (control for endogenous fluorescence) and tissue stained with either complex **1** or **2** were excited by two-photon illumination within 770–860 nm range (Figure 3.3). A continuum of images was captured across the emission spectrum between 416–727 nm, with emission increments of 38.9 nm (Figure 3.3A). The emission intensity of the Re complexes and endogenous signal was quantified using ImageJ software (Figure 3.3B-C). This analysis showed that tissues stained with Re complexes had an emission profile distinctive from endogenous fluorescence of unstained control tissue. The strongest emission was obtained upon excitation in the 790-830 nm range, with the brightest emission from the complexes detected within the 533-610 nm wavelength interval. Given that there was a favourable Re to endogenous fluorescence signal ratio detected upon excitation with 830 nm (Figure

3.3B), this excitation wavelength was used for further analysis. The 533-610 nm emission wavelength range of the complexes within the tissue corresponds to the emission maxima previously detected for these complexes in solution (Figure 3.2), suggesting that there is no chemical modification of the complexes in physiologically environment. The stability is also confirmed by noting that the H-NMR spectra of the two complexes are identical over a period of 24 hours in DMSO solution. This is important as anionic ancillary ligands are known to be susceptible to ligand exchange reactions, and this exchange seems to be responsible for the cytotoxicity of probes such as *fac*-[$Re(CO)_3$(diim)Cl] (Amoroso et al., 2007). However, there were no morphological signs of cytotoxicity detected upon 30 min of treatment with complexes **1** or **2**. Furthermore, no evident signs of cytotoxicity could be detected via MTS assay (Figure 3.4). Importantly, the signal from **1** or **2** was detected within the cells in the first 10 minutes after incubation, indicating that intracellular entry occurs readily and via a mechanism distinct from endocytosis, possibly passive diffusion. A rapid uptake is an extremely desirable attribute for a cellular probe in order to avoid any effect on normal cell physiology and metabolism (Parker, 2011).

The micrographs of the *Drosophila* adipose fat body cells indicate that the complexes **1** and **2** accumulate within specific, yet markedly different, intracellular compartments. To define the organelle specificity, the Re-stained *Drosophila* adipose fat body cells, as well as differentiated human adipose 3T3-L1 cells were counterstained with four commercially available optical probes, which were specific for: i) acidic endosomes and lysosomes, detected by LysoTracker®Green (Figure 3.5); ii) mitochondria, recognised by Mitotracker®Red (Figure 3.6); iii) organelles containing neutral lipids, detected by Oil Red (Figure 3.7); and iv) free cholesterol, detected by Filipin (Figure 3.8). To discriminate between the signals emitted by the Re complexes and the reference probes, the co-

localisation analysis was carried out using different spectral intervals, for LysoTracker®Green and Mitotracker®Red, or spectral unmixing for Filipin (described in Table 3.1). Due to a significant spectral overlap, Oil Red staining was carried out independently from the complexes **1** and **2,** and the conclusion was based on the distinct morphology of the lipid droplets (Figure 3.7).

Complex **1** showed no significant signal in organelles containing LysoTracker®Green (Figure 3.5A, 3.5B) or MitoTracker®Red (Figure 3.6A, 3.6B) in both cell types. By contrast, **2** showed co-localisation with Lysotracker®Green (Figure 3.5C, 3.5D) but not with mitochondria stained by MitoTrackerRed® (Figure 3.6C, 3.6D). Interestingly, **1** appeared to have stained organelles whose morphology is consistent with lipid droplets (Figure 3.7C, 3.7D). The signal intensity from **1** appears *ca.* 5 times higher than the intensity of endogenous fluorescence detected from lipid droplets. The identity of the organelle was confirmed by staining of fixed tissues with Oil Red (Figure 3.7A, 3.7B). Both complex **1** and **2** showed some co-localisation with free cholesterol stain filipin (Figure 3.8E, 3.8F)

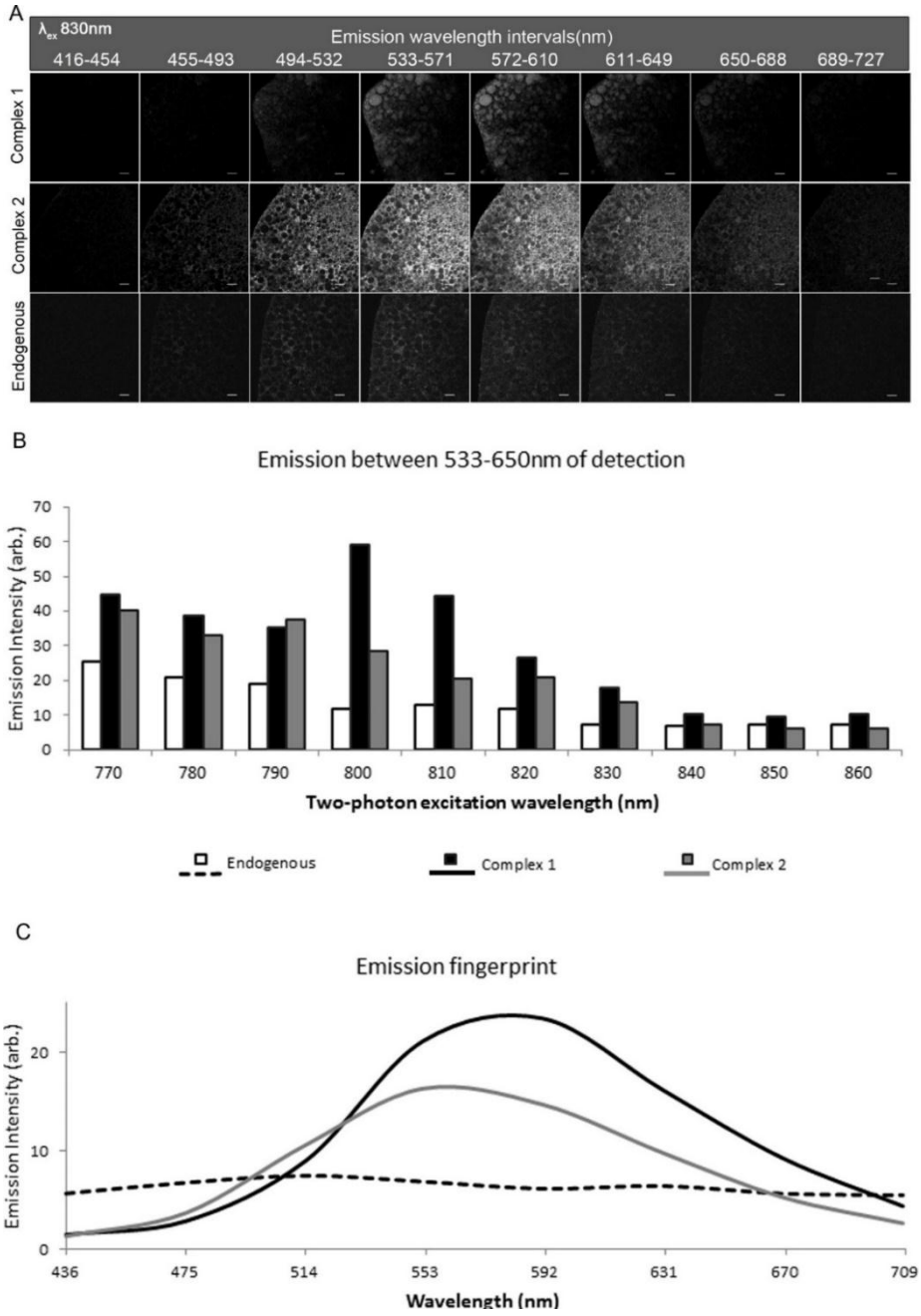


Figure 3.3 Ex vivo emission fingerprinting of complexes 1 and 2 as compared to endogenous fluorescence in *Drosophila* fat body tissue.(A) Representative lambda stack micrographs of fat body cells obtained using the META detection module, sampling emission over the visible spectrum with 38.9 nm wavelength intervals. Representative images of ex vivo tissue stained with **1** (top row), **2** (middle row) and endogenous fluorescence (bottom row), which was excited with a two-photon laser at 830nm. Scale bars = 50 μm. (B) Histogram showing the intensity of emission (within optimal interval 533-650 nm) of **1** (black bars), **2** (grey bars) and endogenous fluorescence (white bars) for two-photon excitation wavelengths between 770-860 nm. (C) Emission fingerprint of tissues stained with **1** (black line) and **2** (grey line) and endogenous emission (dotted line) when excited at with a two-photon laser at 830 nm.

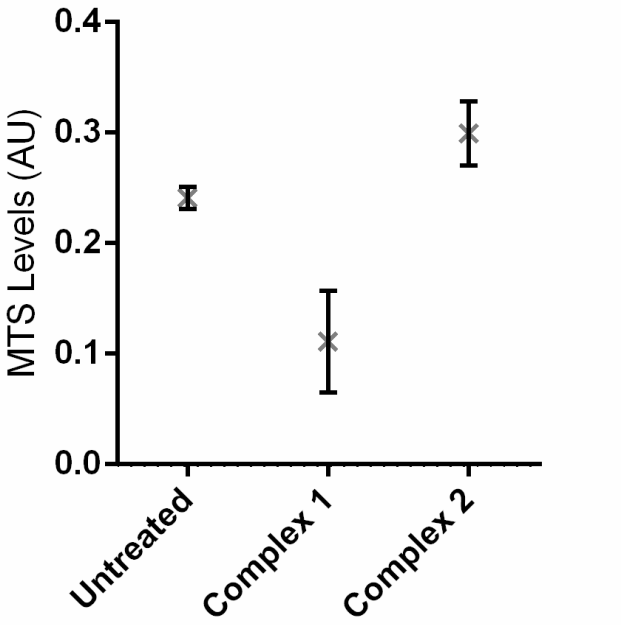


Figure 3.4 Rhenium complexes are not cytotoxic to *Drosophila* tissue.

No significant difference could be detected in the redox state of tissues treated with the Rhenium complexes compared to untreated controls at the concentrations optimal for imaging. Data represent the mean ± s.e.m. of three biological replicates for each treatment group.

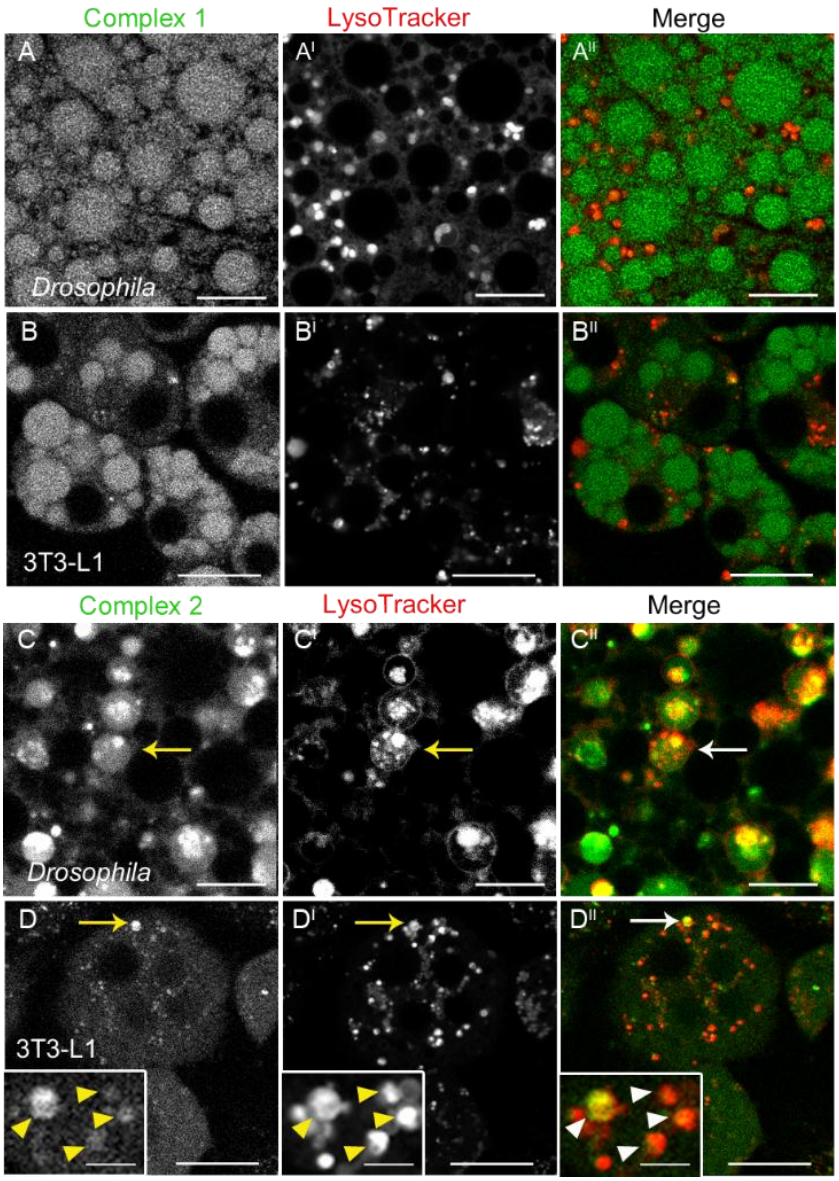


Figure 3.5 Cellular localisation of complexes 1 and 2 in relation to late endosomes.

Cellular localisation of **1** and **2** visualised by two-photon excitation in *Drosophila* fat body (A and C) and 3T3-L1 cells (B and D) in relation to late endosomes. Micrographs showing cells stained with **1** (greyscale in A and B; green in A^{II} and B^{II}) or **2** (greyscale in C and D; green in C^{II} and D^{II}). Late acidic endosomes were depicted by staining with LysoTracker®Green (greyscale in A^{I}, B^{I}; C^{I} and D^{I}; red in A^{II}, B^{II}, C^{II} and D^{II}). Arrows in C-D panels depicts co-localisation between **2** and LysoTracker®Red positive compartments. Enlarged inserts in panel D (left corner) showing co-localisation between **2** and LysoTracker®Red in 3T3-L1 cells, indicated by arrow heads (scale bar = 2µm). Scale bar = 10 µm.

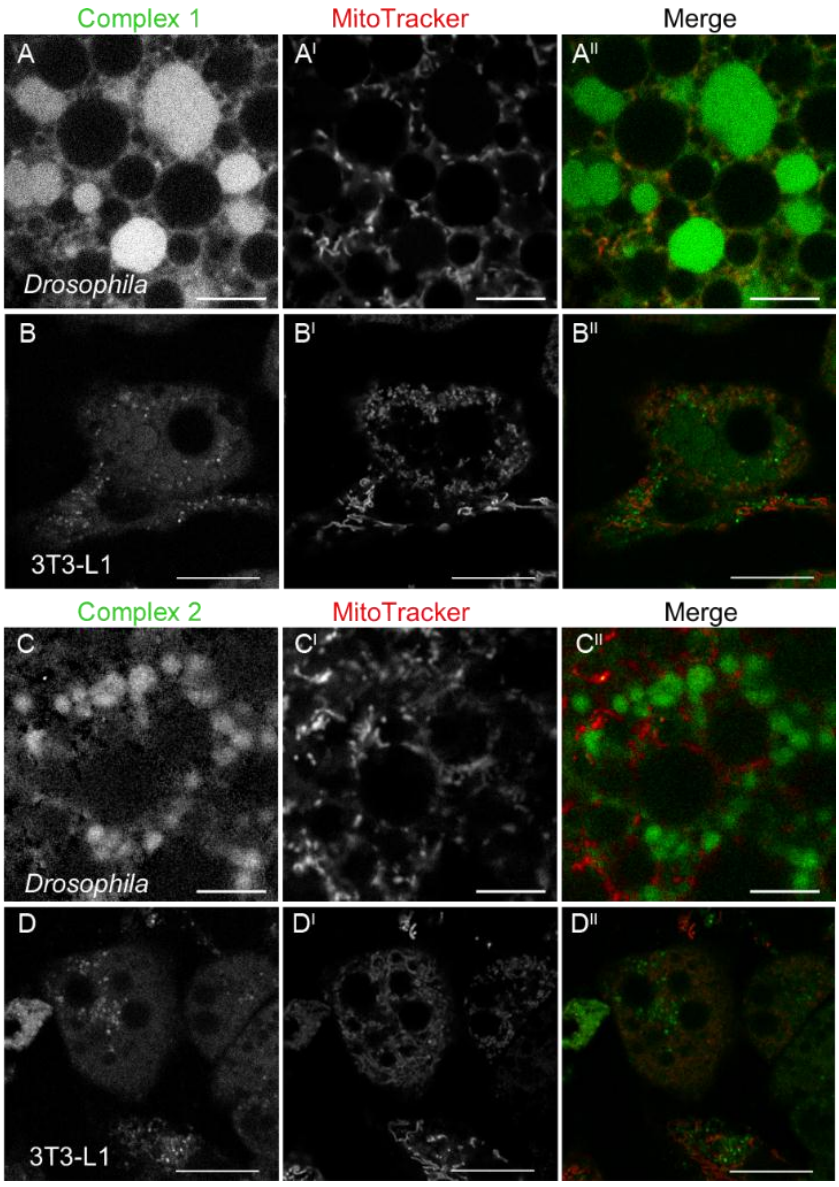


Figure 3.6 Cellular localisation of complexes 1 and 2 in relation to mitochondria.

Cellular localisation of **1** and **2** visualised by two-photon excitationin *Drosophila* fat body (A and C) and 3T3-L1 cells (B and D) in relation to mitochondria. Micrographs showing cells stained with **1** (greyscale in A and B; green in A^{II} and B^{II}) or **2** (greyscale in C and D; green in C^{II} and D^{II}). Mitochondria were depicted by staining with MitoTracker®Red (greyscale in A^{I}, B^{I}, C^{I} and D^{I}; red in A^{II}, B^{II}, C^{II} and D^{II}). Scale bar = 10 μm

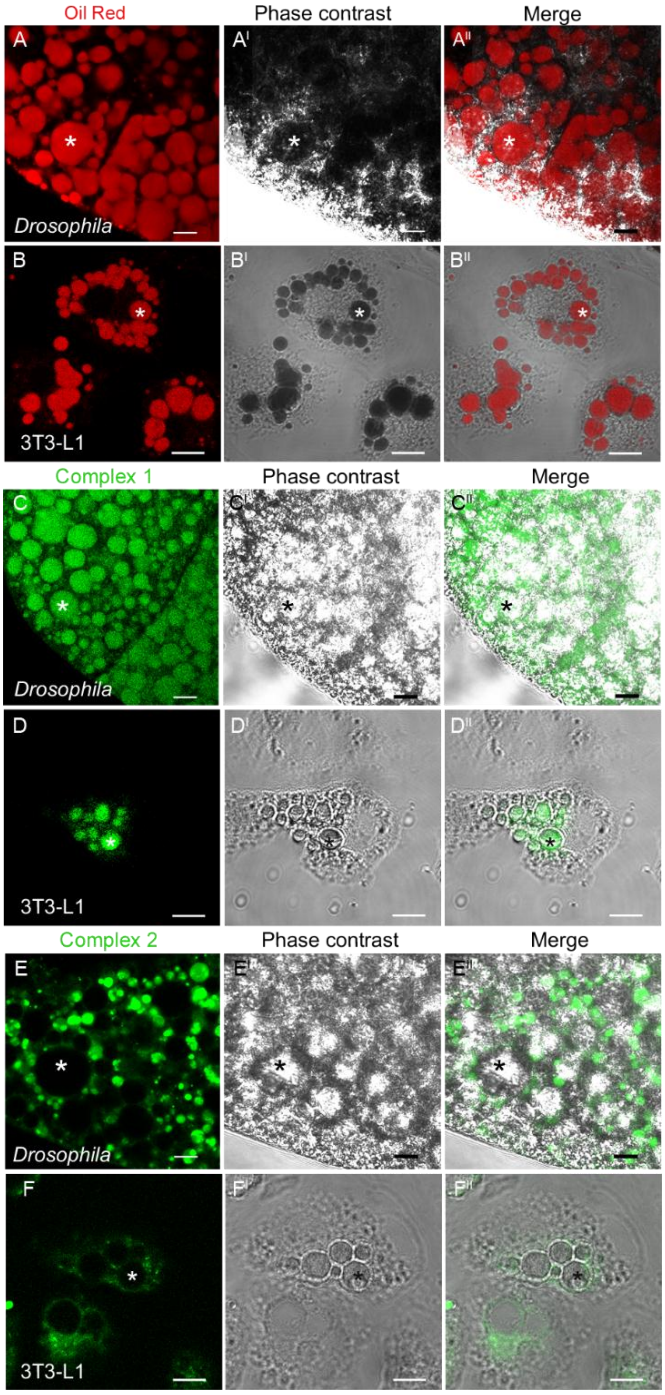


Figure 3.7 Cellular localisation of complexes 1 and 2 in relation to lipid droplets.

Micrographs of *Drosophila* fat body tissue (A, C and E) and 3T3-L cells (B, D and F), showing lipid droplets depicted by staining of fixed cells with Oil Red (red in A and A^{II}, B and B^{II}), in comparison with complex **1** (green in C and C^{II}, D and D^{II}) and **2** (green in E and E^{II}, F and F^{II}). In phase contrast images (A^{I} and B^{I}), the Oil Red light absorption appears as dark areas in lipid droplets (depicted by * in A^{I} and A^{I}). The signal from **1** (green in C and C^{II}, D and D^{II}) locates within lipid droplets (depicted by * in C^{I} and D^{I}, phase contrast image), while complex **2** (green in E and E^{II}, F and F^{II}) is localised outside of lipid droplets (depicted by * in E^{I} and F^{I}, translucent in phase contrast image). Scale bar = 10 μm.

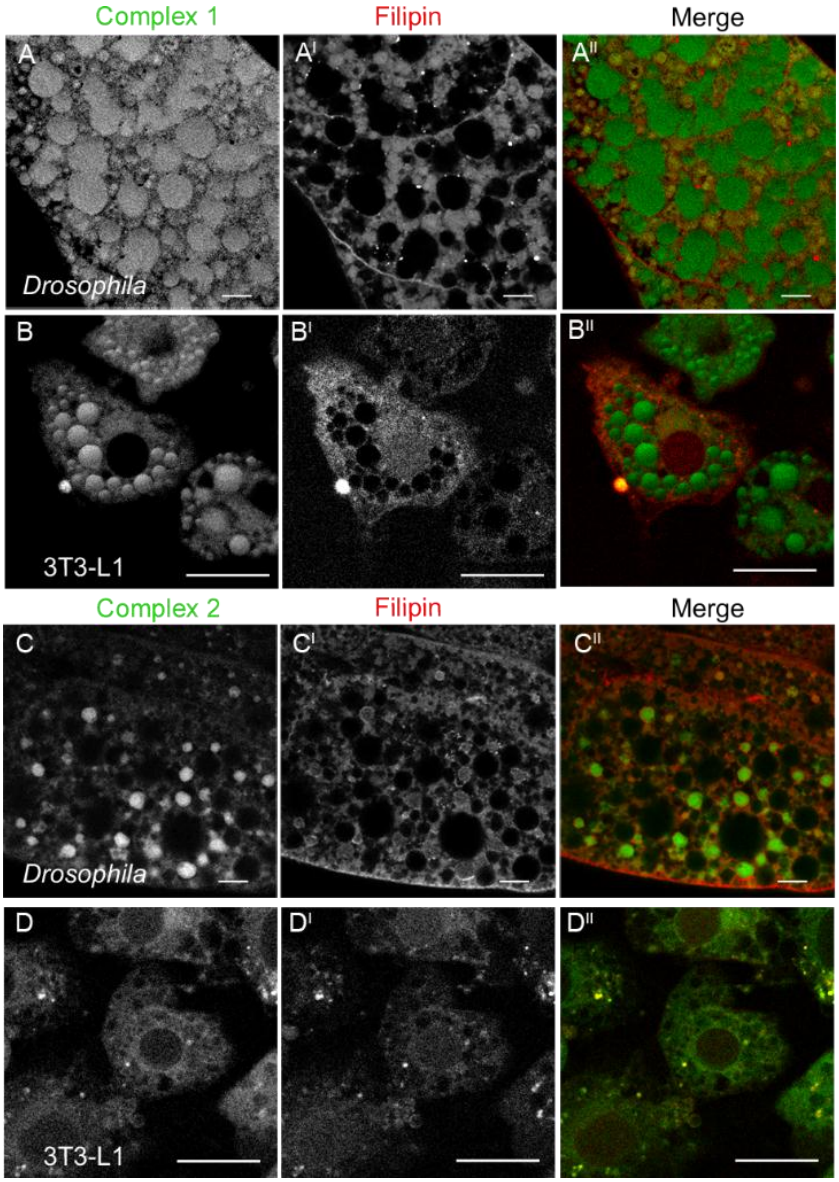


Figure 3.8 Cellular localisation of complexes 1 and 2 in relation to free cholesterol.

Cellular localisation of **1** and **2** visualised by two-photon excitationin *Drosophila* fat body (A and C) and 3T3-L1 cells (B and D) in relation to free cholesterol. Micrographs showing fixed cells stained with **1** (greyscale in A and B; green in A^{II} and B^{II}) or **2** (greyscale in C and D; green in C^{II} and D^{II}). Free cellular cholesterol detected by staining of fixed cells with Filipin (greyscale in A^{I}, B^{I}, C^{I} and D^{I}; red in A^{II}, B^{II}, C^{II} and D^{II}). Scale bar = 10 μm

From these co-localisation studies, it was evident that **1** was an efficient stain for the lipid droplets in live tissues. On the other hand, **2** seems to have a high affinity for acidic organelles, such as late endosome and lysosomes, as it showed 57±2% colocalisation with LysoTracker®-positive compartment in the fat body cells and 95±2% colocalisation in 3T3-L adipocytes. The different behaviour might be rationalised by considering the nature of the ancillary tetrazolato ligand in the two complexes. Complex **1** remains neutral in the cellular environment, as the tetrazolato ligand is too weak as a Brønsted base to undergo protonation. The lack of protonation would confer its high affinity for the neutral lipophilic environment within the lipid droplets. However, **2** is likely to be present in equilibrium with its pyridinium form, which might be responsible for the high affinity of the species for organelles characterised by an acidic environment. This conclusion is based on the fact that conventional lysosomal probes contain fluorescent groups coupled with weakly basic amine functionalities. Again, this differential targeting of two distinct cellular organelles implies that the tetrazolato ligand does not dissociate from the Re centre within cells, making tetrazolato complexes of tricarbonyl Re(I) diimine cores a robust building block in the design of cellular stains with high specificity. Our results provide evidence of how simple and targeted variations in the chemical nature of metal complexes modulate the specificity of the probe in relation to their organelle localisation. This efficient and diverse organelle targeting has been achieved without any conjugation of the metal complex to specific biovectors.

The finding of lipid droplets specificity **1** is of interest as it may offer a probe to uncover the biology of this organelle, which is intricately linked to cell metabolism, many metabolic pathologies, including atherosclerosis and lipodystrophy (Krahmer et al.,

2013b). Therefore, characterisation of the specificity of **1** to lipids interaction/s, as well as its luminescence might be an interesting new direction to follow in the future

In conclusion, two Re tetrazolato complexes have been investigated for their capacity to serve as cellular labels, and their cellular uptake and intracellular localisation suggested a relationship between their structure and specificity for distinct organelles. These studies have utilised two-photon excitation, which has a significant advantage in non-invasive imaging of live cells, while spectral image acquisition allows efficient discrimination between endogenous fluorescence and probe emission. Significantly, these findings open the route to the development of a new generation of phosphorescent and organelle specific dyes for the study of lipid droplets, whose imaging has to date only been achieved with conventional lipophilic fluorophores.

Chapter 4: A Rhenium molecular probe detects lipid droplets and autophagosomes

4.1 Preface

In the preceding chapter two Rhenium(I) tetrazolato complexes were described, which had specific subcellular detection in both *Drosophila* tissues and a human derived cell line. Complex **1**, herein referred to as the Rhenium molecular probe, showed specific localisation to lipid droplets. There are very few fluorescent stains available for the staining of lipid droplets in live cells and those that are compatible with live cell imaging are limited in their use for multicolour imaging. To the best of our knowledge, this is the first demonstration of a metal based probe which localises to this unique organelle and is compatible with live cell multicolour imaging. Lipid droplets are an important organelle, which like autophagy is critical to the cellular regulation of energy and metabolism. Novel interactions between autophagosomes and lipid droplets have been reported in a range of cell types and appear to be involved in the regulation of intracellular lipid homeostasis and metabolism. Thus, we further investigate complex **1**, the Rhenium molecular probe, as a tool to visualise the interaction between lipid droplets and autophagosomes.

Complex **2** (also described in Chapter 3) detected acidic compartments, and is likely to detect autolysosomes following autophagy induction. Further investigation of this complex was not completed as part of this thesis (although some reference to the data set for this molecular probe has been made in the general discussion); as a range of acidotrophic dyes are already available and used extensively in this context.

4.2 Abstract

Lipid droplets are dynamic organelles that mediate the storage of lipids and can act as a source of lipids for energy production in times of metabolic stress. Autophagy is a lysosomal degradation pathway that can also respond to metabolic stress, providing a pathway for the mobilization of lipids from lipid droplets. The interaction between lipid droplets and autophagosomes has important implication for a range of human disease, including metabolic disorders, neurodegenerative diseases and cancers, which commonly display altered lipid metabolism and increased autophagy. The investigation of this important process has been limited by the availability of specific tools to detect lipids in live cells. Here we describe a Rhenium(I) based fluorescent probe, which detected lipid droplets in live cells, and was responsive to autophagic signals. For example, developmental cues during larval to adult transition in *Drosophila*, extreme starvation and the genetic inhibition of TOR all resulted in the Rhenium molecular probe being detected in autophagosomes and autolysosomes. The Rhenium molecular probe was shown to have an affinity for sphingolipids, gangliosides, phospholipids and cholesterol, but did not interact with neutral lipids, including triacylglycerols and cholesterol esters. The Rhenium molecular probe was responsive to pH with a spectral shift, when detected in autolysosomes, allowing a clear distinction between lipids in lipid droplets and autolysosomes. These findings indicated that the Rhenium molecular probe can interact with intracellular lipids in live cells and can be used to investigate the interactions between lipid droplets and autophagosomes during metabolic events.

4.3 Introduction

Lipid droplets act as an important control point for lipid metabolism and are used for the intracellular storage of neutral lipids. Lipid droplet formation can be induced by excess lipids, such as fatty acids, which are converted into neutral lipids by a series of enzyme reactions (Ruggles et al., 2013). These neutral lipids, mainly in the form of triacylglycerol's and sterol esters are contained within the core of lipid droplets, together with other constituents such as structural proteins and various lipases (Bartz et al., 2007). The lipids in the luminal core of lipid droplets can be degraded by lipolysis and released back into the cell to provide energy or utilised as structural components for membrane assembly (Thiam et al., 2013). Autophagosomes are used to traffic these lipids to different cellular locations, but autophagy is also a pathway for the lysosomal degradation of lipids (Liu and Czaja, 2013). Defining the molecular link between the key biological processes of lipid metabolism and autophagy is central to understanding the pathogenesis associated with major diseases like diabetes, obesity, inflammatory diseases and cancer (Greenberg et al., 2011; Krahmer et al., 2013a; Thiele and Spandl, 2008).

The molecular machinery involved in autophagosome formation has been defined and the activation step usually involves the phosphorylation of autophagy related protein Atg13, which facilitates conformational changes and activation of a core Atg1 (human ortholog ULK1) initiation complex (Chang and Neufeld, 2010; Ganley et al., 2009; Hosokawa et al., 2009; Jung et al., 2009; Mehrpour et al., 2010; Nakatogawa et al., 2009). This Atg1 complex acts as a scaffold for the localisation of Atg9 and two ubiquitin like conjugation complexes, Atg12-Atg5 and Atg8-phosphotidylethanolamine (PE), which enable the nucleation, expansion and closure of autophagosomes (Klionsky and Schulman, 2014; Young et al., 2006). When this autophagic machinery is inhibited, by for example, 3-

methyladenine (3-MA) or the specific knockdown of Atg5, lipid droplets accumulate in the intracellular space, demonstrating that autophagy has a function in lipid catabolism and homeostasis (Singh et al., 2009a).

Autophagy is clearly an alternative route for lipid droplet mobilization and degradation, and involves either the sequestering of specific lipids or encapsulating the lipid droplets into a double membrane structure called an autophagosome (Singh and Cuervo, 2011; Singh and Cuervo, 2012; Singh et al., 2009a; Singh et al., 2009b). Autophagosomes normally undergo a maturation process to initially form amphisomes by fusion with endosomes and then ultimately fuse with lysosomes to form autolysosomes. This sequential fusion with endosomes and lysosomes delivers lipases and other hydrolases to the amphisome/autolysosome, which can then beak-down neutral and other lipids (Ouimet et al., 2011; Pearson et al.; Singh and Cuervo, 2012; Singh et al., 2009a).

Autophagosome formation can be regulated by several different mechanisms including the induction of a cellular stress response, which is particularly important during nutrient deprivation. Nutrient sensing pathways include the AMP (adenosine mono-phosphate), insulin and amino acid sensing pathways, converge either directly or indirectly on the target of Rapomycin or TOR (Jin et al., 2014; Kim et al., 2011b; Kim et al., 2013b; Meijer and Dubbelhuis, 2004; Sancak et al., 2008; Yuan et al., 2013); which is a key regulator of autophagy (Noda and Ohsumi, 1998; Scott et al., 2004; Shimobayashi and Hall, 2014; Wang et al., 2001). TOR normally inhibits the activation of autophagy, but upon TOR inactivation Atg13 is phosphorylated, initiating autophagosome formation (Chang and Neufeld, 2010; Mehrpour et al., 2010; Nakatogawa et al., 2009). Lipophagy or the specific degradation of lipids by autophagosomes-autolysosomes operates at a basal level in most

cell types, but can be upregulated in response to stress or the presence of excess lipids and also has an important role in adipocyte differentiation and energy storage (Baerga et al., 2009; Singh et al., 2009b; Zhang et al., 2009b). The complex interplay between lipid pathways and autophagy obviously have a critical role in energy metabolism, but the mechanisms governing these interactions are yet to be fully elucidated.

The lack of appropriate cell biological tools is a major limitation in the investigation of lipid droplet biology, with the chemical nature of neutral lipids making them difficult to visualise (Schnell et al., 2012). In addition, most of the currently available molecular probes require fixation, which can compromise cellular ultrastructure and prevent live cell imaging (Schnell et al., 2012). For example, Oil-Red-O and Nile Red both require sample fixation and both have issues with solubility (Spangenburg et al., 2011). Lipid fixation is particularly problematic when using alcohol based solvents and fixatives, which cause fusion of lipid droplets and or extraction of lipids from cell/tissue samples (Fujimoto and Parton, 2011; Fukumoto and Fujimoto, 2002; Melo et al., 2011b). BODIPY®(493/503) can be used for live or fixed samples (Spangenburg et al., 2011), but its broad excitation and emission profiles and small Stoke shift make it difficult for studies involving dual labelling (Spandl et al., 2009; Yang et al., 2012). Alternatively, coherent anti-Stokes Raman scattering (CARS) microscopy has been used for label-free imaging of lipid droplets *in vivo* (Chien et al., 2011; Dou et al., 2012). This imaging technique involves the overlap of a pump beam and a Stokes beam in a sample, with a wavelength difference set to match the Raman vibrational mode of the sample (Duncan et al., 1982; Wurpel et al., 2002). Although this technique overcomes some of the issues with live cell imaging, it is not compatible with fluorescence imaging making it difficult to investigate interactions between lipid droplets and other cellular components. A number of new organic

flourophores have been described including, monodansylpentane, a blue dye that can be used for multi-photon excitation (Yang et al., 2012) and LD540 which emits in the yellow-green range (Spandl et al., 2009), however these types of dyes often suffer from self-quenching and photobleaching (New et al., 2010). A Rhenium(I) tricarbonyl diimine complex, complex **1**, that exhibits phosphorescent emission has recently been developed for the live cell imaging of lipid droplets (Bader *et al.* 2014; Chapter 3), and exhibited a long excitation half-life and large Stoke shift, which are ideal for cellular imaging (Vaughan et al., 2013). Here we have investigated this Rhenium molecular probe to define its molecular interaction and to investigate lipid droplets during autophagosome formation.

4.4 Material and methods

4.4.1 Fly stocks

All stocks were maintained in standard medium at 25°C. The yeast *GAL4-UAS* system was used for targeted gene expression (Brand and Perrimon, 1993). Fat-body specific expression of transgenes from the UAS were driven by *CG-GAL4* (Asha et al., 2003). Transgenic *UAS-Atg9*^{RNAi} stocks (#34901) and *UAS-Tor*^{TED} stocks (#7013) were obtained from the Bloomington Drosophila Stock Centre (Indiana University, Indiana, USA). *Atg8a-GFP* was driven by an endogenous promoter (Kelso et al., 2004) kindly provided by Dr Erik Baehrecke (University of Massachusetts Medical School, Massachusetts, USA).

4.4.2 Developmental staging

Bromophenol-blue was added to the fly media and used to define different developmental time points (Andres and Thummel, 1994). Third instar larvae at minus eight hours of puparium formation (-8h PF) had a blue gut and were observed wandering in and out of the media, whereas at minus four hours (-4h PF) the guts had little or no blue dye and the larvae were only observed out of the media. Newly formed white pupae (0h PF), were isolated onto moist filter paper and incubated at 25˚C for two hours (+2h PF).

4.4.3 Nutrient deprivation

Third instar larvae at -8h PF were removed from standard media (normally feeding at this developmental stage) and placed on filter paper either soaked in 5% (w/v) sucrose (for amino acid deprivation), or 5% (w/v) tryptone pancreatic digest of casein (BD Bioscience San Jose, USA; for sugar deprivation), or soaked in water (for amino acid and sugar starvation). Larvae were incubated for 4-5 hours prior to tissue isolation and imaging.

4.4.4 Tissue isolation and staining

Fat body tissue was dissected from *Drosophila* larvae or pupae into PBS. The fat body tissue was incubated with 10 μM tricarbonyl phenanthroline (4-cyanophenyltretrazolato) Rhenium(I) in PBS for 15 minutes at room temperature and washed in PBS for 30 seconds. Tissues were counterstained for acidic compartments with LysoTracker® green (prepared according to manufacturer instructions; Invitrogen, Waltham, USA) for 2 minutes at room temperature. Tissues were then mounted in carbomer-940 (Snowdrift farm, Tucson, USA) based optical coupling gel to prevent dehydration prior to imaging (see protocol in Rothstein et al., 2006). For Oil Red O staining, fat body tissue was fixed in 2% (v/v) paraformaldehyde for 20 minutes, washed three times in PBS for ten minutes before incubation in 1/100 Oil Red O for 30 minutes and then washed in PBS before mounting in 80% glycerol.

4.4.5 Imaging and analysis

A Ziess LSM710 META NLO confocal microscope (Zeiss, Oberkochen, Germany), supplemented with a two-photon Mai-Tai® (tunable Ti:Sapphire femtosecond pulse laser, 710–920 nm; Spectra-Physics, Santa Clara, USA) was used for imaging. The images were acquired using a Plan- APOCHROMAT 63X/ NA1.4 oil immersion objective. The Rhenium molecular probe was excited at 830 nm using the two-photon pulse laser and detect at 600-654 nm. LysoTracker® green was imaged by excitation at 488 nm and detected at 497-558 nm. Atg8a-GFP was imaged with the Rhenium molecular probe by excitation at 830 nm (to excite both fluorophores) and resolved using spectral un-mixing using the Zen software package (based on spectral figure-printing of the two components). A spectral profile for the Rhenium molecular probe was acquired in lambda stack mode

(830 nm excitation range, MBS 690+, spectral emission range 416-727 nm, with 9.7 nm intervals).

The Rhenium molecular probe images and co-location analysis involved at least five separate images from five independent biological replicates, and one representative image from each treatment was selected for presentation. For image quantification, two regions of interest (ROI) were selected with an area of 2500 μm^2, to ensure that all regions analysed were in focus and were not outside of the cell boundary. The number of compartments with the Rhenium molecular probe or Atg8a-GFP were counted to give a minimum of ten counts per treatment group. Comparison of means was performed by ANOVA with a Tukey post hoc tested in GraphPad Prism V.6.01 (USA).

The Zen software package (Zeiss, Oberkochen, Germany) was used to obtain the spectral profile of the Rhenium molecular probe in different subcellular compartments. Spectrums were averaged from each of five subcellular compartments in which the Rhenium molecular probe was localised. The emission intensity was calculated for emission maximums in each subcellular compartment and presented as the mean ± s.e.m.

4.4.6 Rhenium molecular probe lipid interaction

To determine the binding properties of the Rhenium molecular probe to various lipids, a probe-lipid overlay was performed. 50 µM of each lipids was loaded on to PVDF membrane (Perkin-Elmer, Waltham, USA). Eleven lipids were analysed including; sphingomyelin (Cat # S0756, Sigma-Aldrich, St Louis, USA), sphingosine (Cat # S7049; Sigma-Aldrich, St Louis, USA), L-α-phosphatidylethanolamine (Cat # P7943, Sigma-Aldrich, St Louis, USA), monosialodanglioside (GM1; Cat # G7641, Sigma-Aldrich, St

Louis, USA), oleoly-L-α-lysophosphatidic acid (Cat # L7260, Sigma-Aldrich, St Louis, USA), palmitic acid (Cat # P5917, Sigma-Aldrich, St Louis, USA), cholesterol (Cat # CO01800100; Scharlau, German), progesterone (Cat # 102722, MP Biomedical, USA), ceramide (Cat # C2137; Sigma-Aldrich, St Louis, USA), triacylglycerol mix C2-C10 (Cat # 17810, Sigma-Aldrich, St Louis, USA) and cholesteryl acetate (Cat # 151114; Sigma-Aldrich, St Louis, USA). Lipids were dissolved in ethanol, methanol or isopropanol for loading depending on solubility. Following lipid loading, membranes were washed for 10`minutes in cold 10% ethanol, before they were incubated with 10 µM of Rhenium molecular probe in cold 10% ethanol for one hour. Membranes were than washed four times for 10 minutes in cold 10% ethanol prior to imaging. Imaging was performed on an Image Quant Las 4000 (GE, Uppsala, Sweden) luminescent image analyser, with the Rhenium molecular probe being detected by excitation at 460 nm using an epi-blue light source, and detected using an 575 nm ethidium bromide filter.

4.5 Results

4.5.1 The Rhenium based molecular probe detected lipid droplets in *Drosophila* fat body tissue, but also localised to an acidic compartment during metamorphosis.

Previously, we described the synthesis of a Rhenium based molecular probe, tricarbonyl phenanthroline (4-cyanophenyltretrazolato) Rhenium(I), which enabled the imaging of lipid droplets in live and fixed cells (Wright et al., 2012; Bader et al., 2014). During *Drosophila* metamorphosis from larvae to adulthood, fat body tissue undergoes a lytic phase, during which lipid droplet storage is decreased, and energy stores are released to support the developmental process (Butterworth et al., 1988). Here we employed this Rhenium molecular probe to assess changes in lipid storage in fat body tissue during development. In fat body tissues explanted at either the onset of puparation, -4h PF or 0h PF, the Rhenium molecular probe was detected in lipid droplets and appeared to be spread evenly throughout the central matrix of these organelles (Figure 4.1A, 4.1A^{II} and Figure 4.1B, 4.1B^{II} respectively). However, at +2h PF, the Rhenium molecular probe was detected in LysoTracker® green positive acidic vesicles (Figure 4.1C^{I}, 4.1C^{II}), as well as lipid droplets (Figure 4.1C, 4.1C^{II}). The size of the lipid droplets did not appear to change dramatically at + 2h PF (Figure 4.1C-4.1C^{II}) compared to either 0h PF (Figure 4.1B-B^{II}) or -4 h PF (Figure 4.1A-A^{II}). In contrast the size of the LysoTracker® green positive compartments increased at 0h PF (Figure 4.1B^{I}) and +2h PF (Figure 4.1C^{I}), when compared to -4h PF (Figure 4.1A^{I}).

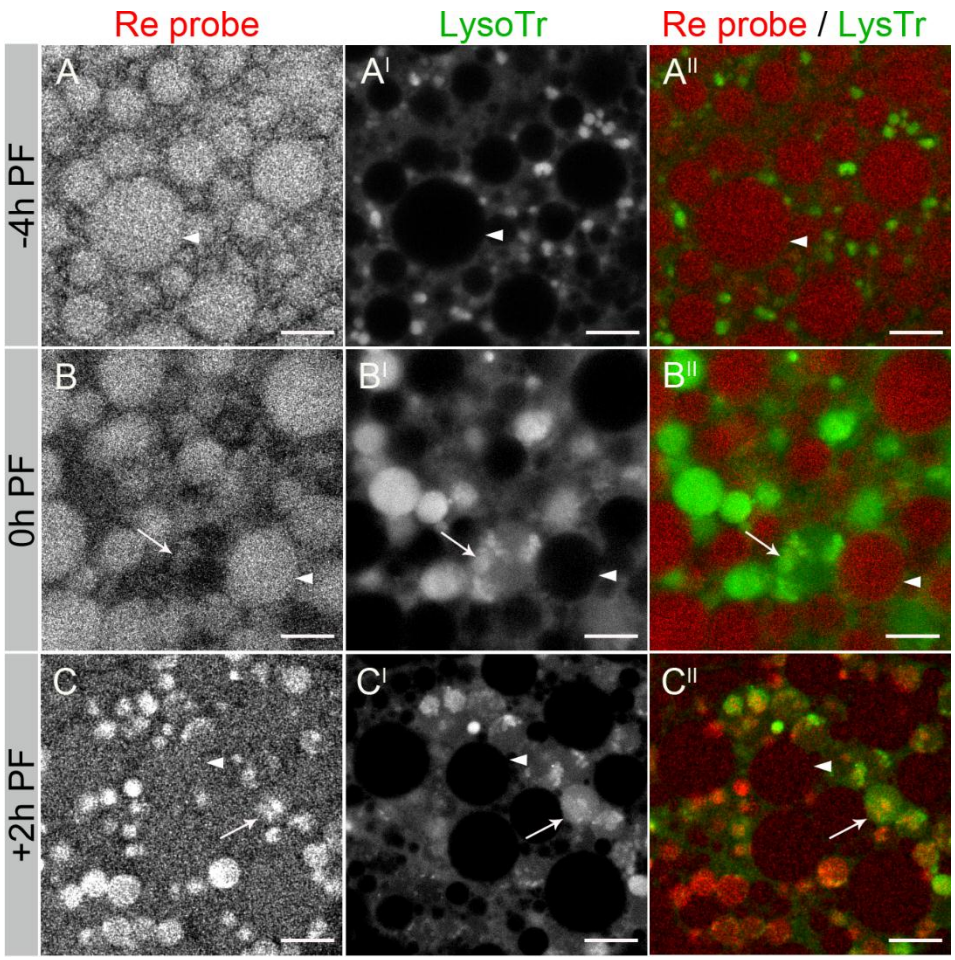


Figure 4.1 The Rhenium molecular probe was detected in Drosophila fat body lipid droplets, but located to acidic compartments during metamorphosis.

Confocal micrographs of fat body cells explanted from WT^{1118} *Drosophila* larvae and pupae at either -4h PF (A-A^{II}), 0h PF (B-B^{II}), or +2h PF (C-C^{II}) and stained with Rhenium molecular probe (grey scale in A, B and C; red in A^{II}, B^{II} and C^{II}) and LysoTracker® green (grey scale in A^{I}, B^{I} and C^{I}; green in A^{II}, B^{II} and C^{II}). Arrowheads indicated lipid droplets (A-C^{II}), arrows indicate colocation of Rhenium molecular probe to LysoTracker® green positive compartments (B-C^{II}). Scale bars = 10 µm.

4.5.2 The spectral profile of the Rhenium molecular probe was dependent on its subcellular location.

In solution, the Rhenium molecular probe has been shown to have different spectral properties following protonation (Werrett et al., 2013), prompting us to define the spectral profile of the Rhenium molecular probe in different subcellular locations. At +2h PF the Rhenium molecular probe was detected in either lipid droplets (Figure 4.2A; green/yellow) with an emission maximum of 557 nm, but was also detected in acidic compartments (Figure 4.2A; cyan) with an emission maximum of 480 nm (Figure 4.2B). The Rhenium molecular probe also had a significantly higher emission intensity ($P = 0.001$) in acidic compartments (intensity of 13889 ± 4377 au at λ_{em} 480 nm; Figure 2B) when compared to lipid droplets (intensity of 1705 ± 256 au at λ_{em} 557 nm; Figure 4.2B).

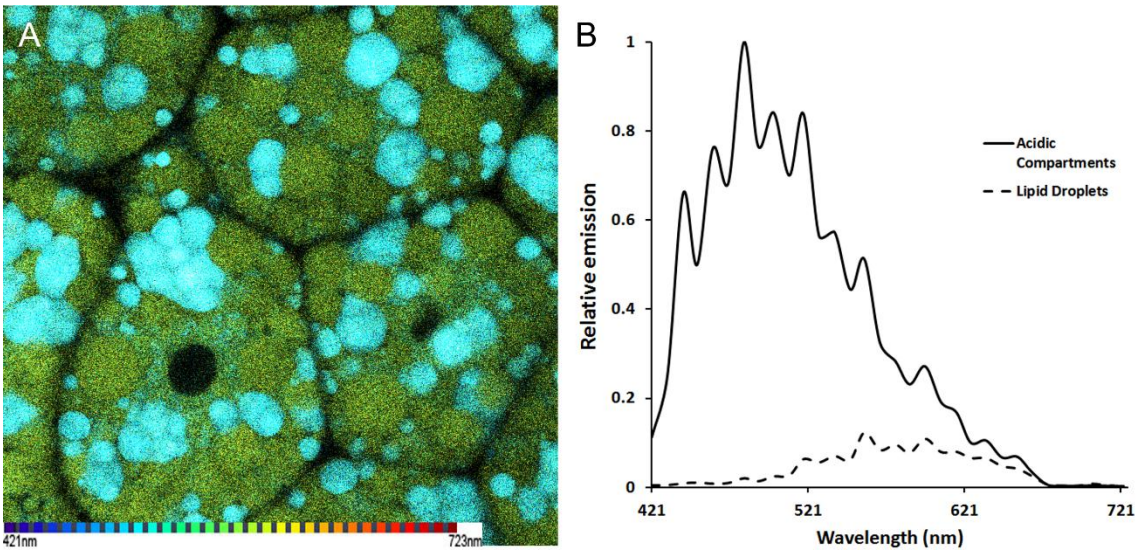


Figure 4.2 Spectral profiling of the Rhenium molecular probe in acidic compartments and lipid droplets.

(A) Confocal micrographs of *Drosophila* fat body at +2h PF stained with Rhenium molecular probe showing spectral profile of probe in acidic compartments (cyan) and lipid droplets (green/yellow). (B) Spectral emissions profile of Rhenium molecular probe in different subcellular compartments (acidic compartments = solid line: lipid droplets = dashed line) relative to emission maxima of acidic compartment (intensity at λ_{em} 480 nm).

4.5.3 The Rhenium molecular probe colocalised with autophagosomes during development and following starvation.

The increased co-localisation of the Rhenium molecular probe with LysoTracker® green positive acidic compartments at +2h PF (Figure 4.1C^{II}) coincided with increased autophagy at this developmental time point (Butterworth et al., 1988; Rusten et al., 2004); which in mammalian cells has been implicated in lipolysis (Singh and Cuervo, 2012). Larvae and pupae expressing the autophagosome marker Atg8a-GFP were investigated to determine if the Rhenium molecular probe was being redistributed into autophagosomes/autolysosomes at +2h PF. Under normal feeding conditions at -4h PF there was minimal or no detectable Atg8a-GFP autophagosomes (Figure 4.3A^{I}) and the Rhenium molecular probe was detected in lipid droplets (Figure 4.3A, 4.3A^{II}). At +2h PF while the Rhenium molecular probe was still detected in lipid droplets it was also detected in Atg8a-GFP autophagosomes/autolysosomes (Figure 4.3E-4.3E^{II}; quantified in Figure 4). Autophagy can also be induced by starvation and we hypothesised that this might also replicate this change in the Rhenium molecular probe's distribution. At early developmental time points there is normally minimal autophagy, as evidenced here by the lack of Atg8a-GFP autophagosomes at -4h PF (Figure 3.3A^{I}, 3.3A^{II}). At this developmental time point amino acid deprivation induced an increase in Atg8a-GFP autophagosomes/autolysosomes (Figure 4.3B^{I}; quantified in Figure 4.4), but no apparent change in the distribution of the Rhenium molecular probe (Figure 4.3B, 4.3B^{II}; quantified in Figure 4.4), when compared to an untreated controls (Figure 4.3A, 4.3A^{II}; quantified in Figure 4.4). Sugar deprivation also induced an increase in Atg8a-GFP autophagosomes/autolysosomes (Figure 4.3C^{I}, 4.3C^{II}) and some change in the distribution of the Rhenium molecular probe (Figure 4.3C, 4.3C^{II}). However, complete starvation (amino acid and sugar deprivation), induced a dramatic redistribution of the Rhenium

molecular probe to Atg8a-GFP autophagosomes-autolysosomes and resulted in both reduced size of the lipid droplets and amount of Rhenium molecular probe staining (Figure 4.3D, 4.3D^{II}). Under these complete starvation conditions an average of 90 ± 11% of the vesicles stained by the Rhenium molecular probe were Atg8a-GFP autophagosomes/autolysosomes.

The pattern of neutral lipid staining detected by Oil Red O was similar to the Rhenium molecular probe under normal feeding conditions (Figure 4.5A, 4.5A^{II} and Figure 4.3A, 4.3A^{II} respectively) and amino acid deprivation (Figure 4.5B, 4.5B^{II} and Figure 4.3B, 4.3B^{II} respectively). Consequently, the formation of Atg8a autophagosomes in response to amino acid starvation (Figure 4.5B^{I}, 4.5B^{II} and Figure 4.3B^{I}, 4.3B^{II}) did not appear to alter either the distribution of Oil Red O staining (Figure 4.5B, 4.5B^{II}) or the Rhenium molecular probe (Figure 4.3B, 4.3B^{II}). Under conditions of sugar deprivation the Oil Red O staining was condensed and the lipid droplets were smaller (Figure 4.5C, 4.5C^{II}) than either amino acid deprived or control fat body cells. In addition, there appeared to be little or no interaction of neutral lipids with Atg8a-GFP autophagosomes following sugar deprivation (Figure 4.5C^{II}), whereas the Rhenium molecular probe showed some co-location with Atg8a-GFP autophagosomes (Figure 4.3C^{II}). There were however significant changes in Oil Red O staining during complete starvation and developmental autophagy (Figure 4.5D-4.5E^{II}), but the pattern of distribution was distinct from that observed for the Rhenium molecular probe (Figure 4.3D-4.3D^{II}). These findings indicated that the Rhenium molecular probe staining was different to that for Oil Red O staining and that the Rhenium molecular probe was most likely not interacting with neutral lipids.

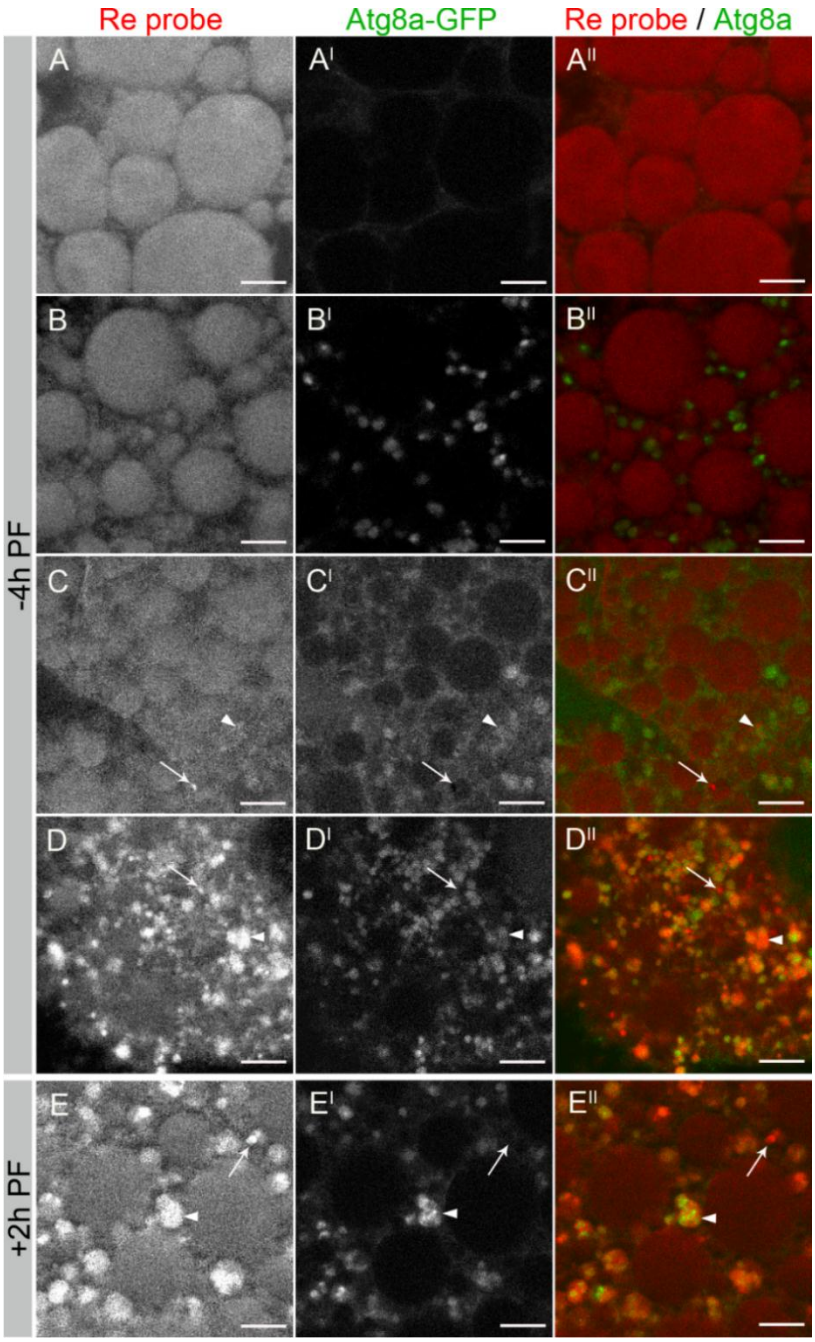


Figure 4.3 The Rhenium molecular probe localised with Atg8aGFP upon starvation and during pupal development.

Confocal micrographs of *Drosophila* fat body tissue from larvae at -4h PF (A-D^{II}) or pupae at +2h PF (E-E^{II}), stained with Rhenium molecular probe (grey scale in A, B, C, D and E; red in A^{II}, B^{II}, C^{II}, D^{II} and E^{II};) and expressing *Atg8a-GFP* (grey scale in A^{I}, B^{I}, C^{I}, D^{I} and E^{I}; green in A^{II}, B^{II}, C^{II}, D^{II} and E^{II}). Tissue from larvae at -4h PF on standard feeding medium (A-A^{II}), -4h PF larvae deprived of amino acids for 4h (B-B^{II}), -4h PF larvae deprived of sugar for 4h (C-C^{II}), -4h PF larvae starved for 4h (deprived of amino acids and sugar; D-D^{II}) and pupae at +2h PF (E-E^{II}). Arrowheads indicate Rhenium molecular probe collocating with Atg8aGFP positive compartments (C-E^{II}), arrows indicate Rhenium molecular probe alone(C-E^{II}). Scale bars = 10 µm.

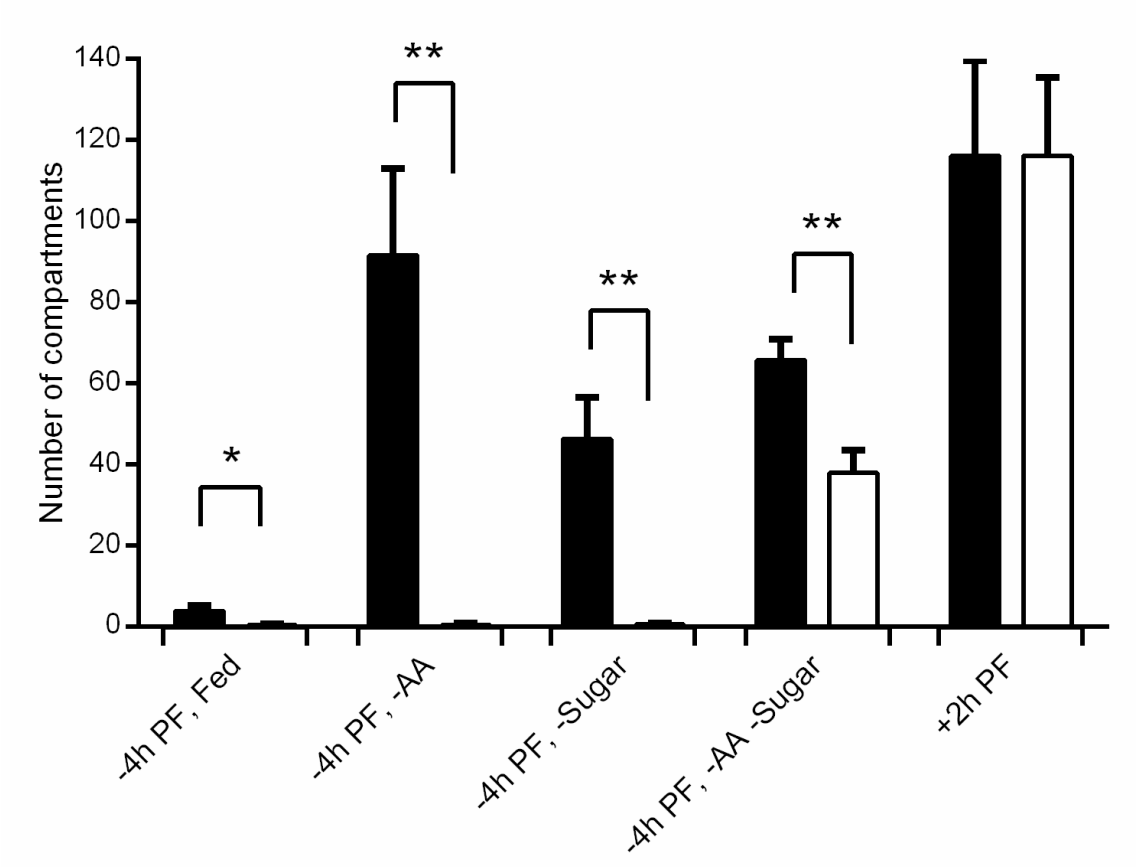


Figure 4.4 Quantification of Atg8aGFP positive compartments and Atg8aGFP/Rhenium molecular probe positive compartments during starvation and development

Histogram showing the number of Atg8aGFP positive compartments (Atg8; black bars) and Atg8aGFP/Rhenium molecular probe positive compartments (Atg8/Re; white bars), present in fat body tissues. Tissues were collected from -4h PF larvae maintained on standard feeding medium (-4h PF, Fed), -4h PF larvae deprived of amino acids for 4h (-4h PF, -AA), -4h PF larvae deprived of sugar for 4h (-4h, -Sugar), -4h PF larvae starved for 4h (-4h PF, -AA-Sugar) and pupae at +2h PF (+2h PF). Results are presented as the mean ± s.e.m (n=10), mean Atg8aGFP positive compartments and Atg8aGFP/Rhenium molecular probe positive compartments were compared for each treatment by student t-test, significance indicated by asterisks, $P < 0.05$.

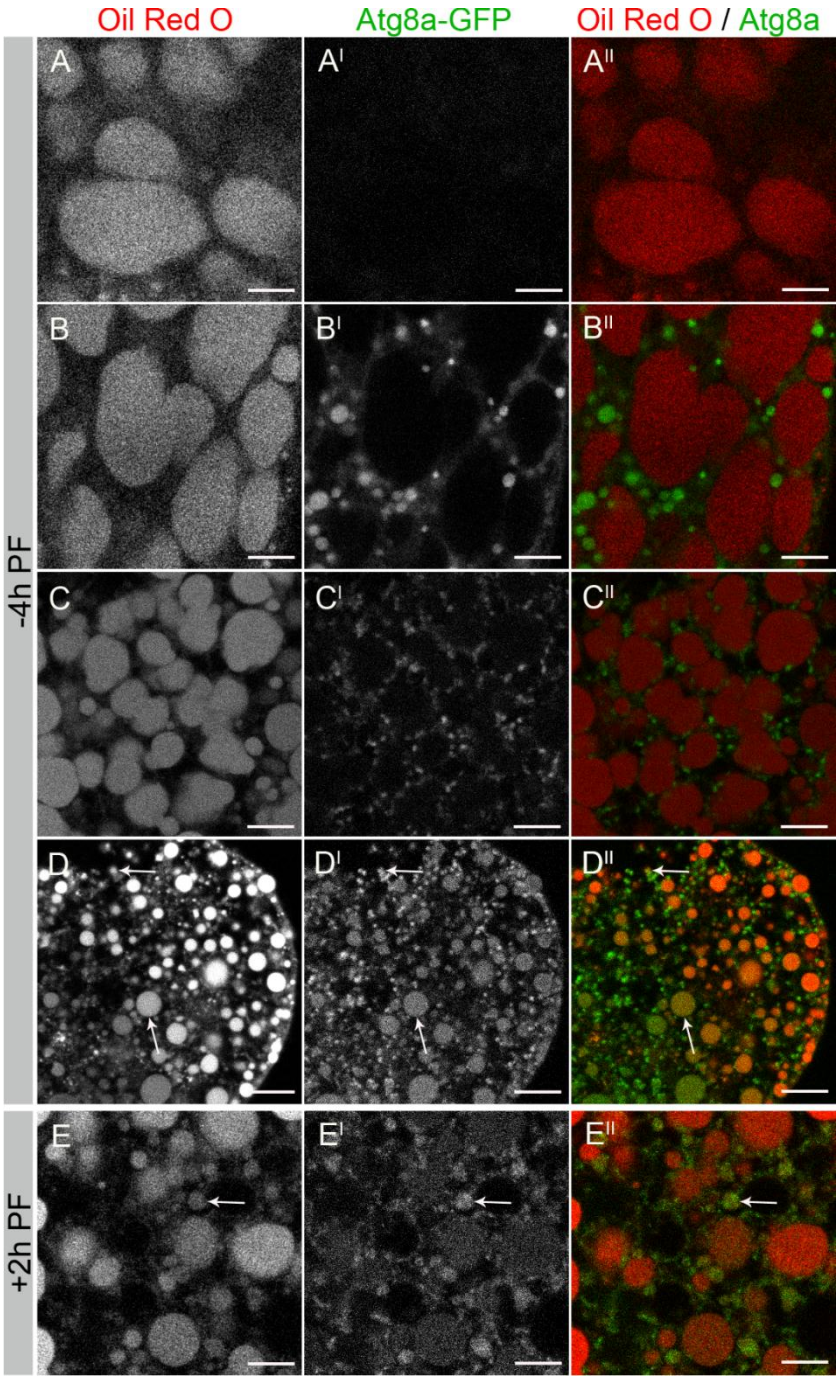


Figure 4.5 Neutral lipid stain Oil Red O localised with Atg8aGFP during either larval starvation or pupal development.

Confocal micrographs of fixed fat body tissue from *Drosophila* larvae at -4h PF (A-D^{II}) or pupae at +2h PF (E-E^{II}), stained with Oil Red O (grey scale in A, B, C,. D and E; red in A^{II}, B^{II}, C^{II}, D^{II} and E^{II}) and expressing *Atg8aGFP* (grey scale in A^{I}, D, C^{I}, D^{I} and E^{I}; green in A^{II}, B^{II}, C^{II}, D^{II} and E^{II}). Images from larvae at -4h PF on standard feeding medium (A-A^{II}), -4h PF larvae deprived of amino acids for 4h (B-B^{II}), -4h PF larvae deprived of sugar for 4h (C-C^{II}), -4h PF larvae starved for 4h (D-D^{II}) or pupae at +2h PF (E-E^{II}). Arrows indicate colocalistation between Oil Red O and Atg8a-GFP (D-E^{II}). Scale bars = 10 µm.

4.5.4 Genetic modulation of autophagy altered the Rhenium molecular probe distribution.

Next we assessed the Rhenium molecular probe distribution in lipid droplets and autophagosomes in response to either the expression of dominant negative *TOR* (*TOR*^{TED}) leading to constitutive activation of autophagy (Noda and Ohsumi, 1998; Scott et al., 2004), or a reduction in autophagosome formation induced by RNAi depletion of the core autophagy protein Atg9 (Low et al., 2013; Nagy et al., 2014a; Tang et al., 2013). At -8h PF (when larvae are normally feeding and there is little or no autophagy) larvae expressing dominant negative *TOR*^{TED} showed significantly more Rhenium molecular probe localised to LysoTracker® green vesicles (Figure 4.6B-4.6B^{II}) when compared to controls (Figure 4.6A-4.6A^{II}; quantified Figure 4.7). Larvae expressing *TOR*^{TED} were unable to be analysed at later developmental time points as the fat body tissue was almost completely degraded. Under normal feeding conditions at -4h PF in larvae expressing *Atg9*^{RNAi} the Rhenium molecular probe was detected mainly in lipid droplets (Figure 4.7B-4.7B^{II}), which was similar to the probe's distribution in controls (Figure 4.7A-4.7A^{II}; quantified Figure 4.9); under these conditions the LysoTracker® green staining was distinct from the Rhenium molecular probe (Figure 4.7A^{II}, 4.7B^{II}. Larvae exposed to amino acid starvation at -4h PF also had Rhenium molecular probe staining in lipid droplets, which was mainly distinct from LysoTracker® green in both controls (Figure 4.7C-4.7C^{II}) and *Atg9*^{RNAi} larvae (Figure 4.7D-4.7D^{II}; quantified in Figure 4.9). In contrast, at -4h PF the complete starvation (-amino acids and -sugar) of control and *Atg9*^{RNAi} larvae, resulted in the Rhenium molecular probe being colocalised with LysoTracker® green (respectively Figure 4.7E^{II}, 4.7F^{II}), and with less staining in lipid droplets, particularly for the *Atg9*^{RNAi} larvae (Figure 4.7F, 4.7F^{II}). However, the number of compartments which were Rhenium molecular probe and LysoTracker® green positive was significantly less in *Atg9*^{RNAi} tissues compared to control

larval fat body (Figure 4.9). At +2h PF both control and *Atg9*^{RNAi} pupae showed Rhenium molecular probe colocalising with LysoTracker® green vesicles (Figure 4.8A-4.8B^{II}), but while there were similar numbers of these compartments (Figure 4.9), the compartment size was reduced in the *Atg9*^{RNAi} pupae (Figure 4.8B-4.8B^{II}) when compared to the controls (Figure 4.8A-4.8A^{II}).

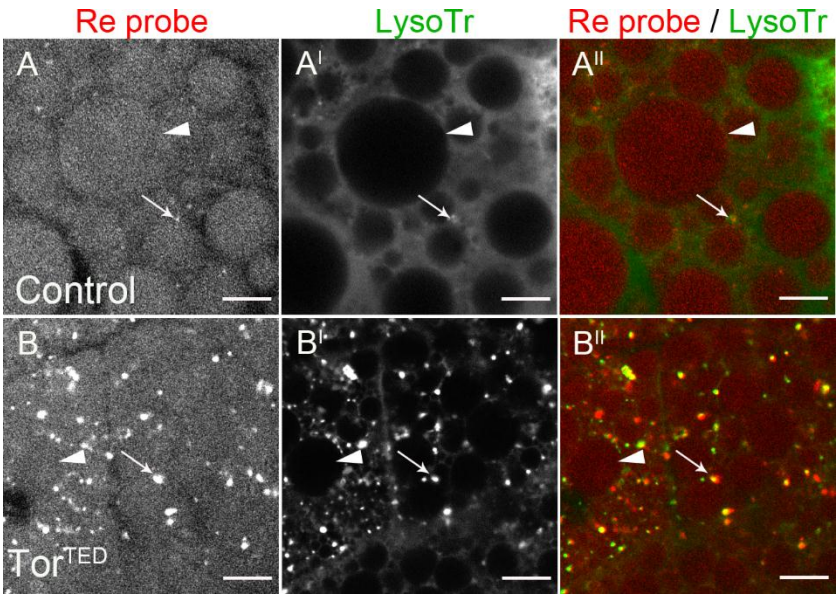


Figure 4.6 The Rhenium molecular probe localised to acidic compartments when autophagy was induced by the inhibition of TOR.

Confocal micrographs of *Drosophila* fat body tissue from larvae at -8h PF larvae on standard feeding medium, stained with the Rhenium molecular probes (grey scale in A and B; red in A^{II} and B^{II}) and LysoTracker® green (grey scale in A^{I} and B^{I}; green in A^{II} and B^{II}). Representative images from controls (A-A^{II}) or TOR^{TED} (B-B^{II}) larvae. Arrowheads indicate lipid droplets, arrows indicate Rhenium molecular probe localised to LysoTracker® green positive compartments. Scale bars = 10 µm.

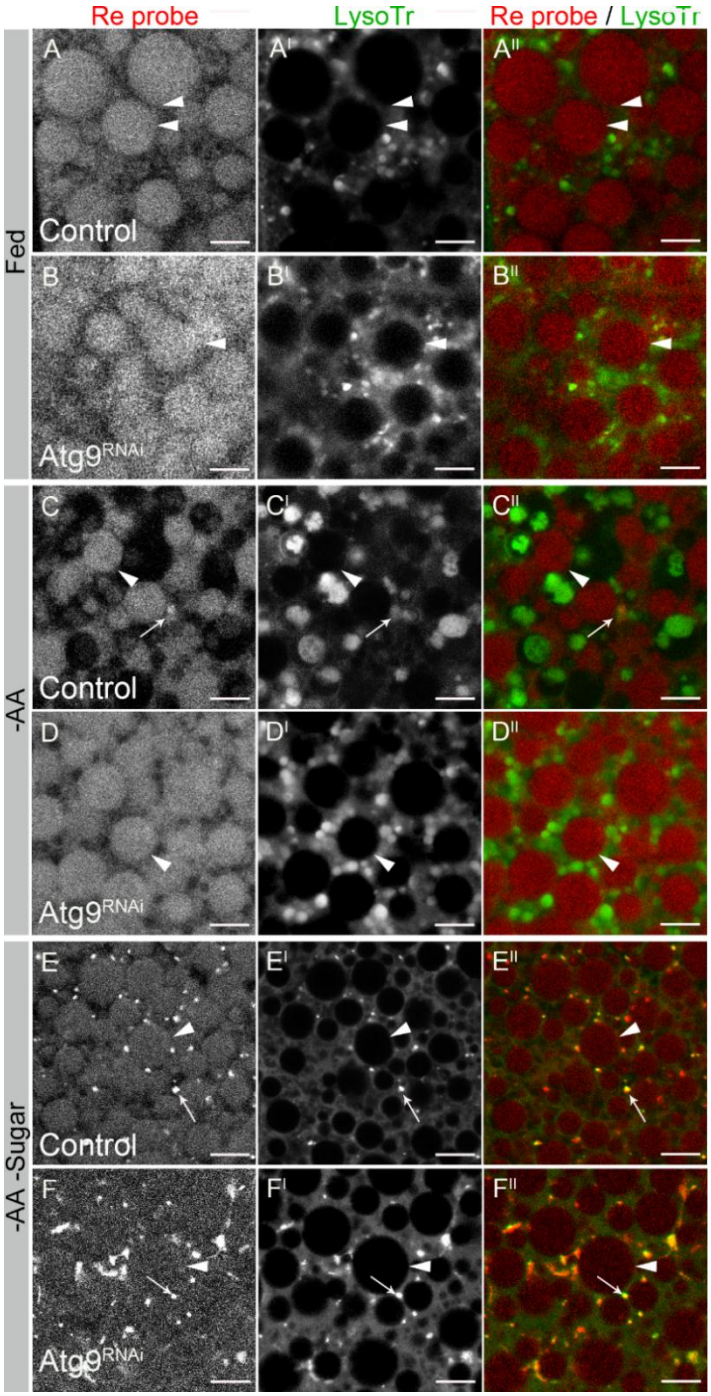


Figure 4.7 Reduced autophagy by Atg9 RNAi silencing was detected with the Rhenium molecular probe.

Confocal micrographs of *Drosophila* fat body tissue from larvae at -4h PF, incubated with the Rhenium molecular probe (grey scale in A, B, C, D, E and F; red in A^{II}, B^{II}, C^{II}, D^{II}, E^{II} and F^{II}) and LysoTracker® green (Grey scale in A^{I}, B^{I}, C^{I}, D^{I}, E^{I} and F^{I}; green in A^{II}, B^{II}, C^{II}, D^{II}, E^{II} and F^{II}). Fat body tissue from -4h PF larvae on standard feeding medium control (A-A^{II}), or $Atg9^{RNAi}$ (B-B^{II}); -4h PF larvae deprived of amino acids for 4h control (C-C^{II}), or $Atg9^{RNAi}$ (D-D^{II}); -4h PF larvae starved for 4h (-amino acids, -sugar) control (E-E^{II}) or $Atg9^{RNAi}$ (F-F^{II}). Arrowheads indicate lipid droplets, arrows indicate Rhenium molecular probe localised to LysoTracker® green positive compartments. Scale bars = 10 µm.

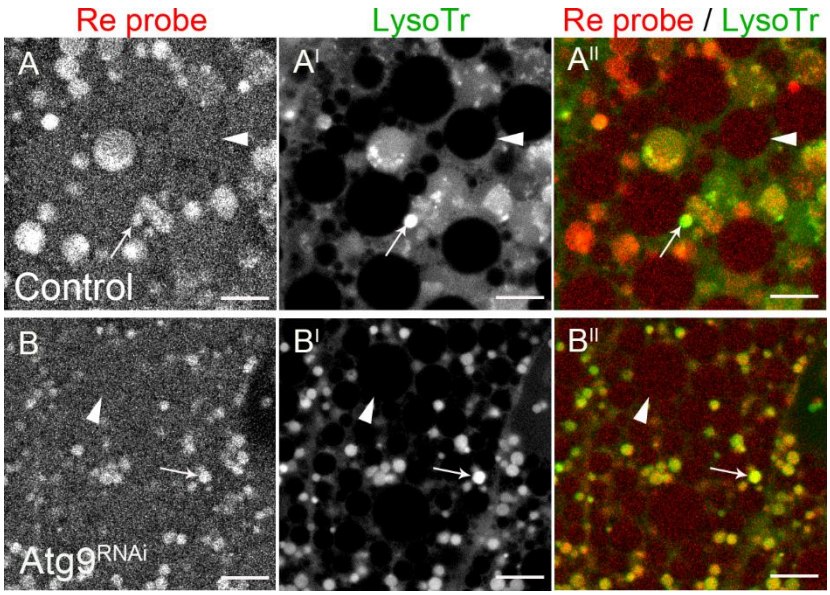


Figure 4.8 Altered developmental autophagy by Atg9 RNAi silencing was detected with the Rhenium molecular probe.

Confocal micrographs of *Drosophila* fat body tissue from pupae at +2h PF, incubated with Rhenium molecular probe (grey scale in A and B; red in A^{II} and B^{II}) and LysoTracker® green (Grey scale in A^{I} and B^{I}; green in A^{II} and B^{II}). Representative images from control (A-A^{II}) or $Atg9^{RNAi}$ (B-B^{II}) pupae. Arrowheads indicate lipid droplets, arrows indicate Rhenium molecular probe localised to LysoTracker® green positive compartments. Scale bars = 10 µm.

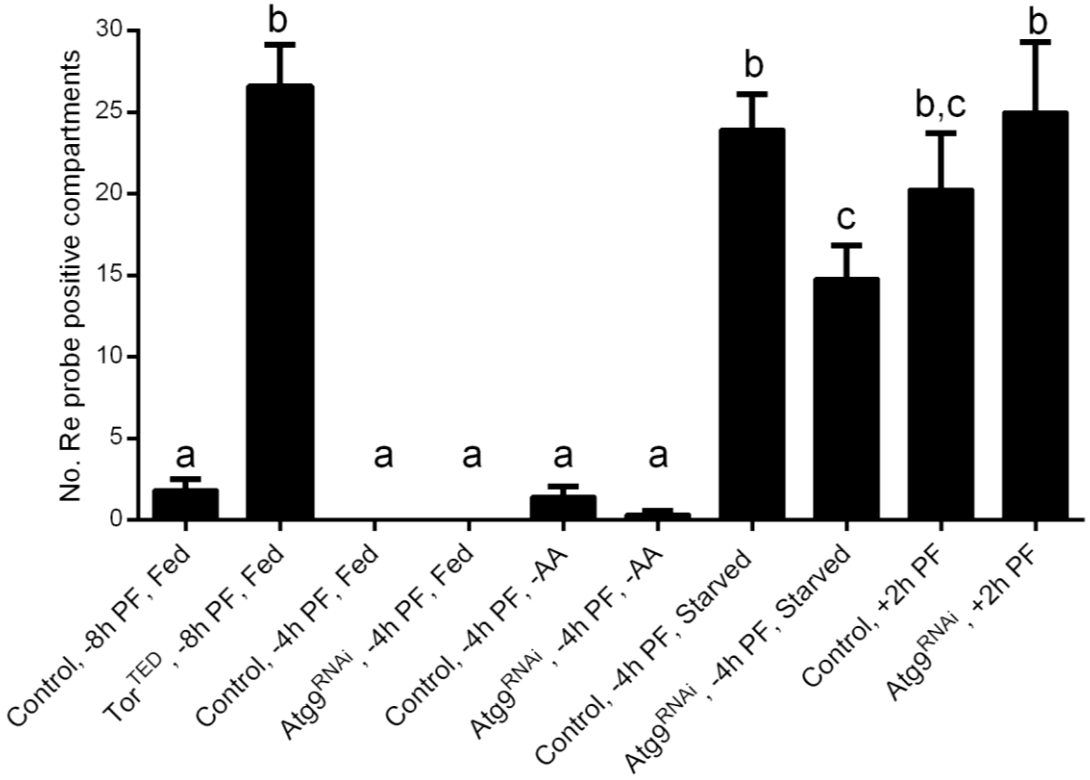


Figure 4.9 Quantification of Rhenium molecular probe and LysoTracker® positive compartments during starvation and development.

Histogram showing the number of Rhenium molecular probe and LysoTracker® green positive compartments, present in fat body tissues. Fat body tissue from -8h PF larvae on standard feeding medium, controls (Control, -8h FP, Fed) or TOR^{TED} (TOR^{TED}, -8h FP, Fed); -4h PF larvae on standard feeding, controls (Control, -4h FP, Fed), or $Atg9^{RNAi}$ ($Atg9^{RNAi}$, -4h FP, Fed); -4h PF larvae deprived of amino acids for 4h, controls (Control, -4h PF, -AA) or $Atg9^{RNAi}$ ($Atg9^{RNAi}$, -4h PF, -AA); -4h PF larvae starved for 4h (-amino acids, -sugar), controls (Control, -4h PF, Starved) or $Atg9^{RNAi}$ ($Atg9^{RNAi}$, -4h PF, Starved) or pupae at +2h PF, controls (Control, +2h PF) or $Atg9^{RNAi}$ ($Atg9^{RNAi}$, =2h PF). Results are presented as the mean ± s.e.m. (n=10), treatments compared by ANOVA with Tukey post-hoc test, different letters indicates significance difference between means, $P < 0.05$.

4.5.5 The Rhenium molecular probe interacted with specific lipids.

In overlay experiments the Rhenium molecular probe interacted with monosialoganglioside (GM1), sphingomyelin and sphingosine (Figure 4.10). The probe also interacted with phosphatidylethanolamine (PE), lysophosphatidic acid, cholesterol and progesterone, but the affinity of the interaction appeared to be reduced when compared with the three lipids above (Figure 4.10). No interaction was detected between the Rhenium molecular probe and ceramide, triacylglycerol's (for which a mixture containing 5 species was tested), fatty acid species, palmitic acid or esterified cholesterol, cholesteryl acetate (Figure 4.10).

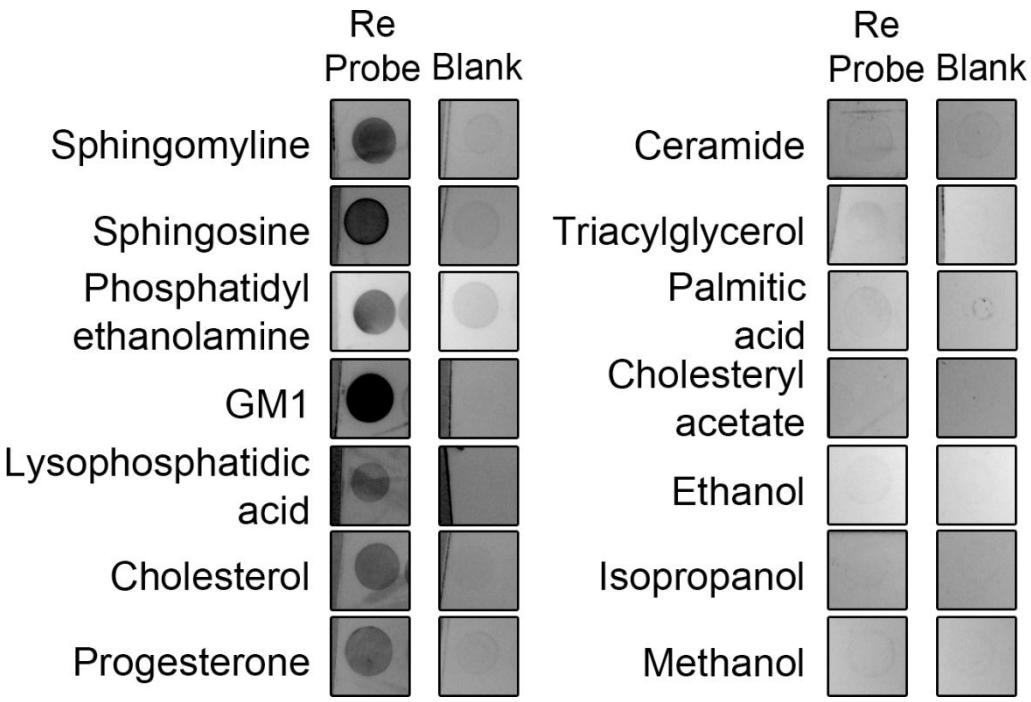


Figure 4.10 The Rhenium molecular probe interacted with specific lipids

Rhenium molecular probe-lipid overlay, showing an interaction between the Rhenium molecular probe (Re Probe) and seven lipid species on the left and no interaction with four lipid species on the right or controls (ethanol, isopropanol or methanol). Blank shows detection of lipid background, without Rhenium molecular probe incubation.

4.6 Discussion

Cells utilise lipid droplets as a storage site for excess lipids, which are usually sequestered as triglycerides and sterol esters. Lipid droplets act as a critical energy source for cells during high demand or nutrient deprivation and also isolate potentially toxic lipids from other metabolic processes. Autophagy has a pivotal role in lipid localisation, orchestrating the vesicular trafficking and secretion of triglyceride rich lipoproteins, as well as mediating the transient storage of lipids in lipid droplets (Ouimet, 2013; Pan et al., 2008). Autophagosomes can also recruit lipids for membrane expansion (Dupont et al., 2014) and have a specific role in lipid degradation and the fuelling of energy generating pathways involving β-oxidation in mitochondria (Singh and Cuervo, 2012). The dynamic balance between lipid droplets and autophagosomes therefore has a fundamental role in lipid homeostasis, energy metabolism and cellular function.

In addition to lipids in the form of triacylglycerol and sterol esters, lipid droplets also contain free fatty acids, cholesterol, shingolipids and phospholipids, as well as lipases and other proteins (Bartz et al., 2007). A number of methods have been developed to detect lipid droplets in cells, and these rely mainly on either dyes or molecular probes that interact with core lipids in these vital organelles. For example, the two most common dyes used to detect lipid droplets are the phenoxazone dye, Nile red, which has been used for the fluorescent detection of neutral lipids (Gocze and Freeman, 1994; Greenspan et al., 1985) and the lysochrome or fat soluble diazo dye Oil Red O, which detects neutral triacylglycerols (Andersson et al., 2006; Spangenburg et al., 2011). The Rhenium(I) tricarbonyl diimine complex that was investigated here interacted with a molecular constituents of lipid droplets that were evenly distributed throughout the matrix of the lipid droplets. Unlike other lipid droplets stains, the Rhenium molecular probe did not

interact *ex vivo* with the core lipid components triacylglycerols or cholesterol esters. The molecular probe was shown to interact with other lipid species that are associated with lipid droplets including; sphingolipids, sphingosine, sphingomyelin and ganglioside, monosialodanglioside (GM1); phospholipid, phosphotidalyethanolamine (PE) and the phospholipid derivative lysophosphatidic acid (LPA); as well as, cholesterol and its sterol derivative progesterone (Atshaves et al., 2000; Bartz et al., 2007; Grillitsch et al., 2011; McIntosh et al., 2010; Tauchi-Sato et al., 2002). There was some variation in the degree of Rhenium molecular probe interaction with the lipid species, and this may have been a result of the ethanol washes, as some lipids are more soluble in ethanol, thus we cannot comment on the affinity of the interaction by this method. Although a number of the lipid species detected by the molecular probe are also major constituents of biological membranes (Bartz et al., 2007; Chiantia and London, 2013; Grillitsch et al., 2011; Maxfield and van Meer, 2010; Tauchi-Sato et al., 2002), *in vivo* the dye did not appear to associate directly with biological membranes. This suggested the Rhenium molecular probe does not primarily interact with these lipids via the polar head group, which would be exposed when these lipids are present in membranes.

The dynamic relationship that is emerging between lipid droplets and autophagy appears to be central in key cell biological processes like energy sensing and metabolism (Singh and Cuervo, 2012). The fundamental interactions that have already been elucidated include: the transfer of membrane constituents from lipid droplets to facilitate autophagosome formation and biogenesis (Dupont et al., 2014); the transfer of neutral lipids, triacylglycerols and cholesterol esters to autophagosomes as a substrate; the control of intracellular lipid content to maintain membrane composition and energy/metabolic pathways (Atshaves et al., 2000; Ouimet et al., 2011; Singh et al., 2009a); and complete

lipid droplet organelle turnover by autophagosomes (Eid et al., 2013; Singh et al., 2009a; Yang et al., 2014). The Rhenium tetrazolato complex acted as a molecular probe that was detected in both lipid droplets and autophagosomes, and this was evident at specific developmental time-points and in response to a number of conditions that induced autophagy. The Rhenium molecular probe was detected in lipid droplets, in *Drosophila* fat body tissue, as well as the autophagosomes-autolysosomes at the developmental stage of two hours following puparium formation, when autophagy is upregulated by prolonged starvation and hormonal cues (Butterworth et al., 1988; Rusten et al., 2004). Similarly, in response to either, combined glucose and amino acid starvation, or the inactivation of the target of Rapamycin (TOR^{TED}), the Rhenium molecular probe localised to autophagosomes-autolysosomes, as well as lipid droplets. This indicated that the Rhenium molecular probe might be a reporter for a specific event during the interaction of lipid droplets and autophagosomes.

The Rhenium molecular probe predominately interacted *ex vivo* with lipid species that are associated with lipid membranes, which could suggest that membrane expansion events may be detected by the molecular probe. The molecular target for the Rhenium molecular probe *in vivo*, however, did not appear to be involved in autophagosome formation, as under conditions of either amino acid or sugar deprivation, autophagosomes were formed, but there was little or no molecular probe interaction with these autophagosomes. The Rhenium molecular probe did, however, associate with autophagosomes under conditions of extreme starvation (combined amino acid and sugar starvation), during larval to adult development (+2h PF), and when autophagy was induce, by the inhibition of TOR signalling. The detection of the Rhenium molecular probe in autophagosomes, coincided with the detection of neutral lipids in the autophagosomes by Oil Red O stain, suggesting

that lipid droplets were being sequestered as a substrate for autophagy under these conditions. However, the Rhenium molecular probe did not appear to interacting with the neutral lipid components of the lipid droplets as there were differences in the cellular distribution of Oil Red O and the Rhenium molecular probe; although both were detected in autophagic compartments under the above mentioned conditions. This is in line with observations in mouse hepatocytes, where prolonged starvation and inhibition of TOR increased the lipid content of autophagosomes and the association between autophagosomes and lipid droplets (Singh et al., 2009a). This suggested that the Rhenium molecular probe may be used to specifically detect lipophagy, but not other general forms of autophagy.

It is possible that the Rhenium molecular probe detected an increase in lipid content in the autophagosomes, which could be derived from sources other than the lipid droplet. The inclusion of lipid droplets into autophagosomes can occur together with the inclusion of lipid membranes, for example from other organelles and the plasma membrane, resulting in increased levels of cholesterol, sphingolipids and GM1 in autophagosomes (Yang et al., 2014). It is unclear in *Drosophila* fat body, if lipid membrane content in autophagosomes is increased under certain conditions, however this may be an alternative explanation for the detection of the Rhenium molecular probe in autophagic compartments. There is also increasing evidence that autophagy is utilized for the regulation of cellular cholesterol and sphingolipid species (Alexaki et al., 2014; Cheng et al., 2006; Lajoie et al., 2005; Liao et al., 2007; Lieberman et al., 2012; Ouimet, 2013; Ouimet et al., 2011; Pacheco and Lieberman, 2008), however it remains to be seen if the Rhenium molecular probe is able to detect autophagy mediated efflux of these lipid species.

Down regulation of autophagy by genetic or pharmacological inhibition, reduces lipid transfer to autophagosomes (Kaushik et al., 2011; Singh et al., 2009a). In Atg9 knock-down tissues, there was a reduction in the number of autophagic compartments positive for the Rhenium molecular probe following larval exposure to complete starvation. This suggested that autophagic machinery is required for lipid transfer, and this decreases in the number of lipid containing autophagosomes could be detected by the Rhenium molecular probe. Furthermore, Atg9 depletion resulted in smaller autophagic compartments detected by the Rhenium molecular probe during metamorphosis (at +2h PF), when compared to controls. This was consistent with results reported in Chapter 2 for Atg9 depletion during puparation. The number of autophagic compartments detected in Atg9 depleted cells at +2h PF, however, was not reduced as was seen at 0h PF (as reported in Chapter 2), this may indicate an accumulation of un-degraded autolysosomes, as we suspected there is impaired maturation of autophagosomes in Atg9 depleted tissues.

Protonation of the Rhenium molecular probe is possible at the tetrazylatoe ring, and the protonated species is more emissive and has a blue emissions shift, when compared to the non-protonated species (Werrett et al., 2013). When detected in acidic compartments, *in vivo*, we also demonstrated that the Rhenium molecular probe had an increased emission and a blue shift in spectral profile, when compared to its profile in lipid droplets. Thus, this Rhenium molecular probe may act as a pH sensor, as well as a lipid dye, making it an ideal tool to distinguish between lipid stores and lipids localised in acidified compartment such as lysosomes and autolysosomes.

The bidirectional interactions between autophagy and lipid metabolism have important implications for disease pathophysiology and there is a defined need to image these

processes (Liu and Czaja, 2013). Consequently, the Rhenium molecular probe described here could be used to visualise the pathogenic process in for example: the altered lipid metabolism associated with fatty liver disease; the increased autophagy and altered degradation of lipids observed in Alzheimer's disease; the altered cholesterol deposition and plaque formation in cardiovascular disease; or the altered balance between lipid metabolism and autophagy in cancer. Therefore the Rhenium molecular probe could provide a promising new tools for live cell imaging for both the research into and diagnosis of such pathologies.

Chapter 5: General discussion

Autophagy plays a critical role in the turnover of cytoplasmic content, by delivering cellular constitutes to endosomes and lysosomes for degradation (Colombo and Simon, 2009; Jia and Sowers, 2014; Kundu and Thompson, 2008; Mehrpour et al., 2010). Autophagy also has important roles in energy metabolism and has recently been identified to function in lipid metabolism (Singh and Cuervo, 2012). For example, lipids stored in lipid droplets can be targeted by autophagosomes to liberate lipids for energy generation during metabolic stress (Singh et al., 2009a). Additionally, autophagy functions to maintain the cellular lipid content in different cellular pools and has been shown to have a role in controlling the amount of sphingolipid, ganglioside, sterol and phospholipid (Alexaki et al., 2014; Ouimet, 2013; Ouimet et al., 2011; Zhou et al., 2002). These lipids have structural roles, but also function in autophagy signalling and regulation, providing cells with a feedback mechanism for autophagy mediated lipid regulation (Dall'Armi et al., 2013; Xu et al., 2010). Phospholipids and sphingolipids are important for membrane formation during autophagosome biogenesis (Dall'Armi et al., 2013; Dupont et al., 2014; Sims et al., 2010), however, the source of these lipids and the autophagic machinery that governs this early step in autophagy remains an area of debate in the field (Lamb et al., 2013b).

Sphingolipids, gangliosides, sterols and phospholipids are important regulatory and signalling molecules, participating in a range of cellular processes; including cell growth, proliferation, differentiation, survival, apoptosis, inflammation, motility and membrane homeostasis (Breslow and Weissman, 2010; Huang and Freter, 2015). The maintenance of cellular lipid composition is therefore critically important for normal cellular homeostasis, with altered lipid efflux via lysosomes observed in a range of neurodegenerative and metabolic disorders (Pan and Yue, 2014; Parkinson-Lawrence et al., 2010; Shimada and

Klionsky, 2012; Tan et al., 2014; Winslow et al., 2010; Wolfe et al., 2013). Although a number of important links between autophagy and lipids have been identified, the details of these interactions remains unclear. One of the biggest challenges facing research in this field is a lack of tools for the detection of lipids in live cells, leading to a dependence on protein centred approaches, which make assumptions about protein function that are not always clearly defined.

Atg9 is the only transmembrane protein involved in the core autophagic machinery and is generally accepted to function during initial membrane recruitment and phagophore formation (Shibutani and Yoshimori, 2014). In yeast, Atg9 is essential for autophagosome formation, with the fusion of Atg9 vesicles at the PAS contributing to the initial phagophore membrane (Papinski et al., 2014; Yamamoto et al., 2012). The function of Atg9 in autophagosome formation is less crucial in higher eukaryotes, where the loss of Atg9 reduces, but does not completely abrogate, autophagosome formation. Furthermore, Atg9 associates with early autophagic structures, but does not become incorporated into the autophagosome membrane (Orsi et al., 2012; Saitoh et al., 2009). Following the induction of autophagy, Atg9 has been shown to redistribute to peripheral sites, including late endosomes, an observation that has previously been attributed to a role in membrane recruitment to the forming autophagosome (Longatti et al., 2012; Orsi et al., 2012; Young et al., 2006). We have shown that Atg9 is also required for the presence of intraluminal vesicles in amphisomes and autolysosomes, leading us to question if Atg9 has an alternate function at the late endosome. Atg9 could facilitate the recruitment of the molecular machinery that is required for intraluminal vesicular formation either at the late endosome, to form multivesicular endosomes or at the amphisome-autolysosome following endosome fusion. During autophagy initiation, Atg9 has been shown to be involved in the

recruitment of a range of molecular machinery including tethering proteins, Rab trafficking proteins and autophagy proteins (Kakuta et al., 2012; Papinski and Kraft, 2014; Papinski et al., 2014; Wang et al., 2013), and it may play a similar role at the late endosome or amphisome-autolysosome.

Although intraluminal vesicle formation has not previously been reported in autophagosomes a number of studies have shown that the ESCRT machinery, which is responsible for intraluminal vesicle formation in late endosomes (Wollert and Hurley, 2010), is required for autophagosome maturation (Fader and Colombo, 2009; Manil-Segalen et al., 2012; Rusten et al., 2007). The function of ESCRT complexes during autophagosome maturation has been a matter of debate, with the assumption that intraluminal vesicle formation does not occur as part of the autophagic maturation process (Manil-Segalen et al., 2012; Rusten and Stenmark, 2009). Observations here, however, indicate that intraluminal vesicles are present in amphisomes and autolysosomes of *Drosophila* fat body cells. The presence of endosomal and autophagic markers on these intraluminal compartments could suggest that vesicles form following autophagosome-endosome fusion, possibly explaining the functional role of the ESCRT machinery during autophagosome maturation. Intraluminal vesicle formation in the autophagosome may facilitate cargo sorting, in a manner similar to late endosomes. Cargo sorting may be necessary for autophagosomes, as not all proteins targeted by autophagy are destined for lysosomal degradation and autophagy can also act as a trafficking pathway for proteins such as, interleukins and lipoproteins (Deretic et al., 2012; Ouimet, 2013; Pan et al., 2008). Intraluminal vesicles may also be important in establishing local pH gradients, as variations in intraluminal acidity were detected by LysoTracker® following Atg9 depletion. This localised acidification may facilitate the degradation of specific cargo that

is not destined for a trafficking pathway. The reduced intraluminal vesicle formation and its effect on acidification were associated with altered degradation of larval tissue during *Drosophila* metamorphosis. Further investigation into the nature of these intraluminal vesicles is required to fully elucidate their role in autophagosome maturation and autolysosome degradation and to define the site and the molecular machinery involved in of the formation of these vesicles.

During *Drosophila* development, autophagy is important for the degradation and remodelling of larval tissue, but may also function in lipid mobilization from lipid droplets. The fat body is the major tissue for lipid storage and during larval development large amounts of lipids accumulate in lipid droplets, which can then be mobilized to provide energy or structural lipids to the developing tissues during metamorphosis (Gronke et al., 2007; Kuhnlein, 2012). The mobilization of lipids during metamorphosis is in part facilitated by lipases, such as lipid droplet associated Brummer and lysosomal acid lipase-1, the expression of which are induced by the insect steroid hormone ecdysone (Grönke et al., 2005; Gronke et al., 2007; Hossain et al., 2013; Wang et al., 2010). The involvement of lysosomal associated lipases and the identification of autophagy as a route for lipid delivery to the lysosome (Singh et al., 2009a) has led to the speculation that lipophagy has an important function during *Drosophila* metamorphosis (Nezis, 2012; Tracy and Baehrecke, 2013). We have detected lipids in autophagosomes of pupal fat body cells, providing the first evidence to support a function for autophagy in lipid mobilization during development. In autophagosomes and autolysosomes, we detected both neutral lipids by Oil Red O staining, as well as polar lipid species by the newly described molecular probe: tricarbonyl diimine Rhenium(I) complex. Autophagy induction in larvae by TOR suppression or by complete starvation also resulted in the

detection of lipids in autophagosomes-autolysosomes. This suggested that lipophagy may regulate lipid mobilization in *Drosophila* fat body during development, but may also have a role in energy maintenance during times of extreme nutrient deprivation.

Lipid droplets store lipids primarily in the form of neutral lipids, triacylglyerols and sterol esters, but can also contain a number of polar lipids (Bartz et al., 2007). The Rhenium molecular probe described in Chapter 4 (complex **1**), was shown *ex vivo* to interact with polar lipids, but did not interact with neutral lipids. The interaction of complex **1** therefore differs from many of the existing lipid droplet dyes, which interact with neutral lipids in lipid droplets (Andersson et al., 2006; Gocze and Freeman, 1994; Greenspan et al., 1985; Spangenburg et al., 2011). Complex **1** interacted with sphingosine, sphingomyelin and monosialoganglioside (GM1), phosphatidylethanolamine (PE), lysophosphatidic acid, cholesterol and the cholesterol derived hormone progesterone (Figure 5.1). Other sphingolipids, gangliosides, phospholipids and cholesterol species, that were not assessed here, may also interact with this complex. Polar lipids can be detected in lipid droplets, however, they are thought to exist predominately in cells as a component of membranes (Lingwood and Simons, 2010; Suetsugu et al., 2014). Complex **1** did not appear to interact with membranes *in vivo* and this could indicate that the membrane structure interferes with the interaction between complex **1** and polar lipids. Autophagosomes have been shown to sequester polar lipids including sphingolipid, gangliosides, phospholipids and cholesterol to maintain the cellular homeostasis of these lipids (Alexaki et al., 2014; Cheng et al., 2006; Lajoie et al., 2005; Liao et al., 2007; Lieberman et al., 2012; Ouimet, 2013; Ouimet et al., 2011; Pacheco and Lieberman, 2008). It is therefore possible that the polar lipids detected by complex **1** in autophagosomes, were derived from membranes as well as sequestration from lipid droplets. This could involve increased membrane turn-over by

autophagosomes during *Drosophila* development and in response to complete starvation or inhibition of TOR.

Initial results for a second tricarbonyl diimine Rhenium(I) complex described in Chapter 3 (complex **2**), demonstrated a localisation to acidic compartments. This distribution was attributed to the basic nature of this molecule, and this is a characteristic of many acidotrophic dyes (Bader et al., 2014; Pierzynska-Mach et al., 2014). Recently obtained results suggested that complex **2** also had an affinity for polar lipids, in lipid over lay experiments (Figure 5.1). Under these test conditions complex **2** appeared to have a higher affinity to GM1 then other lipids tested, however, further testing is required to determine the strength of interaction between the complex and particular lipid species. Polar lipids including GM1 are constitutively degraded via the endosome-lysosome pathway (Kolter and Sandhoff, 1999), and thus the subcellular localisation of complex **2** to acidic compartments, which could include late endosomes and lysosomes, may relate to the detection of polar lipids trafficked for degradation by the lysosome. Like complex **1**, complex **2** did not appear to detect membranes, where the majority of cells polar lipids are contained (Ledeen and Wu, 2011; Sandhoff and Harzer, 2013). This is consistent with the hypothesis that these Rhenium complexes do not interact with polar lipids via their exposed head group.

Dysregulation of autophagy and the accumulation of lipids in lysosomes is observed in a number of human diseases including, a range of neurodegenerative diseases and metabolic disorders (Pan and Yue, 2014; Parkinson-Lawrence et al., 2010; Shimada and Klionsky, 2012; Tan et al., 2014; Winslow et al., 2010; Wolfe et al., 2013). For example, increased amounts of sphingolipids, gangliosides and cholesterol have been reported in endosomal-

lysosomal compartments for lysosomal storage disorders (Parkinson-Lawrence et al., 2010), Alzheimer's disease (Wood et al., 2014; Yang et al., 2014), Huntington's disease (Karasinska and Hayden, 2011) and Parkinson's disease (de Lau et al., 2006). These diseases also display altered autophagosome maturation, but it is unclear as to how these pathologies contribute to disease progression (Lieberman et al., 2012; Tan et al., 2014). In lysosomal storage disorders the storage of lipids results in neurodegenerative disease, and it is thought that autophagy may be up regulated to compensate for lysosomal dysfunction (Pacheco et al., 2007), but this may also result from altered autophagosome maturation (Cheng et al., 2006; Ko et al., 2005; Liao et al., 2007; Sarkar et al., 2013). Understanding the mechanisms that govern the interactions between lipids, autophagy and lysosomes will provide insight into these and other human diseases. The Rhenium base complexes described herein could provide investigators with new information about these interactions as well as potential diagnostic tools.

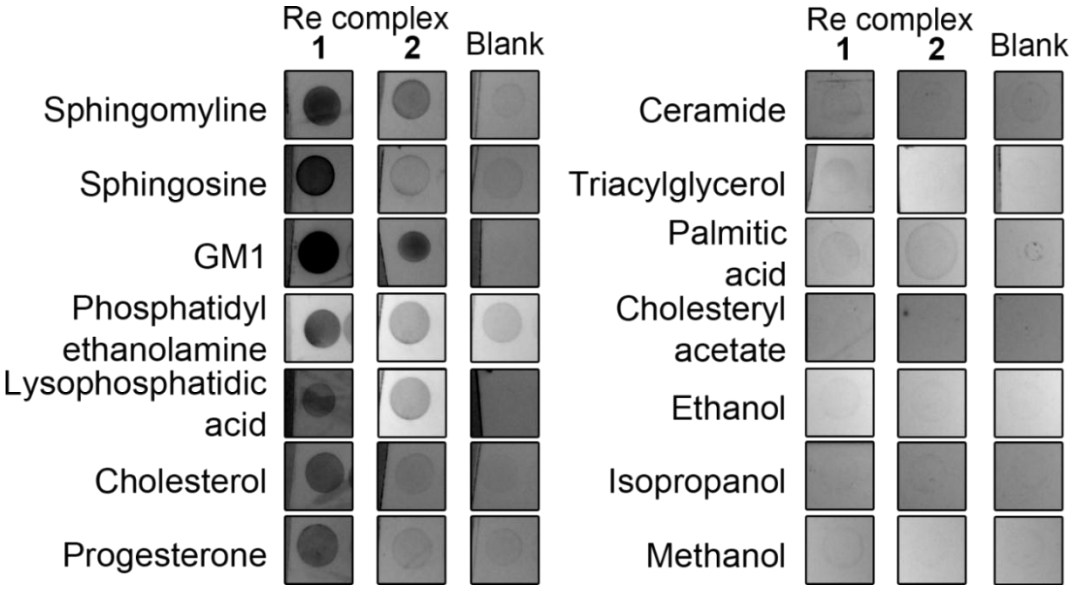


Figure 5.1 The Rhenium tetrazolate complexes 1 and 2 had an affinity for polar lipids

Rhenium molecular probe-lipid overlay, showing the affinity of complex **1** and **2** for eleven lipid or controls (ethanol, isopropanol or methanol). Blank shows detection of lipid background, without incubation with the Rhenium molecular probe.

The tricarbonyl diimine Rhenium(I) complexes have the potential to be further developed as lipid specific probes for use in research and diagnosis for lipid related pathologies. The tools currently available for the investigation of polar lipid species are primarily based on fluorescent labelled analogues, but their behaviour does not always match that of the endogenous lipids (Steck et al., 2013). Filipin is one of the few stains available for the detection of polar lipids and is widely used for the detection of cholesterol. The mode of interaction between filipin and cholesterol has not been defined and recent studies have demonstrated that it interacts with GM1 and GM2 gangliosides with higher affinity than cholesterol, thus conclusions based on filipin staining must take into account these other interactions (Arthur et al., 2011; Hannich et al., 2011; Maxfield and Wüstner, 2012). Moreover, filipin and other compounds detecting polar lipids can be cytotoxic and require cell fixation before staining, making these dyes incompatible with live cell imaging (Gimpl, 2010). The Rhenium based complexes had little or no detectable cytotoxicity and were suitable for live cell imaging (Bader et al., 2014). We also showed that the sub-cellular distribution of the Rhenium based complexes could be modulated by changing the tetrazolato ligand complexed to the tricarbonyl Re(I) diimine core. Variations in the tetrazolato ligand may facilitate the interaction of these modified complexes with specific lipid species, and therefore, there is a potential to develop a range of lipid dyes based on the tricarbonyl Rhenium(I) diimine core. These complexes may also be developed to have targeted applications in disease treatment, using the photodynamic properties of the molecular probes to develop them as therapeutics. For example, Rhenium(I) indolato complexes have been shown to induce cell death in cancer cells upon photoactivation, however, a related class of compounds the Rhenium(I) tricarbonyl polypyridine complexes did not elicit an apoptotic response (Kastl et al., 2013); indicating that small variations in Rhenium based complexes can dramatically alter the bioactivity of these

compounds. Although initial results indicated that the tricarbonyl Rhenium(I) diimine complexes do not have cytotoxic effects, the photodynamic properties of the molecular probes have not been fully characterised and cancer cells are yet to be investigated with these complexes. Photodynamic therapies are a promising alternative to conventional chemotherapy as they could provide spatially controlled cytotoxicity and a low risk of developing resistance (Dolmans et al., 2003).

The tricarbonyl diimine Rhenium(I) complexes may also function as molecular biosensors, which are able to detect changes in local pH. When localised to acidified compartments complex **1** had an increase in fluorescence intensity and the emission profile showed a blue shift. These altered photo-physical properties, upon detection in acidic compartments, was consistent with changes observed upon protonation of this complex in solution (Werrett et al., 2013). Thus, it is possible that acidic conditions within autolysosomes leads to the protonation of complex **1**, altering its emission profile. It is yet to be determined if the same spectral shift is achieved with other Rhenium complexes and further spectral profiling of complex **1** is required in order to define the pH-dependent optical properties. Initial results indicate that complex **1** could provide a tool for assessing compartment acidity as well as lipid content, which would have direct applications for the investigation of pathologies that present upon lipid accumulation in lysosomes and autolysosomes.

It is likely that other factors besides lipid affinity influence the subcellular distribution of the Rhenium molecular complexes. Although both complex **1** and **2** had an affinity for polar lipids, the cellular detection of the two complexes differed dramatically. Complex **1** is a neutral complex and appeared to interact more strongly *ex vivo* with a range of lipids

and this may contribute to its localisation to the more lipophilic, lipid droplets under normal cellular conditions. The more hydrophobic nature of complex **1** may also allow the complex to diffuse across the plasma membrane with a mode of cellular entry that has been shown for other charge neutral, Rhenium complexes (Balasingham et al., 2012a). Complex **2**, by comparison is more basic and this may contribute to its lysosomal distribution, but may also mean that the complex has an alternate mode of cellular entry. Metal complexes can enter cells via endocytosis, which may result in their detection in endosomes and lysosomes (Coogan and Fernandez-Moreira, 2014). Interestingly viral interaction with GM1 at the cell surface can induce the endocytosis of the virus (Ewers et al., 2010), and it is therefore possible that the Rhenium based complexes induced their own endocytosis via interaction with GM1 or with other lipid signalling molecules at the cell surface. Future studies plan to define the mode of cellular entry for these different Rhenium molecular complexes so that we may better understand the cellular behaviour of these molecular probes.

Preliminary results indicate that the modification of the chemical structure of tricarbonyl diimine Rhenium(I) complex can lead to specific organelle targeting and potentially enable the development of lipid targeting probes for live cell imaging. This is the first investigation of tricarbonyl diimine Rhenium(I) complexes with a tetrazolato ligand as molecular probes, and provides initial information for the rational based design of other related complexes. Finally, complex **1** has shown significant promise for the investigation of lipid specific autophagy, which is emerging as an important regulatory mechanism in metabolic and other disease progression (Lieberman et al., 2012; Singh and Cuervo, 2012).

Reference

Alexaki, A., S.D. Gupta, S. Majumder, M. Kono, G. Tuymetova, J.M. Harmon, T.M. Dunn, and R.L. Proia. 2014. Autophagy regulates sphingolipid levels in the liver. *Journal of Lipid Research*. 55:2521-2531.

Amoroso, A.J., R.J. Arthur, M.P. Coogan, J.B. Court, V. Fernandez-Moreira, A.J. Hayes, D. Lloyd, C. Millet, and S.J.A. Pope. 2008. 3-Chloromethylpyridyl bipyridine fac-tricarbonyl rhenium: a thiol-reactive luminophore for fluorescence microscopy accumulates in mitochondria. *New Journal of Chemistry*. 32:1097-1102.

Amoroso, A.J., M.P. Coogan, J.E. Dunne, V. Fernandez-Moreira, J.B. Hess, A.J. Hayes, D. Lloyd, C. Millet, S.J.A. Pope, and C. Williams. 2007. Rhenium fac tricarbonyl bisimine complexes: biologically useful fluorochromes for cell imaging applications. *Chemical Communications*. 3066-3068.

Andersson, L., P. Boström, J. Ericson, M. Rutberg, B. Magnusson, D. Marchesan, M. Ruiz, L. Asp, P. Huang, M.A. Frohman, J. Borén, and S.-O. Olofsson. 2006. PLD1 and ERK2 regulate cytosolic lipid droplet formation. *Journal of Cell Science*. 119:2246-2257.

Andres, A.J., and C.S. Thummel. 1994. Methods for quantitative analysis of transcription in larvae and prepupae. *Methods in Cell Biology*. 44:565-573.

Arstila, A.U., and B.F. Trump. 1968. Studies on cellular autophagocytosis. The formation of autophagic vacuoles in the liver after glucagon administration. *The American Journal of Pathology*. 53:687-733.

Arthur, J.R., K.A. Heinecke, and T.N. Seyfried. 2011. Filipin recognizes both GM1 and cholesterol in GM1 gangliosidosis mouse brain. *Journal of Lipid Research*. 52:1345-1351.

Asha, H., I. Nagy, G. Kovacs, D. Stetson, I. Ando, and C.R. Dearolf. 2003. Analysis of Ras-induced overproliferation in Drosophila hemocytes. *Genetics*. 163:203-215.

Atshaves, B.P., O. Starodub, A. McIntosh, A. Petrescu, J.B. Roths, A.B. Kier, and F. Schroeder. 2000. Sterol carrier protein-2 alters high density lipoprotein-mediated cholesterol efflux. *The Journal of Biological Chemistry*. 275:36852-36861.

Babst, M. 2011. MVB vesicle formation: ESCRT-dependent, ESCRT-independent and everything in between. *Current Opinion in Cell Biology*. 23:452-457.

Bader, C.A., R.D. Brooks, Y.S. Ng, A. Sorvina, M.V. Werrett, P.J. Wright, A.G. Anwer, D.A. Brooks, S. Stagni, S. Muzzioli, M. Silberstein, B.W. Skelton, E.M. Goldys, S.E. Plush, T. Shandala, and M. Massi. 2014. Modulation of the organelle specificity in Re(I) tetrazolato complexes leads to labeling of lipid droplets. *Royal Society of Chemistry Advances*. 4:16345-16351.

Baenke, F., B. Peck, H. Miess, and A. Schulze. 2013. Hooked on fat: the role of lipid synthesis in cancer metabolism and tumour development. *Disease Models & Mechanisms*. 6:1353-1363.

Baerga, R., Y. Zhang, P.H. Chen, S. Goldman, and S. Jin. 2009. Targeted deletion of autophagy-related 5 (atg5) impairs adipogenesis in a cellular model and in mice. *Autophagy*. 5:1118-1130.

Bagshaw, R.D., J.W. Callahan, and D.J. Mahuran. 2006. The Arf-family protein, Arl8b, is involved in the spatial distribution of lysosomes. *Biochemical and Biophysical Research Communications* . 344:1186-1191.

Balasingham, R.G., M.P. Coogan, and F.L. Thorp-Greenwood. 2011. Complexes in context: attempting to control the cellular uptake and localisation of rhenium fac-tricarbonyl polypyridyl complexes. *Dalton Transactions*. 40:11663-11674.

Balasingham, R.G., F.L. Thorp-Greenwood, C.F. Williams, M.P. Coogan, and S.J.A. Pope. 2012a. Biologically compatible, phosphorescent dimetallic Rhenium complexes linked through functionalized alkyl chains: syntheses, spectroscopic properties, and applications in imaging microscopy. *Inorganic Chemistry*. 51:1419-1426.

Balasingham, R.G., C.F. Williams, H.J. Mottram, M.P. Coogan, and S.J.A. Pope. 2012b. Gold(I) complexes derived from alkynyloxy-substituted anthraquinones: syntheses, luminescence, preliminary cytotoxicity, and cell imaging studies. *Organometallics*. 31:5835-5843.

Bar-Peled, L., L.D. Schweitzer, R. Zoncu, and D.M. Sabatini. 2012. Ragulator is a GEF for the rag GTPases that signal amino acid levels to mTORC1. *Cell*. 150:1196-1208.

Barth, J.M.I., and K. Kohler. 2014. How to take autophagy and endocytosis up a Notch. *BioMed Research International*. 2014:12.

Bartz, R., W.H. Li, B. Venables, J.K. Zehmer, M.R. Roth, R. Welti, R.G. Anderson, P. Liu, and K.D. Chapman. 2007. Lipidomics reveals that adiposomes store ether lipids and mediate phospholipid traffic. *Journal of Lipid Research*. 48:837-847.

Bejarano, E., A. Yuste, B. Patel, R.F. Stout, Jr., D.C. Spray, and A.M. Cuervo. 2014. Connexins modulate autophagosome biogenesis. *Nature Cell Biology*. 16:401-414.

Berg, T.O., M. Fengsrud, P.E. Strømhaug, T. Berg, and P.O. Seglen. 1998. Isolation and characterization of rat liver amphisomes: evidence for fusion of autophagosomes with both early and late endosomes. *Journal of Biological Chemistry*. 273:21883-21892.

Botchway, S.W., M. Charnley, J.W. Haycock, A.W. Parker, D.L. Rochester, J.A. Weinstein, and J.A.G. Williams. 2008. Time-resolved and two-photon emission imaging microscopy of live cells with inert platinum complexes. *Proceedings of the National Academy of Sciences of the United States of America*. 105:16071-16076.

Brand, A.H., and N. Perrimon. 1993. Targeted gene expression as a means of altering cell fates and generating dominant phenotypes. *Development*. 118:401-415.

Brasaemle, D.L., and Jeffrey C. Hansen. 2006. Developmental Biology: Holding Pattern for Histones. *Current Biology*. 16:R918-R920.

Breslow, D.K., and J.S. Weissman. 2010. Membranes in balance: mechanisms of sphingolipid homeostasis. *Molecular Cell*. 40:267-279.

Bright, N.A., M.J. Gratian, and J.P. Luzio. 2005. Endocytic delivery to lysosomes mediated by concurrent fusion and kissing events in living cells. *Current Biology*. 15:360-365.

Brooks, D.A., Bader, C., Ng, Y.S., Brooks, R.D., Borlace, G.N. and Shandala,T. 2012. At the Intersection of the pathways for exocytosis and autophagy. *In* Crosstalk and Integration of Membrane Trafficking Pathways. R. Weigert, editor. InTech.

Butterworth, F.M., L. Emerson, and E.M. Rasch. 1988. Maturation and degeneration of the fat body in the *Drosophila* larva and pupa as revealed by morphometric analysis. *Tissue & Cell*. 20:255-268.

Cai, N., X. Zhao, Y. Jing, K. Sun, S. Jiao, X. Chen, H. Yang, Y. Zhou, and L. Wei. 2014. Autophagy protects against palmitate-induced apoptosis in hepatocytes. *Cell & Bioscience*. 4:28.

Cao, Y., U. Nair, K. Yasumura-Yorimitsu, and D.J. Klionsky. 2009. A multiple ATG gene knockout strain for yeast two-hybrid analysis. *Autophagy*. 5:699-705.

Cermelli, S., Y. Guo, S.P. Gross, and M.A. Welte. 2006. The lipid-droplet proteome reveals that droplets are a protein-storage depot. *Current Biology*. 16:1783-1795.

Chan, J., S.C. Dodani, and C.J. Chang. 2012. Reaction-based small-molecule fluorescent probes for chemoselective bioimaging. *Nature Chemistry*. 4:973-984.

Chang, Y.Y., and T.P. Neufeld. 2009. An Atg1/Atg13 complex with multiple roles in TOR-mediated autophagy regulation. *Molecular Biology of the Cell*. 20:2004-2014.

Chang, Y.Y., and T.P. Neufeld. 2010. Autophagy takes flight in Drosophila. *FEBS Letters*. 584:1342-1349.

Chen, D., W. Fan, Y. Lu, X. Ding, S. Chen, and Q. Zhong. 2012. A mammalian autophagosome maturation mechanism mediated by TECPR1 and the Atg12-Atg5 conjugate. *Molecular Cell*. 45:629-641.

Chen, J.J., J. Jing, H. Chang, Y. Rong, Y. Hai, J. Tang, J.L. Zhang, and P. Xu. 2013. A sensitive and quantitative autolysosome probe for detecting autophagic activity in live and prestained fixed cells. *Autophagy*. 9:894-904.

Chen, Y., and L. Yu. 2013. Autophagic lysosome reformation. *Experimental Cell Research*. 319:142-146.

Cheng, J., Y. Ohsaki, K. Tauchi-Sato, A. Fujita, and T. Fujimoto. 2006. Cholesterol depletion induces autophagy. *Biochemical and Biophysical Research Communications* . 351:246-252.

Chiang, H.L., S.R. Terlecky, C.P. Plant, and J.F. Dice. 1989. A role for a 70-kilodaton heat shock protein in lysosomal degradation of intracellular proteins. Science. 246:382-385.

Chiantia, S., and E. London. 2013. Sphingolipids and membrane domains: recent advances. *Handbook of Experimental Pharmacology*:33-55.

Chien, C.H., W.W. Chen, J.T. Wu, and T.C. Chang. 2011. Label-free imaging of Drosophila in vivo by coherent anti-Stokes Raman scattering and two-photon excitation autofluorescence microscopy. *Journal of Biomedical Optics*. 16:016012.

Chintagari, N.R., N. Jin, P. Wang, T.A. Narasaraju, J. Chen, and L. Liu. 2006. Effect of cholesterol depletion on exocytosis of alveolar type II cells. *American Journal of Respiratory Cell and Molecular Biology*. 34:677-687.

Choi, A.M., S.W. Ryter, and B. Levine. 2013. Autophagy in human health and disease. *The New England Jounal of Medicine*. 368:651-662.

Chung, C.Y.S., S.P.Y. Li, M.W. Louie, K.K.W. Lo, and V.W.W. Yam. 2013. Induced self-assembly and disassembly of water-soluble alkynylplatinum(II) terpyridyl complexes with "switchable" near-infrared (NIR) emission modulated by metal-metal interactions over physiological pH: demonstration of pH-responsive NIR luminescent probes in cell-imaging studies. *Chemical Science*. 4:2453-2462.

Colombo, M.I., and H.U. Simon. 2009. Autophagy. *Autophagy*. John Wiley & Sons, Ltd, Sussex

Coogan, M.P., and V. Fernandez-Moreira. 2014. Progress with, and prospects for, metal complexes in cell imaging. *Chemical Communications*. 50:384-399.

Dall'Armi, C., K.A. Devereaux, and G. Di Paolo. 2013. The role of lipids in the control of autophagy. *Current Biology*. 23:R33-45.

Danielsen, E.T., M.E. Moeller, and K.F. Rewitz. 2013. Chapter 2 - Nutrient signaling and developmental timing of maturation. *In* Current topics in developmental biology. Vol. Volume 105. E.R. Ann and B.O.C. Michael, editors. Academic Press. 37-67.

De Duve, C. and Wattiaux, R. 1966. Functions of lysosomes. *Annu Rev Physiol.* 28, 435-492.

de Lau, L.M., P.J. Koudstaal, A. Hofman, and M.M. Breteler. 2006. Serum cholesterol levels and the risk of Parkinson's disease. *American Journal of Epidemiology*. 164:998-1002.

Delmas, D., V. Aires, D.J. Colin, E. Limagne, A. Scagliarini, A.K. Cotte, and F. Ghiringhelli. 2013. Importance of lipid microdomains, rafts, in absorption, delivery, and biological effects of resveratrol. *Annals of the New York Academy of Sciences*. 1290:90-97.

Denef, N., Y. Chen, S.D. Weeks, G. Barcelo, and T. Schüpbach. 2008. Crag regulates epithelial architecture and polarized deposition of basement membrane proteins in *Drosophila*. *Developmental Cell*. 14:354-364.

Denton, D., M.T. Aung-Htut, N. Lorensuhewa, S. Nicolson, W. Zhu, K. Mills, D. Cakouros, A. Bergmann, and S. Kumar. 2013. UTX coordinates steroid hormone-mediated autophagy and cell death. *Nature Communications*. 4:2916.

Denton, D., B. Shravage, R. Simin, K. Mills, D.L. Berry, E.H. Baehrecke, and S. Kumar. 2009. Autophagy, not apoptosis, is essential for midgut cell death in *Drosophila*. *Current Biology*. 19:1741-1746.

Denzer, K., M.J. Kleijmeer, H.F. Heijnen, W. Stoorvogel, and H.J. Geuze. 2000. Exosome: from internal vesicle of the multivesicular body to intercellular signaling device. *Journal of Cell Science*. 113 Pt 19:3365-3374.

Deretic, V. 2009. Links between autophagy, innate immunity, inflammation and Crohn's disease. *Digestive Diseases* 27:246-251.

Deretic, V., S. Jiang, and N. Dupont. 2012. Autophagy intersections with conventional and unconventional secretion in tissue development, remodeling and inflammation. *Trends in Cell Biology*. 22:397-406.

Digel, M., R. Ehehalt, and J. Fullekrug. 2010. Lipid droplets lighting up: Insights from live microscopy. *Febs Letters*. 584:2168-2175.

Dirkx, R., and M. Solimena. 2012. Cholesterol-enriched membrane rafts and insulin secretion. *Journal of Diabetes Investigation*. 3:339-346.

Dollar, G., E. Struckhoff, J. Michaud, and R.S. Cohen. 2002. Rab11 polarization of the *Drosophila* oocyte: a novel link between membrane trafficking, microtubule organization, and oskar mRNA localization and translation. *Development*. 129:517-526.

Dolman, N.J., K.M. Chambers, B. Mandavilli, R.H. Batchelor, and M.S. Janes. 2013. Tools and techniques to measure mitophagy using fluorescence microscopy. *Autophagy*. 9:1653-1662.

Dolmans, D.E., D. Fukumura, and R.K. Jain. 2003. Photodynamic therapy for cancer. *Nature Reviews Cancer*. 3:380-387.

Dou, W., D. Zhang, Y. Jung, J.X. Cheng, and D.M. Umulis. 2012. Label-free imaging of lipid-droplet intracellular motion in early *Drosophila* embryos using femtosecond-stimulated Raman loss microscopy.*Biophysical Journal*. 102:1666-1675.

Doyotte, A., M.R. Russell, C.R. Hopkins, and P.G. Woodman. 2005. Depletion of TSG101 forms a mammalian "Class E" compartment: a multicisternal early endosome with multiple sorting defects. *Journal of Cell Science*. 118:3003-3017.

Duffy, J.B. 2002. GAL4 system in Drosophila: a fly geneticist's Swiss army knife. *Genesis*. 34:1-15.

Duncan, M.D., J. Reintjes, and T.J. Manuccia. 1982. Scanning coherent anti-Stokes Raman microscope. *Optics Letters*. 7:350-352.

Dunn, W.A. 1990. Studies on the mechanisms of autophagy: maturation of the autophagic vacuole. *The Journal of Cell Biology*. 110:1935-1945.

Dupont, N., S. Chauhan, J. Arko-Mensah, E.F. Castillo, A. Masedunskas, R. Weigert, H. Robenek, T. Proikas-Cezanne, and V. Deretic. 2014. Neutral lipid stores and lipase PNPLA5 contribute to autophagosome biogenesis. *Current Biology*. 24:609-620.

Egan, D., J. Kim, R.J. Shaw, and K.L. Guan. 2011. The autophagy initiating kinase ULK1 is regulated via opposing phosphorylation by AMPK and mTOR. *Autophagy*. 7:643-644.

Eid, N., Y. Ito, K. Maemura, and Y. Otsuki. 2013. Elevated autophagic sequestration of mitochondria and lipid droplets in steatotic hepatocytes of

chronic ethanol-treated rats: an immunohistochemical and electron microscopic study. *Journal of Molecular Histology*. 44:311-326.

Eskelinen, E.L. 2006. Roles of LAMP-1 and LAMP-2 in lysosome biogenesis and autophagy. *Journal of Molecular Histology*. 27:495-502.

Ewers, H., W. Romer, A.E. Smith, K. Bacia, S. Dmitrieff, W. Chai, R. Mancini, J. Kartenbeck, V. Chambon, L. Berland, A. Oppenheim, G. Schwarzmann, T. Feizi, P. Schwille, P. Sens, A. Helenius, and L. Johannes. 2010. GM1 structure determines SV40-induced membrane invagination and infection. *Nature Cell Biology*. 12:11-18.

Fader, C.M., and M.I. Colombo. 2009. Autophagy and multivesicular bodies: two closely related partners. *Cell Death and Differentiation*. 16:70-78.

Fader, C.M., D. Sanchez, M. Furlan, and M.I. Colombo. 2008. Induction of autophagy promotes fusion of multivesicular bodies with autophagic vacuoles in k562 cells. *Traffic*. 9:230-250.

Fader, C.M., D.G. Sanchez, M.B. Mestre, and M.I. Colombo. 2009. TI-VAMP/VAMP7 and VAMP3/cellubrevin: two v-SNARE proteins involved in specific steps of the autophagy/multivesicular body pathways. *Biochimica et Biophysica Acta*. 1793:1901-1916.

Farese, R.V., Jr., and T.C. Walther. 2009. Lipid droplets finally get a little R-E-S-P-E-C-T. *Cell*. 139:855-860.

Fengsrud, M., N. Roos, T. Berg, W. Liou, J.W. Slot, and P.O. Seglen. 1995. Ultrastructural and immunocytochemical characterization of autophagic vacuoles in isolated hepatocytes: effects of vinblastine and asparagine on vacuole distributions. *Experimental Cell Research*. 221:504-519.

Ferguson, C.J., G.M. Lenk, and M.H. Meisler. 2009. Defective autophagy in neurons and astrocytes from mice deficient in PI(3,5)P2. *Human Molecular Genetics*. 18:4868-4878.

Fernández-Moreira, V., M.L. Ortego, C.F. Williams, M.P. Coogan, M.D. Villacampa, and M.C. Gimeno. 2012. Bioconjugated Rhenium(I) complexes with amino acid derivatives: synthesis, photophysical properties, and cell imaging studies. *Organometallics*. 31:5950-5957.

Fernandez-Moreira, V., F.L. Thorp-Greenwood, and M.P. Coogan. 2010. Application of d6 transition metal complexes in fluorescence cell imaging. *Chemical Communications*. 46:186-202.

Ferri, E., D. Donghi, M. Panigati, G. Prencipe, L. D'Alfonso, I. Zanoni, C. Baldoli, S. Maiorana, G. D'Alfonso, and E. Licandro. 2010. Luminescent conjugates between dinuclear rhenium(I) complexes and peptide nucleic acids (PNA) for cell imaging and DNA targeting. *Chemical Communications*. 46:6255-6257.

Filimonenko, M., S. Stuffers, C. Raiborg, A. Yamamoto, L. Malerød, E.M.C. Fisher, A. Isaacs, A. Brech, H. Stenmark, and A. Simonsen. 2007. Functional multivesicular bodies are required for autophagic clearance of protein aggregates associated with neurodegenerative disease. *The Journal of Cell Biology*. 179:485-500.

Forgac, M. 2007. Vacuolar ATPases: rotary proton pumps in physiology and pathophysiology. *Nature Reviews Molecular Cell Biologyl*. 8:917-929.

Fraldi, A., F. Annunziata, A. Lombardi, H.J. Kaiser, D.L. Medina, C. Spampanato, A.O. Fedele, R. Polishchuk, N.C. Sorrentino, K. Simons, and A. Ballabio. 2010. Lysosomal fusion and SNARE function are impaired by cholesterol accumulation in lysosomal storage disorders. *The EMBO Journal*. 29:3607-3620.

Fritsch, C., G. Ploeger, and D.J. Arndt-Jovin. 2006. Drosophila under the lens: imaging from chromosomes to whole embryos. *Chromosome research : an international journal on the molecular, supramolecular and evolutionary aspects of chromosome biology*. 14:451-464.

Fujimoto, T., and R.G. Parton. 2011. Not just fat: the structure and function of the lipid droplet. *Cold Spring Harbor Perspectives in Biology*. 3.

Fujita, N., M. Hayashi-Nishino, H. Fukumoto, H. Omori, A. Yamamoto, T. Noda, and T. Yoshimori. 2008a. An Atg4B mutant hampers the lipidation of LC3 paralogues and causes defects in autophagosome closure. *Molecular Biology of the Cell*. 19:4651-4659.

Fujita, N., T. Itoh, M. Fukuda, T. Noda, and T. Yoshimori. 2008b. The Atg16L complex specifies the site of LC3 lipidation for membrane biogenesis in autophagy. *Molecular Biology of the Cell*. 19:2092-2100.

Fukumoto, S., and T. Fujimoto. 2002. Deformation of lipid droplets in fixed samples. *Histochemistry and Cell Biology*. 118:423-428.

Ganley, I.G., H. Lam du, J. Wang, X. Ding, S. Chen, and X. Jiang. 2009. ULK1.ATG13.FIP200 complex mediates mTOR signaling and is essential for autophagy. *The Journal of Biological Chemistry*. 284:12297-12305.

Gao, W., J.H. Kang, Y. Liao, W.X. Ding, A.A. Gambotto, S.C. Watkins, Y.J. Liu, D.B. Stolz, and X.M. Yin. 2010. Biochemical isolation and characterization of the tubulovesicular LC3-positive autophagosomal compartment. *The Journal of Biological Chemistry*. 285:1371-1383.

Geng, J., and D.J. Klionsky. 2008. The Atg8 and Atg12 ubiquitin-like conjugation systems in macroautophagy. *EMBO Reports*. 9:859-864.

Gimpl, G. 2010. Cholesterol-protein interaction: methods and cholesterol reporter molecules. *Sub-cell Biochemistry*. 51:1-45.

Gocze, P.M., and D.A. Freeman. 1994. Factors underlying the variability of lipid droplet fluorescence in MA-10 Leydig tumor cells. *Cytometry*. 17:151-158.

Gordon, P.B., and P.O. Seglen. 1988. Prelysosomal convergence of autophagic and endocytic pathways. *Biochemical and Biophysical Research Communications* . 151:40-47.

Greenberg, A.S., R.A. Coleman, F.B. Kraemer, J.L. McManaman, M.S. Obin, V. Puri, Q.W. Yan, H. Miyoshi, and D.G. Mashek. 2011. The role of lipid droplets in metabolic disease in rodents and humans. *Journal of Clinical Investigation*. 121:2102-2110.

Greenberg, A.S., and M.S. Obin. 2008. Many roads lead to the lipid droplet. *Cell Metabolism*. 7:472-473.

Greenspan, P., E.P. Mayer, and S.D. Fowler. 1985. Nile red: a selective fluorescent stain for intracellular lipid droplets. *The Journal of Cell Biology*. 100:965-973.

Grillitsch, K., M. Connerth, H. Köfeler, T.N. Arrey, B. Rietschel, B. Wagner, M. Karas, and G. Daum. 2011. Lipid particles/droplets of the yeast Saccharomyces cerevisiae revisited: Lipidome meets Proteome. *Biochimica et Biophysica Acta*. 1811:1165-1176.

Grönke, S., A. Mildner, S. Fellert, N. Tennagels, S. Petry, G. Müller, H. Jäckle, and R.P. Kühnlein. 2005. Brummer lipase is an evolutionary conserved fat storage regulator in *Drosophila*. *Cell Metabolism*. 1:323-330.

Gronke, S., G. Muller, J. Hirsch, S. Fellert, A. Andreou, T. Haase, H. Jackle, and R.P. Kuhnlein. 2007. Dual lipolytic control of body fat storage and mobilization in *Drosophila*. *PLoS Biology*. 5:e137.

Gutierrez, M.G., D.B. Munafo, W. Beron, and M.I. Colombo. 2004. Rab7 is required for the normal progression of the autophagic pathway in mammalian cells. *Journal of Cell Science*. 117:2687-2697.

Haberkant, P., and J.C.M. Holthuis. 2014. Fat & fabulous: Bifunctional lipids in the spotlight. *Biochimica et Biophysica Acta - Molecular and Cell Biology of Lipids*. 1841:1022-1030.

Hailey, D.W., A.S. Rambold, P. Satpute-Krishnan, K. Mitra, R. Sougrat, P.K. Kim, and J. Lippincott-Schwartz. 2010. Mitochondria supply membranes for autophagosome biogenesis during starvation. *Cell*. 141:656-667.

Hanada, T., N.N. Noda, Y. Satomi, Y. Ichimura, Y. Fujioka, T. Takao, F. Inagaki, and Y. Ohsumi. 2007. The Atg12-Atg5 conjugate has a novel E3-like activity for protein lipidation in autophagy. *The Journal of Biological Chemistry*. 282:37298-37302.

Hannich, J.T., K. Umebayashi, and H. Riezman. 2011. Distribution and functions of sterols and sphingolipids. *Cold Spring Harbor Perspectives in Biology*. 3.

Hanson, P.I., and A. Cashikar. 2012. Multivesicular body morphogenesis. *Annual Review of Cell and Developmental Biology*. 28:337-362.

Harding, T.M., K.A. Morano, S.V. Scott, and D.J. Klionsky. 1995. Isolation and characterization of yeast mutants in the cytoplasm to vacuole protein targeting pathway. *The Journal of Cell Biology*. 131:591-602.

Hayashi-Nishino, M., N. Fujita, T. Noda, A. Yamaguchi, T. Yoshimori, and A. Yamamoto. 2009. A subdomain of the endoplasmic reticulum forms a cradle for autophagosome formation. *Nature Cell Biology*. 11:1433-1437.

Hazelrigg, T., and J.H. Mansfield. 2006. Green fluorescent protein applications in Drosophila. *Methods of Biochemical Analysis*. 47:227-257.

He, C., M. Baba, Y. Cao, and D.J. Klionsky. 2008. Self-interaction is critical for Atg9 transport and function at the phagophore assembly site during autophagy. *Molecular Biology of the Cell*. 19:5506-5516.

He, L., C.-P. Tan, R.-R. Ye, Y.-Z. Zhao, Y.-H. Liu, Q. Zhao, L.-N. Ji, and Z.-W. Mao. 2014. Theranostic Iridium(III) complexes as one- and two-photon phosphorescent trackers to monitor autophagic lysosomes. *Angewandte Chemie International Edition*: 53:12137–12141.

He, S., D. Ni, B. Ma, J.H. Lee, T. Zhang, I. Ghozalli, S.D. Pirooz, Z. Zhao, N. Bharatham, B. Li, S. Oh, W.H. Lee, Y. Takahashi, H.G. Wang, A. Minassian, P. Feng, V. Deretic, R. Pepperkok, M. Tagaya, H.S. Yoon, and C. Liang. 2013. PtdIns(3)P-bound UVRAG coordinates Golgi-ER retrograde and Atg9 transport by differential interactions with the ER tether and the beclin 1 complex. *Nature Cell Biology*. 15:1206-1219.

Ho, C.L., K.L. Wong, H.K. Kong, Y.M. Ho, C.T.L. Chan, W.M. Kwok, K.S.Y. Leung, H.L. Tam, M.H.W. Lam, X.F. Ren, A.M. Ren, J.K. Feng, and W.Y. Wong. 2012. A strong two-photon induced phosphorescent Golgi-specific in vitro marker based on a heteroleptic iridium complex. *Chemical Communications*. 48:2525-2527.

Hosogi, S., K. Kusuzaki, T. Inui, X.D. Wang, and Y. Marunaka. 2014. Cytosolic chloride ion is a key factor in lysosomal acidification and function of autophagy in human gastric cancer cell. *Journal of Cellular and Molecular Medicine*. 18:1124-1133.

Hosokawa, N., T. Hara, T. Kaizuka, C. Kishi, A. Takamura, Y. Miura, S. Iemura, T. Natsume, K. Takehana, N. Yamada, J.L. Guan, N. Oshiro, and N. Mizushima. 2009. Nutrient-dependent mTORC1 association with the ULK1-Atg13-FIP200 complex required for autophagy. *Molecular Biology of the Cell*. 20:1981-1991.

Hossain, M.S., Y. Liu, S. Zhou, K. Li, L. Tian, and S. Li. 2013. 20-Hydroxyecdysone-induced transcriptional activity of FoxO upregulates brummer and acid lipase-1 and promotes lipolysis in *Bombyx* fat body. *Insect Biochemistry and Molecular Biology*. 43:829-838.

Hoyvik, H., P.B. Gordon, T.O. Berg, P.E. Stromhaug, and P.O. Seglen. 1991. Inhibition of autophagic-lysosomal delivery and autophagic lactolysis by asparagine. J Cell Biol. 113:1305-1312.

Huang, C., and C. Freter. 2015. Lipid Metabolism, Apoptosis and Cancer Therapy. *International Journal of Molecular Sciences*. 16:924-949.

Hyttinen, J.M.T., M. Niittykoski, A. Salminen, and K. Kaarniranta. 2013. Maturation of autophagosomes and endosomes: A key role for Rab7. *Biochimica et Biophysica Acta - Molecular Cell Research*. 1833:503-510.

Ichimura, Y., T. Kirisako, T. Takao, Y. Satomi, Y. Shimonishi, N. Ishihara, N. Mizushima, I. Tanida, E. Kominami, M. Ohsumi, T. Noda, and Y. Ohsumi. 2000. A ubiquitin-like system mediates protein lipidation. *Nature*. 408:488-492.

Idrees, M., K. Thangavelu, M. Sikaroodi, C. Smith, J. Sivaraman, P.M. Gillevet, and H. Bokhari. 2014. Novel fluorescent protein from *Hydnophora rigida* possesses green emission. *Biochemical and Biophysical Research Communications* . 448:33-38.

Inoki, K., T. Zhu, and K.L. Guan. 2003. TSC2 mediates cellular energy response to control cell growth and survival. *Cell*. 115:577-590.

Inokuchi-Shimizu, S., E.J. Park, Y.S. Roh, L. Yang, B. Zhang, J. Song, S. Liang, M. Pimienta, K. Taniguchi, X. Wu, K. Asahina, W. Lagakos, M.R. Mackey, S. Akira, M.H. Ellisman, D.D. Sears, J.M. Olefsky, M. Karin, D.A. Brenner, and E. Seki. 2014. TAK1-mediated autophagy and fatty acid oxidation prevent hepatosteatosis and tumorigenesis. *The Journal of Clinical Investigation*. 124:3566-3578.

Itakura, E., C. Kishi-Itakura, and N. Mizushima. 2012. The hairpin-type tail-anchored SNARE syntaxin 17 targets to autophagosomes for fusion with endosomes/lysosomes. *Cell*. 151:1256-1269.

Itakura, E., and N. Mizushima. 2013. Syntaxin 17: the autophagosomal SNARE. *Autophagy*. 9:917-919.

Jäger, S., C. Bucci, I. Tanida, T. Ueno, E. Kominami, P. Saftig, and E.-L. Eskelinen. 2004. Role for Rab7 in maturation of late autophagic vacuoles. *Journal of Cell Science*. 117:4837-4848.

Jia, G., and J.R. Sowers. 2014. Autophagy: A housekeeper in cardiorenal metabolic health and disease. *Biochimica et Biophysica Acta*

Jiang, L., S.L. Rogers, and S.T. Crews. 2007. The Drosophila Dead end Arf-like3 GTPase controls vesicle trafficking during tracheal fusion cell morphogenesis. *Developmental Biology*. 311:487-499.

Jin, M., and D.J. Klionsky. 2014. Transcriptional regulation of by the Pho23-Rpd3 complex modulates the frequency of autophagosome formation. *Autophagy*. 10:1681-1682.

Jin, N., K. Mao, Y. Jin, G. Tevzadze, E.J. Kauffman, S. Park, D. Bridges, R. Loewith, A.R. Saltiel, D.J. Klionsky, and L.S. Weisman. 2014. Roles for PI(3,5)P2 in nutrient sensing through TORC1. *Molecular Biology of the Cell*. 25:1171-1185.

Juhasz, G., J.H. Hill, Y. Yan, M. Sass, E.H. Baehrecke, J.M. Backer, and T.P. Neufeld. 2008. The class III PI(3)K Vps34 promotes autophagy and endocytosis but not TOR signaling in *Drosophila*. *The Journal of Cell Biology*. 181:655-666.

Juhasz, G., and T. Neufeld. 2008. Experimental control and characterization of autophagy in *Drosophila*. *Methods in molecular biology*. 445:125 - 133.

Juhasz, G., and T.P. Neufeld. 2006. Autophagy: A forty-year search for a missing membrane source. *PLoS Biology*. 4:161-164.

Juhasz, G., L.G. Puskas, O. Komonyi, B. Erdi, P. Maroy, T.P. Neufeld, and M. Sass. 2007. Gene expression profiling identifies FKBP39 as an inhibitor of autophagy in larval *Drosophila* fat body. *Cell Death and Differentiation*. 14:1181-1190.

Jung, C.H., C.B. Jun, S.H. Ro, Y.M. Kim, N.M. Otto, J. Cao, M. Kundu, and D.H. Kim. 2009. ULK-Atg13-FIP200 complexes mediate mTOR signaling to the autophagy machinery. *Molecular Biology of the Cell*. 20:1992-2003.

Jung, D., K. Min, J. Jung, W. Jang, and Y. Kwon. 2013. Chemical biology-based approaches on fluorescent labeling of proteins in live cells. *Molecular bioSystems*. 9:862-872.

Kakuta, S., H. Yamamoto, L. Negishi, C. Kondo-Kakuta, N. Hayashi, and Y. Ohsumi. 2012. Atg9 vesicles recruit vesicle-tethering proteins Trs85 and Ypt1 to the autophagosome formation site. *The Journal of Biological Chemistry*. 287:44261-44269.

Karasinska, J.M., and M.R. Hayden. 2011. Cholesterol metabolism in Huntington disease. *Nature Reviews. Neurology*. 7:561-572.

Kastl, A., S. Dieckmann, K. Wahler, T. Volker, L. Kastl, A.L. Merkel, A. Vultur, B. Shannan, K. Harms, M. Ocker, W.J. Parak, M. Herlyn, and E. Meggers. 2013. Rhenium complexes with visible-light-induced anticancer activity. *ChemMedChem*. 8:924-927.

Kaushik, S., A.C. Massey, and A.M. Cuervo. 2006. Lysosome membrane lipid microdomains: novel regulators of chaperone-mediated autophagy. *The EMBO Journal*. 25:3921-3933.

Kaushik, S., J.A. Rodriguez-Navarro, E. Arias, R. Kiffin, S. Sahu, G.J. Schwartz, A.M. Cuervo, and R. Singh. 2011. Autophagy in hypothalamic AgRP neurons regulates food intake and energy balance. *Cell Metabolism*. 14:173-183.

Kelso, R.J., M. Buszczak, A.T. Quinones, C. Castiblanco, S. Mazzalupo, and L. Cooley. 2004. Flytrap, a database documenting a GFP protein-trap insertion screen in *Drosophila melanogaster*. *Nucleic Acids Research*. 32:D418-420.

Kim, J., M. Kundu, B. Viollet, and K.L. Guan. 2011. AMPK and mTOR regulate autophagy through direct phosphorylation of Ulk1. *Nature Cell Biology*. 13:132-141.

Kim, M., H.L. Park, H.W. Park, S.H. Ro, S.G. Nam, J.M. Reed, J.L. Guan, and J.H. Lee. 2013a. *Drosophila* Fip200 is an essential regulator of autophagy that attenuates both growth and aging. *Autophagy*. 9:1201-1213.

Kim, S., S.A. Naylor, and A. DiAntonio. 2012. *Drosophila* Golgi membrane protein Ema promotes autophagosomal growth and function. *Proceedings of the National Academy of Sciences*. 109:E1072–E1081.

Kim, S.G., G.R. Hoffman, G. Poulogiannis, G.R. Buel, Y.J. Jang, K.W. Lee, B.Y. Kim, R.L. Erikson, L.C. Cantley, A.Y. Choo, and J. Blenis. 2013b. Metabolic stress controls mTORC1 lysosomal localization and dimerization by regulating the TTT-RUVBL1/2 complex. *Molecular Cell*. 49:172-185.

Kirisako, T., Y. Ichimura, H. Okada, Y. Kabeya, N. Mizushima, T. Yoshimori, M. Ohsumi, T. Takao, T. Noda, and Y. Ohsumi. 2000. The reversible modification regulates the membrane-binding state of Apg8/Aut7 essential for autophagy and the cytoplasm to vacuole targeting pathway. *Journal of Cell Biology*. 151:263-276.

Klionsky, D., F. Abdalla, H. Abeliovich, R. Abraham, A. Acevedo-Arozena, K. Adeli, L. Agholme, M. Agnello, P. Agostinis, J. Aguirre-Ghiso, H. Ahn, O. Ait-Mohamed, S. Ait-Si-Ali, T. Akematsu, S. Akira, H. Al-Younes, M. Al-Zeer, M. Albert, R. Albin, J. Alegre-Abarrategui, M. Aleo, M. Alirezaei, A. Almasan, M. Almonte-Becerril, A. Amano, R. Amaravadi, S. Amarnath, A. Amer, N. Andrieu-Abadie, and V. Anantharam. 2012. Guidelines for the use and interpretation of assays for monitoring autophagy. *Autophagy*. 8:445 - 544.

Klionsky, D.J., H. Abeliovich, P. Agostinis, D.K. Agrawal, G. Aliev, D.S. Askew, M. Baba, E.H. Baehrecke, B.A. Bahr, A. Ballabio, B.A. Bamber, D.C. Bassham, E. Bergamini, X. Bi, M. Biard-Piechaczyk, J.S. Blum, D.E. Bredesen, J.L. Brodsky, J.H. Brumell, U.T. Brunk, W. Bursch, N. Camougrand, E. Cebollero, F. Cecconi, Y. Chen, L.S. Chin, A. Choi, C.T. Chu, J. Chung, P.G. Clarke, R.S. Clark, S.G. Clarke, C. Clave, J.L. Cleveland, P. Codogno, M.I. Colombo, A. Coto-Montes, J.M. Cregg, A.M. Cuervo, J. Debnath, F. Demarchi, P.B. Dennis, P.A. Dennis, V. Deretic, R.J. Devenish, F. Di Sano, J.F. Dice, M. Difiglia, S. Dinesh-Kumar, C.W. Distelhorst, M. Djavaheri-Mergny, F.C. Dorsey, W. Droge, M. Dron, W.A. Dunn, Jr., M. Duszenko, N.T. Eissa, Z. Elazar, A. Esclatine, E.L. Eskelinen, L. Fesus, K.D. Finley, J.M. Fuentes, J. Fueyo, K. Fujisaki, B. Galliot, F.B. Gao, D.A. Gewirtz, S.B. Gibson, A. Gohla, A.L. Goldberg, R. Gonzalez, C. Gonzalez-Estevez, S. Gorski, R.A. Gottlieb, D. Haussinger, Y.W. He, K. Heidenreich, J.A. Hill, M. Hoyer-Hansen, X. Hu, W.P. Huang, A. Iwasaki, M. Jaattela, W.T. Jackson, X. Jiang, S. Jin, T. Johansen, J.U. Jung, M. Kadowaki, C. Kang, A. Kelekar, D.H. Kessel, J.A. Kiel, H.P. Kim, A.

Kimchi, T.J. Kinsella, K. Kiselyov, K. Kitamoto, E. Knecht, et al. 2008. Guidelines for the use and interpretation of assays for monitoring autophagy in higher eukaryotes. *Autophagy*. 4:151-175.

Klionsky, D.J., and B.A. Schulman. 2014. Dynamic regulation of macroautophagy by distinctive ubiquitin-like proteins. *Nature Structural & Molecular Biology*. 21:336-345.

Ko, D.C., L. Milenkovic, S.M. Beier, H. Manuel, J. Buchanan, and M.P. Scott. 2005. Cell-autonomous death of cerebellar purkinje neurons with autophagy in Niemann-Pick type C disease. *PLoS Genetics*. 1:81-95.

Koga, H., S. Kaushik, and A.M. Cuervo. 2010. Altered lipid content inhibits autophagic vesicular fusion. *FASEB journal : official publication of the Federation of American Societies for Experimental Biology*. 24:3052-3065.

Kogure, T., S. Karasawa, T. Araki, K. Saito, M. Kinjo, and A. Miyawaki. 2006. A fluorescent variant of a protein from the stony coral *Montipora* facilitates dual-color single-laser fluorescence cross-correlation spectroscopy. *Nature Biotechnology*. 24:577-581.

Kohlwein, S.D., M. Veenhuis, and I.J. van der Klei. 2013. Lipid droplets and peroxisomes: key players in cellular lipid homeostasis or a matter of fat--store 'em up or burn 'em down. *Genetics*. 193:1-50.

Kolter, T., and K. Sandhoff. 1999. Sphingolipids—their metabolic pathways and the pathobiochemistry of neurodegenerative diseases. *Angewandte Chemie International Edition*. 38:1532-1568.

Korolchuk, V.I., S. Saiki, M. Lichtenberg, F.H. Siddiqi, E.A. Roberts, S. Imarisio, L. Jahreiss, S. Sarkar, M. Futter, F.M. Menzies, C.J. O'Kane, V. Deretic, and D.C. Rubinsztein. 2011. Lysosomal positioning coordinates cellular nutrient responses. *Nature Cell Biology*. 13:453-460.

Koyama-Honda, I., E. Itakura, T.K. Fujiwara, and N. Mizushima. 2013. Temporal analysis of recruitment of mammalian ATG proteins to the autophagosome formation site. *Autophagy*. 9:1491-1499.

Krahmer, N., R.V. Farese, Jr., and T.C. Walther. 2013a. Balancing the fat: lipid droplets and human disease. *EMBO Molecular Medicine*. 5:905-915.

Krahmer, N., R.V. Farese, and T.C. Walther. 2013b. Balancing the fat: lipid droplets and human disease. *EMBO Molecular Medicine*. 5:973-983.

Kroemer, G., G. Marino, and B. Levine. 2010. Autophagy and the integrated stress response. *Molecular Cell*. 40:280-293.

Kuerschner, L., C. Moessinger, and C. Thiele. 2008. Imaging of lipid biosynthesis: how a neutral lipid enters lipid droplets. *Traffic*. 9:338-352.

Kuhnlein, R.P. 2012. Thematic review series: Lipid droplet synthesis and metabolism: from yeast to man. Lipid droplet-based storage fat metabolism in Drosophila. *Journal of Lipid Research*. 53:1430-1436.

Kuma, A., N. Mizushima, N. Ishihara, and Y. Ohsumi. 2002. Formation of the approximately 350-kDa Apg12-Apg5.Apg16 multimeric complex, mediated by Apg16 oligomerization, is essential for autophagy in yeast. *Journal of Biological Chemistry*. 277:18619-18625.

Kundu, M., and C.B. Thompson. 200a. Autophagy: basic principles and relevance to disease. *Annual Reviews of Pathology*. 3:427-455.

Lajoie, P., G. Guay, J.W. Dennis, and I.R. Nabi. 2005. The lipid composition of autophagic vacuoles regulates expression of multilamellar bodies. *Journal of Cell Science*. 118:1991-2003.

Lamb, C.A., H.C. Dooley, and S.A. Tooze. 2013a. Endocytosis and autophagy: Shared machinery for degradation. *Bioessays*. 35:34-45.

Lamb, C.A., T. Yoshimori, and S.A. Tooze. 2013b. The autophagosome: origins unknown, biogenesis complex. *Nature Reviews Molecular Cell Biologyl*. 14:759-774.

Lang, T. 2007. SNARE proteins and 'membrane rafts'. *Journal of Physiology*. 585:693-698.

Laplante, M., and D.M. Sabatini. 2012. mTOR signaling in growth control and disease. *Cell*. 149:274-293.

Ledeen, R., and G. Wu. 2011. New findings on nuclear gangliosides: overview on metabolism and function. *Journal of Neurochemistry*. 116:714-720.

Lee, C.Y., B.A. Cooksey, and E.H. Baehrecke. 2002. Steroid regulation of midgut cell death during *Drosophila* development. *Developmental Biology*. 250:101-111.

Lee, J.A., A. Beigneux, S.T. Ahmad, S.G. Young, and F.B. Gao. 2007. ESCRT-III dysfunction causes autophagosome accumulation and neurodegeneration. *Current Biology*. 17:1561-1567.

Lee, J.W., S. Park, Y. Takahashi, and H.G. Wang. 2010. The association of AMPK with ULK1 regulates autophagy. *PLoS One*. 5:e15394.

Lenk, G.M., and M.H. Meisler. 2014. Mouse models of PI(3,5)P2 deficiency with impaired lysosome function. *Methods in Enzymology*. 534:245-260.

Levine, B., and G. Kroemer. 2008. Autophagy in the pathogenesis of disease. *Cell*. 132:27-42.

Li, M., Y. Hou, J. Wang, X. Chen, Z.M. Shao, and X.M. Yin. 2011. Kinetics comparisons of mammalian Atg4 homologues indicate selective preferences toward diverse Atg8 substrates. *The Journal of Biological Chemistry*. 286:7327-7338.

Liang, C., J.S. Lee, K.S. Inn, M.U. Gack, Q. Li, E.A. Roberts, I. Vergne, V. Deretic, P. Feng, C. Akazawa, and J.U. Jung. 2008. Beclin1-binding UVRAG targets the class C Vps complex to coordinate autophagosome maturation and endocytic trafficking. *Nature Cell Biology*. 10:776-787.

Liao, G., Y. Yao, J. Liu, Z. Yu, S. Cheung, A. Xie, X. Liang, and X. Bi. 2007. Cholesterol accumulation is associated with lysosomal dysfunction and autophagic stress in Npc1 -/- mouse brain. *American Journal of Pathology*. 171:962-975.

Lieberman, A.P., R. Puertollano, N. Raben, S. Slaugenhaupt, S.U. Walkley, and A. Ballabio. 2012. Autophagy in lysosomal storage disorders. *Autophagy*. 8:719-730.

Lindmo, K., A. Simonsen, A. Brech, K. Finley, T.E. Rusten, and H. Stenmark. 2006. A dual function for Deep orange in programmed autophagy in the *Drosophila melanogaster* fat body. *Experimental Cell Research*. 312:2018-2027.

Ling, D., M. Magallanes, and P.M. Salvaterra. 2014. Accumulation of amyloid-like Abeta1-42 in AEL (autophagy-endosomal-lysosomal) vesicles: potential implications for plaque biogenesis. *ASN neuro*. 6.

Lingwood, D., and K. Simons. 2010. Lipid Rafts As a Membrane-Organizing Principle. *Science*. 327:46-50.

Lisenbee, C.S., S.K. Karnik, and R.N. Trelease. 2003. Overexpression and mislocalization of a tail-anchored GFP redefines the identity of peroxisomal ER. *Traffic*. 4:491-501.

Liu, E.Y., and K.M. Ryan. 2012. Autophagy and cancer--issues we need to digest. *Journal of Cell Science*. 125:2349-2358.

Liu, H., Q. Jia, G. Tettamanti, and S. Li. 2013. Balancing crosstalk between 20-hydroxyecdysone-induced autophagy and caspase activity in the fat body during *Drosophila* larval-prepupal transition. *Insect Biochemistry and Molecular Biology*. 43:1068-1078.

Liu, K., and M.J. Czaja. 2013. Regulation of lipid stores and metabolism by lipophagy. *Cell Death and Differentiation*. 20:3-11.

Lo, K.K., A.W. Choi, and W.H. Law. 2012. Applications of luminescent inorganic and organometallic transition metal complexes as biomolecular and cellular probes. *Dalton Transactions*. 41:6021-6047.

Lo, K.K., T.K. Lee, J.S. Lau, W.L. Poon, and S.H. Cheng. 2008. Luminescent biological probes derived from ruthenium(II) estradiol polypyridine complexes. *Inorganic Chemistry*. 47:200-208.

Lo, K.K.W., W.K. Hui, C.K. Chung, K.H.K. Tsang, D.C.M. Ng, N.Y. Zhu, and K.K. Cheung. 2005. Biological labelling reagents and probes derived from luminescent transition metal polypyridine complexes. *Coordination Chemistry Reviews*. 249:1434-1450.

Lo, K.K.W., W.H.T. Law, J.C.Y. Chan, H.W. Liu, and K.Y. Zhang. 2013. Photophysical and cellular uptake properties of novel phosphorescent cyclometalated iridium(III) bipyridine D-fructose complexes. *Metallomics*. 5:808-812.

Lo, W.S., W.M. Kwok, G.L. Law, C.T. Yeung, C.T.L. Chan, H.L. Yeung, H.K. Kong, C.H. Chen, M.B. Murphy, K.L. Wong, and W.T. Wong. 2011. Impressive europium red emission induced by two-photon excitation for biological applications. *Inorganic Chemistry*. 50:5309-5311.

Longatti, A., C.A. Lamb, M. Razi, S. Yoshimura, F.A. Barr, and S.A. Tooze. 2012. TBC1D14 regulates autophagosome formation via Rab11- and ULK1-positive recycling endosomes. *The Journal of Cell Biology*. 197:659-675.

Longatti, A., and S.A. Tooze. 2009. Vesicular trafficking and autophagosome formation. *Cell Death and Differentiation*. 16:956-965.

Louie, M.W., H.W. Liu, M.H. Lam, Y.W. Lam, and K.K. Lo. 2011. Luminescent rhenium(I) polypyridine complexes appended with an alpha-D-glucose moiety as novel biomolecular and cellular probes. *Chemistry*. 17:8304-8308.

Low, P., A. Varga, K. Pircs, P. Nagy, Z. Szatmari, M. Sass, and G. Juhasz. 2013. Impaired proteasomal degradation enhances autophagy via hypoxia signaling in *Drosophila*. *BMC Cell Biology*. 14:29.

Lynch-Day, M.A., D. Bhandari, S. Menon, J. Huang, H. Cai, C.R. Bartholomew, J.H. Brumell, S. Ferro-Novick, and D.J. Klionsky. 2010. Trs85 directs a Ypt1 GEF, TRAPPIII, to the phagophore to promote autophagy.

Proceedings of the National Academy of Sciences of the United States of America. 107:7811-7816.

Mack, H.I., B. Zheng, J.M. Asara, and S.M. Thomas. 2012. AMPK-dependent phosphorylation of ULK1 regulates ATG9 localization. *Autophagy*. 8:1197-1214.

Maggioni, D., F. Fenili, L. D'Alfonso, D. Donghi, M. Panigati, I. Zanoni, R. Marzi, A. Manfredi, P. Ferruti, G. D'Alfonso, and E. Ranucci. 2012. Luminescent rhenium and ruthenium complexes of an amphoteric poly(amidoamine) functionalized with 1,10-phenanthroline. *Inorganic Chemistry*. 51:12776-12788.

Manil-Segalen, M., C. Lefebvre, E. Culetto, and R. Legouis. 2012. Need an ESCRT for autophagosomal maturation? *Communicative & Integrative Biology*. 5:566-571.

Mari, C., M. Panigati, L. D'Alfonso, I. Zanoni, D. Donghi, L. Sironi, M. Collini, S. Maiorana, C. Baldoli, G. D'Alfonso, and E. Licandro. 2012. Luminescent conjugates between dinuclear Rhenium complexes and peptide nucleic acids (PNA): synthesis, photophysical characterization, and cell uptake. *Organometallics*. 31:5918-5928.

Mari, M., J. Griffith, E. Rieter, L. Krishnappa, D.J. Klionsky, and F. Reggiori. 2010. An Atg9-containing compartment that functions in the early steps of autophagosome biogenesis. *Journal of Cell Biology*. 190:1005-1022.

Mari, M., S.A. Tooze, and F. Reggiori. 2011. The puzzling origin of the autophagosomal membrane. *F1000 biology reports*. 3:25.

Masanta, G., C.S. Lim, H.J. Kim, J.H. Han, H.M. Kim, and B.R. Cho. 2011. A mitochondrial-targeted two-photon probe for Zinc ion. *Journal of the American Chemical Society*. 133:5698-5700.

Matsushita, M., S. Tanaka, N. Nakamura, H. Inoue, and H. Kanazawa. 2004. A novel kinesin-like protein, KIF1Bbeta3 is involved in the movement of lysosomes to the cell periphery in non-neuronal cells. *Traffic*. 5:140-151.

Maxfield, F.R., and G. van Meer. 2010. Cholesterol, the central lipid of mammalian cells. *Current Opinion in Cell Biology*. 22:422-429.

Maxfield, F.R., and D. Wüstner. 2012. Chapter 17 - Analysis of cholesterol trafficking with fluorescent probes. *In* Methods in Cell Biology. Vol. Volume 108. P. Gilbert Di and R.W. Markus, editors. Academic Press. 367-393.

McIntosh, A.L., S.M. Storey, and B.P. Atshaves. 2010. Intracellular lipid droplets contain dynamic pools of sphingomyelin: ADRP binds phospholipids with high affinity. *Lipids*. 45:465-477.

McPhee, C.K., and E.H. Baehrecke. 2009. Autophagy in *Drosophila melanogaster*. *Biochimica et Biophysica Acta*. 1793:1452-1460.

Mehrpour, M., A. Esclatine, I. Beau, and P. Codogno. 2010. Overview of macroautophagy regulation in mammalian cells. *Cell Research*. 20:748-762.

Meijer, A.J., and P. Codogno. 2004. Regulation and role of autophagy in mammalian cells. *The International Journal of Biochemistry & Cell Biology.* 36:2445-2462.

Meijer, A.J., and P.F. Dubbelhuis. 2004. Amino acid signalling and the integration of metabolism. *Biochemical and Biophysical Research Communications* . 313:397-403.

Melo, R.C., H. D'Avila, H.C. Wan, P.T. Bozza, A.M. Dvorak, and P.F. Weller. 2011a. Lipid bodies in inflammatory cells: structure, function, and current imaging techniques. *The Journal of Histochemistry and Cytochemistry*. 59:540-556.

Melo, R.C., H. D'Avila, H.C. Wan, P.T. Bozza, A.M. Dvorak, and P.F. Weller. 2011b. Lipid bodies in inflammatory cells: structure, function, and current imaging techniques. *Journal of Histochemistry & Cytochemistry*. 59:540-556.

Mindell, J.A. 2012. Lysosomal Acidification Mechanisms. *Annual Review of Physiology*. 74:69-86.

Mizushima, N., B. Levine, A. Cuervo, and D. Klionsky. 2008. Autophagy fights disease through cellular self-digestion. *Nature*. 451:1069 - 1075.

Mizushima, N., T. Noda, T. Yoshimori, Y. Tanaka, T. Ishii, M.D. George, D.J. Klionsky, M. Ohsumi, and Y. Ohsumi. 1998. A protein conjugation system essential for autophagy. *Nature*. 395:395-398.

Montgomery, C.P., B.S. Murray, E.J. New, R. Pal, and D. Parker. 2009. Cell-penetrating metal complex optical probes: targeted and responsive systems based on lanthanide luminescence. *Accounts of Chemical Research*. 42:925-937.

Moreau, K., B. Ravikumar, M. Renna, C. Puri, and D.C. Rubinsztein. 2011. Autophagosome precursor maturation requires homotypic fusion. *Cell*. 146:303-317.

Mousavi, S.A., R. Kjeken, T.O. Berg, P.O. Seglen, T. Berg, and A. Brech. 2001. Effects of inhibitors of the vacuolar proton pump on hepatic heterophagy and autophagy. *Biochimica et Biophysica Acta -Biomembranes*. 1510:243-257.

Mulakkal, N.C., P. Nagy, S. Takats, R. Tusco, G. Juhasz, and I.P. Nezis. 2014. Autophagy in *Drosophila*: from historical studies to current knowledge. *BioMed Research International*. 2014:273473.

Murphy, L., A. Congreve, L.O. Palsson, and J.A.G. Williams. 2010. The time domain in co-stained cell imaging: time-resolved emission imaging microscopy using a protonatable luminescent iridium complex. *Chemical Communications*. 46:8743-8745.

Nagy, P., K. Hegedus, K. Pircs, A. Varga, and G. Juhasz. 2014a. Different effects of Atg2 and Atg18 mutations on Atg8a and Atg9 trafficking during starvation in *Drosophila*. *FEBS Letters*. 588:408-413.

Nagy, P., K. Hegedus, K. Pircs, A. Varga, and G. Juhasz. 2014b. Different effects of Atg2 and Atg18 mutations on Atg8a and Atg9 trafficking during starvation in *Drosophila*. *FEBS Letters*. 588:408-413.

Nagy, P., M. Karpati, A. Varga, K. Pircs, Z. Venkei, S. Takats, K. Varga, B. Erdi, K. Hegedus, and G. Juhasz. 2014c. Atg17/FIP200 localizes to perilysosomal Ref(2)P aggregates and promotes autophagy by activation of Atg1 in *Drosophila*. *Autophagy*. 10:453-467.

Nagy, P., A. Varga, K. Pircs, K. Hegedus, and G. Juhasz. 2013. Myc-driven overgrowth requires unfolded protein response-mediated induction of autophagy and antioxidant responses in *Drosophila melanogaster*. *PLoS Genetics*. 9:e1003664.

Nakatogawa, H., Y. Ichimura, and Y. Ohsumi. 2007. Atg8, a ubiquitin-like protein required for autophagosome formation, mediates membrane tethering and hemifusion. *Cell*. 130:165-178.

Nakatogawa, H., K. Suzuki, Y. Kamada, and Y. Ohsumi. 2009. Dynamics and diversity in autophagy mechanisms: lessons from yeast. *Nature Reviews Molecular Cell Biologyl*. 10:458-467.

Nazarko, V.Y., and Q. Zhong. 2013. ULK1 targets Beclin-1 in autophagy. *Nature Cell Biology*. 15:727-728.

Neufeld, T.P. 2008a. Chapter 36 - Genetic manipulation and monitoring of autophagy in *Drosophila*. *In* Methods in Enzymology. Vol. Volume 451. J.K. Daniel, editor. Academic Press. 653-667.

Neufeld, T.P. 2008b. Genetic manipulation and monitoring of autophagy in Drosophila. *Methods in Enzymology*. 451:653-667.

New, E.J., A. Congreve, and D. Parker. 2010. Definition of the uptake mechanism and sub-cellular localisation profile of emissive lanthanide complexes as cellular optical probes. *Chemical Science*. 1:111-118.

Nezis, I.P. 2012. The selectivity and specificity of autophagy in Drosophila. *Cells*. 1:248-262.

Nicklin, P., P. Bergman, B. Zhang, E. Triantafellow, H. Wang, B. Nyfeler, H. Yang, M. Hild, C. Kung, C. Wilson, V.E. Myer, J.P. MacKeigan, J.A. Porter, Y.K. Wang, L.C. Cantley, P.M. Finan, and L.O. Murphy. 2009. Bidirectional transport of amino acids regulates mTOR and autophagy. *Cell*. 136:521-534.

Nobukuni, T., M. Joaquin, M. Roccio, S.G. Dann, S.Y. Kim, P. Gulati, M.P. Byfield, J.M. Backer, F. Natt, J.L. Bos, F.J. Zwartkruis, and G. Thomas. 2005. Amino acids mediate mTOR/raptor signaling through activation of class 3 phosphatidylinositol 3OH-kinase. *PNAS*. 102:14238-14243.

Noda, T., and Y. Ohsumi. 1998. Tor, a phosphatidylinositol kinase homologue, controls autophagy in yeast. *The Journal of Biological Chemistry*. 273:3963-3966.

Ogawa, M., Y. Yoshikawa, T. Kobayashi, H. Mimuro, M. Fukumatsu, K. Kiga, Z. Piao, H. Ashida, M. Yoshida, S. Kakuta, T. Koyama, Y. Goto, T. Nagatake, S. Nagai, H. Kiyono, M. Kawalec, J.M. Reichhart, and C. Sasakawa. 2011. A Tecpr1-dependent selective autophagy pathway targets bacterial pathogens. *Cell Host & Microbe*. 9:376-389.

Ohsaki, Y., Y. Shinohara, M. Suzuki, and T. Fujimoto. 2010. A pitfall in using BODIPY dyes to label lipid droplets for fluorescence microscopy. *Histochemistry and Cell Biology*. 133:477-480.

Ohsumi, Y. 2014. Historical landmarks of autophagy research. *Cell Res*. 24:9-23.

Ong, W.J., S. Alvarez, I.E. Leroux, R.S. Shahid, A.A. Samma, P. Peshkepija, A.L. Morgan, S. Mulcahy, and M. Zimmer. 2011. Function and structure of GFP-like proteins in the protein data bank. *Molecular bioSystems*. 7:984-992.

Orsi, A., M. Razi, H.C. Dooley, D. Robinson, A.E. Weston, L.M. Collinson, and S.A. Tooze. 2012. Dynamic and transient interactions of Atg9 with

autophagosomes, but not membrane integration, are required for autophagy. *Molecular Biology of the Cell*. 23:1860-1873.

Ouimet, M. 2013. Autophagy in obesity and atherosclerosis: Interrelationships between cholesterol homeostasis, lipoprotein metabolism and autophagy in macrophages and other systems. *Biochimica et Biophysica Acta*. 1831:1124-1133.

Ouimet, M., V. Franklin, E. Mak, X. Liao, I. Tabas, and Y.L. Marcel. 2011. Autophagy regulates cholesterol efflux from macrophage foam cells via lysosomal acid lipase. *Cell Metabolism*. 13:655-667.

Pacheco, C.D., R. Kunkel, and A.P. Lieberman. 2007. Autophagy in Niemann-Pick C disease is dependent upon Beclin-1 and responsive to lipid trafficking defects. *Human Molecular Genetics*. 16:1495-1503.

Pacheco, C.D., and A.P. Lieberman. 2008. The pathogenesis of Niemann-Pick type C disease: a role for autophagy? *Expert Reviews in Molecular Medicine*. 10:e26.

Pan, M., V. Maitin, S. Parathath, U. Andreo, S.X. Lin, C. St Germain, Z. Yao, F.R. Maxfield, K.J. Williams, and E.A. Fisher. 2008. Presecretory oxidation, aggregation, and autophagic destruction of apoprotein-B: a pathway for late-stage quality control. *Proceedings of the National Academy of Sciences of the United States of America*. 105:5862-5867.

Pan, P.Y., and Z. Yue. 2014. Genetic causes of Parkinson's disease and their links to autophagy regulation. *Parkinsonism & Related Disorders*. 20 Suppl 1:S154-157.

Pankiv, S., E.A. Alemu, A. Brech, J.-A. Bruun, T. Lamark, A. Øvervatn, G. Bjørkøy, and T. Johansen. 2010. FYCO1 is a Rab7 effector that binds to LC3 and PI3P to mediate microtubule plus end–directed vesicle transport. *The Journal of Cell Biology*. 188:253-269.

Papinski, D., and C. Kraft. 2014. Atg1 kinase organizes autophagosome formation by phosphorylating Atg9. *Autophagy*. 10:1338-1340.

Papinski, D., M. Schuschnig, W. Reiter, L. Wilhelm, C.A. Barnes, A. Maiolica, I. Hansmann, T. Pfaffenwimmer, M. Kijanska, I. Stoffel, S.S. Lee, A. Brezovich, J.H. Lou, B.E. Turk, R. Aebersold, G. Ammerer, M. Peter, and C. Kraft. 2014. Early steps in autophagy depend on direct phosphorylation of Atg9 by the Atg1 kinase. *Molecular Cell*. 53:471-483.

Parker, D. 2011. Critical design factors for optical imaging with metal coordination complexes. *Australian Journal of Chemistry*. 64:239-243.

Parkinson-Lawrence, E.J., T. Shandala, M. Prodoehl, R. Plew, G.N. Borlace, and D.A. Brooks. 2010. Lysosomal storage disease: revealing lysosomal function and physiology. *Physiology*. 25:102-115.

Pattingre, S., C. Bauvy, S. Carpentier, T. Levade, B. Levine, and P. Codogno. 2009. Role of JNK1-dependent Bcl-2 phosphorylation in ceramide-induced macroautophagy. *The Journal of Biological Chemistry*. 284:2719-2728.

Peake, K.B., and J.E. Vance. 2010. Defective cholesterol trafficking in Niemann-Pick C-deficient cells. *FEBS Letters*. 584:2731-2739.

Pearson, G.L., N. Mellett, K.Y. Chu, J. Cantley, A. Davenport, P. Bourbon, C.C. Cosner, P. Helquist, P.J. Meikle, and T.J. Biden. 2014. Lysosomal acid lipase and lipophagy are constitutive negative regulators of glucose-stimulated insulin secretion from pancreatic beta cells. *Diabetologia*. 57:129-139.

Pierzynska-Mach, A., P.A. Janowski, and J.W. Dobrucki. 2014. Evaluation of acridine orange, LysoTracker Red, and quinacrine as fluorescent probes for long-term tracking of acidic vesicles. *Cytom Part A*. 85A:729-737.

Pircs, K., P. Nagy, A. Varga, Z. Venkei, B. Erdi, K. Hegedus, and G. Juhasz. 2012. Advantages and limitations of different p62-based assays for estimating autophagic activity in *Drosophila*. *PLoS One*. 7:e44214.

Polson, H.E., J. de Lartigue, D.J. Rigden, M. Reedijk, S. Urbe, M.J. Clague, and S.A. Tooze. 2010. Mammalian Atg18 (WIPI2) localizes to omegasome-

anchored phagophores and positively regulates LC3 lipidation. *Autophagy*. 6.

Popovic, D., and I. Dikic. 2014. TBC1D5 and the AP2 complex regulate ATG9 trafficking and initiation of autophagy. *EMBO Reports*. 15:392-401.

Puckett, C.A., R.J. Ernst, and J.K. Barton. 2010. Exploring the cellular accumulation of metal complexes. *Dalton Transactions*. 39:1159-1170.

Pulipparacharuvil, S., M.A. Akbar, S. Ray, E.A. Sevrioukov, A.S. Haberman, J. Rohrer, and H. Kramer. 2005. *Drosophila* Vps16A is required for trafficking to lysosomes and biogenesis of pigment granules. *Journal of Cell Science*. 118:3663-3673.

Puri, C., M. Renna, C.F. Bento, K. Moreau, and D.C. Rubinsztein. 2013. Diverse autophagosome membrane sources coalesce in recycling endosomes. *Cell*. 154:1285-1299.

Puri, C., M. Renna, C.F. Bento, K. Moreau, and D.C. Rubinsztein. 2014. ATG16L1 meets ATG9 in recycling endosomes: additional roles for the plasma membrane and endocytosis in autophagosome biogenesis. *Autophagy*. 10:182-184.

Quan, W., and M.S. Lee. 2013. Role of autophagy in the control of body metabolism. *Endocrinology and Metabolism*. 28:6-11.

Ragusa, M.J., R.E. Stanley, and J.H. Hurley. 2012. Architecture of the Atg17 Complex as a scaffold for autophagosome biogenesis. *Cell*. 151:1501-1512.

Raiborg, C., and H. Stenmark. 2009. The ESCRT machinery in endosomal sorting of ubiquitylated membrane proteins. *Nature*. 458:445-452.

Ravikumar, B., K. Moreau, L. Jahreiss, C. Puri, and D.C. Rubinsztein. 2010. Plasma membrane contributes to the formation of pre-autophagosomal structures. *Nature Cell Biology*. 12:747-757.

Reggiori, F., and S.A. Tooze. 2012. Autophagy regulation through Atg9 traffic. *The Journal of Cell Biology*. 198:151-153.

Richards, P., C. Didszun, S. Campesan, A. Simpson, B. Horley, K.W. Young, P. Glynn, K. Cain, C.P. Kyriacou, F. Giorgini, and P. Nicotera. 2011. Dendritic spine loss and neurodegeneration is rescued by Rab11 in models of Huntington's disease. *Cell Death and Differentiation*. 18:191-200.

Rink, J., E. Ghigo, Y. Kalaidzidis, and M. Zerial. 2005. Rab conversion as a mechanism of progression from early to late endosomes. *Cell*. 122:735-749.

Romanov, J., M. Walczak, I. Ibiricu, S. Schüchner, E. Ogris, C. Kraft, and S. Martens. 2012. Mechanism and functions of membrane binding by the Atg5–Atg12/Atg16 complex during autophagosome formation. *The EMBO Journal*. 4304-4317 pp.

Rothstein, E.C., M. Nauman, S. Chesnick, and R.S. Balaban. 2006. Multi-photon excitation microscopy in intact animals. *Journal of Microscopy*. 222:58-64.

Rubinsztein, D.C., T. Shpilka, and Z. Elazar. 2012. Mechanisms of autophagosome biogenesis. *Current Biology*. 22:R29-34.

Ruggles, K.V., A. Turkish, and S.L. Sturley. 2013. Making, baking, and breaking: the synthesis, storage, and hydrolysis of neutral lipids. *Annual Review of Nutrition*. 33:413-451.

Russell, R.C., Y. Tian, H. Yuan, H.W. Park, Y.Y. Chang, J. Kim, H. Kim, T.P. Neufeld, A. Dillin, and K.L. Guan. 2013. ULK1 induces autophagy by phosphorylating Beclin-1 and activating VPS34 lipid kinase. *Nature Cell Biology*. 15:741-750.

Rusten, T., K. Lindmo, G. Juhasz, M. Sass, P. Seglen, A. Brech, and H. Stenmark. 2004. Programmed autophagy in the *Drosophila* fat body is induced by ecdysone through regulation of the PI3K pathway. *Developmental Cell*. 7:179 - 192.

Rusten, T.E., L.M. Rodahl, K. Pattni, C. Englund, C. Samakovlis, S. Dove, A. Brech, and H. Stenmark. 2006. Fab1 phosphatidylinositol 3-phosphate 5-kinase controls trafficking but not silencing of endocytosed receptors. *Molecular Biology of the Cell*. 17:3989-4001.

Rusten, T.E., and H. Stenmark. 2009. How do ESCRT proteins control autophagy? *Journal of Cell Science*. 122:2179-2183.

Rusten, T.E., T. Vaccari, K. Lindmo, L.M. Rodahl, I.P. Nezis, C. Sem-Jacobsen, F. Wendler, J.P. Vincent, A. Brech, D. Bilder, and H. Stenmark. 2007. ESCRTs and Fab1 regulate distinct steps of autophagy. *Current Biology*. 17:1817-1825.

Saitoh, T., N. Fujita, T. Hayashi, K. Takahara, T. Satoh, H. Lee, K. Matsunaga, S. Kageyama, H. Omori, T. Noda, N. Yamamoto, T. Kawai, K. Ishii, O. Takeuchi, T. Yoshimori, and S. Akira. 2009. Atg9a controls dsDNA-driven dynamic translocation of STING and the innate immune response. *Proceedings of the National Academy of Sciences of the United States of America*. 106:20842-20846.

Sancak, Y., L. Bar-Peled, R. Zoncu, A.L. Markhard, S. Nada, and D.M. Sabatini. 2010. Ragulator-Rag complex targets mTORC1 to the lysosomal surface and is necessary for its activation by amino acids. *Cell*. 141:290-303.

Sancak, Y., T.R. Peterson, Y.D. Shaul, R.A. Lindquist, C.C. Thoreen, L. Bar-Peled, and D.M. Sabatini. 2008. The Rag GTPases bind raptor and mediate amino acid signaling to mTORC1. *Science*. 320:1496-1501.

Sandhoff, K., and K. Harzer. 2013. Gangliosides and Gangliosidoses: Principles of Molecular and Metabolic Pathogenesis. *The Journal of Neuroscience*. 33:10195-10208.

Sarkar, S., B. Carroll, Y. Buganim, D. Maetzel, A.H. Ng, J.P. Cassady, M.A. Cohen, S. Chakraborty, H. Wang, E. Spooner, H. Ploegh, J. Gsponer, V.I. Korolchuk, and R. Jaenisch. 2013. Impaired autophagy in the lipid-storage disorder Niemann-Pick type C1 disease. *Cell Reports*. 5:1302-1315.

Sato, T.K., P. Rehling, M.R. Peterson, and S.D. Emr. 2000. Class C Vps protein complex regulates vacuolar SNARE pairing and is required for vesicle docking/fusion. *Molecular Cell*. 6:661-671.

Satoh, A.K., J.E. O'Tousa, K. Ozaki, and D.F. Ready. 2005. Rab11 mediates post-Golgi trafficking of rhodopsin to the photosensitive apical membrane of *Drosophila* photoreceptors. *Development*. 132:1487-1497.

Satori, C.P., M.M. Henderson, E.A. Krautkramer, V. Kostal, M.D. Distefano, and E.A. Arriaga. 2013. Bioanalysis of eukaryotic organelles. *Chemical Reviews*. 113:2733-2811.

Savina, A., C.M. Fader, M.T. Damiani, and M.I. Colombo. 2005. Rab11 promotes docking and fusion of multivesicular bodies in a calcium-dependent manner. *Traffic*. 6:131-143.

Scarlatti, F., C. Bauvy, A. Ventruti, G. Sala, F. Cluzeaud, A. Vandewalle, R. Ghidoni, and P. Codogno. 2004. Ceramide-mediated macroautophagy involves inhibition of protein kinase B and up-regulation of beclin 1. *The Journal of Biological Chemistry*. 279:18384-18391.

Schnell, U., F. Dijk, K.A. Sjollema, and B.N. Giepmans. 2012. Immunolabeling artifacts and the need for live-cell imaging. *Nature Methods*. 9:152-158.

Schoer, J.K., A.M. Gallegos, A.L. McIntosh, O. Starodub, A.B. Kier, J.T. Billheimer, and F. Schroeder. 2000. Lysosomal membrane cholesterol dynamics. *Biochemistry-Us*. 39:7662-7677.

Schroder, B.A., C. Wrocklage, A. Hasilik, and P. Saftig. 2010. The proteome of lysosomes. *Proteomics*. 10:4053-4076.

Scott, R.C., O. Schuldiner, and T.P. Neufeld. 2004. Role and regulation of starvation-induced autophagy in the *Drosophila* fat body. *Developmental Cell*. 7:167-178.

Sekito, T., T. Kawamata, R. Ichikawa, K. Suzuki, and Y. Ohsumi. 2009. Atg17 recruits Atg9 to organize the pre-autophagosomal structure. *Genes Cells*. 14:525-538.

Settembre, C., A. Fraldi, L. Jahreiss, C. Spampanato, C. Venturi, D. Medina, R. de Pablo, C. Tacchetti, D.C. Rubinsztein, and A. Ballabio. 2008a. A block of

autophagy in lysosomal storage disorders. *Human Molecular Genetics*. 17:119-129.

Settembre, C., A. Fraldi, D.C. Rubinsztein, and A. Ballabio. 2008b. Lysosomal storage diseases as disorders of autophagy. *Autophagy*. 4:113-114.

Shandala, T., J.M. Woodcock, Y. Ng, L. Biggs, E.M. Skoulakis, D.A. Brooks, and A.F. Lopez. 2011. Drosophila 14-3-3epsilon has a crucial role in anti-microbial peptide secretion and innate immunity. *Journal of Cell Science*. 124:2165-2174.

Shaw, R. J., Bardeesy, N., Manning, B. D., Lopez, L., Kosmatka, M., DePinho, R. A. and Cantley, L. C. (2004). The LKB1 tumor suppressor negatively regulates mTOR signaling. Cancer Cell 6, 91-99

Shen, H.M., and N. Mizushima. 2014. At the end of the autophagic road: an emerging understanding of lysosomal functions in autophagy. *Trends in Biochemical Sciences*. 39:61-71.

Shibata, M., K. Yoshimura, N. Furuya, M. Koike, T. Ueno, M. Komatsu, H. Arai, K. Tanaka, E. Kominami, and Y. Uchiyama. 2009. The MAP1-LC3 conjugation system is involved in lipid droplet formation. *Biochemical and Biophysical Research Communications* . 382:419-423.

Shibutani, S.T., and T. Yoshimori. 2014. A current perspective of autophagosome biogenesis. *Cell Res*. 24:58-68.

Shimada, Y., and D.J. Klionsky. 2012. Autophagy contributes to lysosomal storage disorders. *Autophagy*. 8:715-716.

Shimobayashi, M., and M.N. Hall. 2014. Making new contacts: the mTOR network in metabolism and signalling crosstalk. *Nature Reviews Molecular Cell Biologyl*. 15:155-162.

Shintani, T., W.P. Huang, P.E. Stromhaug, and D.J. Klionsky. 2002. Mechanism of cargo selection in the cytoplasm to vacuole targeting pathway. *Developmental Cell*. 3:825-837.

Simonsen, A., and S.A. Tooze. 2009. Coordination of membrane events during autophagy by multiple class III PI3-kinase complexes. *Journal of Cell Biology*. 186:773-782.

Sims, K., C.A. Haynes, S. Kelly, J.C. Allegood, E. Wang, A. Momin, M. Leipelt, D. Reichart, C.K. Glass, M.C. Sullards, and A.H. Merrill, Jr. 2010. Kdo2-lipid A, a TLR4-specific agonist, induces de novo sphingolipid biosynthesis in RAW264.7 macrophages, which is essential for induction of autophagy. *The Journal of Biological Chemistry*. 285:38568-38579.

Singh, R., and A.M. Cuervo. 2011. Autophagy in the cellular energetic balance. *Cell Metabolism*. 13:495-504.

Singh, R., and A.M. Cuervo. 2012. Lipophagy: connecting autophagy and lipid metabolism. *International Journal of Cell Biology*. 2012:282041.

Singh, R., S. Kaushik, Y. Wang, Y. Xiang, I. Novak, M. Komatsu, K. Tanaka, A.M. Cuervo, and M.J. Czaja. 2009a. Autophagy regulates lipid metabolism. *Nature*. 458:1131-1135.

Singh, R., Y. Xiang, Y. Wang, K. Baikati, A.M. Cuervo, Y.K. Luu, Y. Tang, J.E. Pessin, G.J. Schwartz, and M.J. Czaja. 2009b. Autophagy regulates adipose mass and differentiation in mice. *The Journal of Clinical Investigation*. 119:3329-3339.

Smith, D.G., R. Pal, and D. Parker. 2012. Measuring equilibrium bicarbonate concentrations directly in cellular mitochondria and in human serum using europium/terbium emission intensity ratios. *Chemistry*. 18:11604-11613.

Solinger, J.A., and A. Spang. 2013. Tethering complexes in the endocytic pathway: CORVET and HOPS. *The FEBS journal*. 280:2743-2757.

Son, S.M., H. Song, J. Byun, K.S. Park, H.C. Jang, Y.J. Park, and I. Mook-Jung. 2012. Accumulation of autophagosomes contributes to enhanced amyloidogenic APP processing under insulin-resistant conditions. *Autophagy*. 8:1842-1844.

Spandl, J., D.J. White, J. Peychl, and C. Thiele. 2009. Live cell multicolor imaging of lipid droplets with a new dye, LD540. *Traffic*. 10:1579-1584.

Spangenburg, E.E., S.J. Pratt, L.M. Wohlers, and R.M. Lovering. 2011. Use of BODIPY (493/503) to visualize intramuscular lipid droplets in skeletal muscle. *Journal of Biomedicine and Biotechnology*. 2011:598358.

Spowart, J., and J.J. Lum. 2010. Opening a new DOR to autophagy. *EMBO Reports*. 11:4-5.

St Pierre, S.E., L. Ponting, R. Stefancsik, P. McQuilton, and C. FlyBase. 2014. FlyBase 102--advanced approaches to interrogating FlyBase. *Nucleic Acids Research*. 42:D780-D788.

Stanley, R.E., M.J. Ragusa, and J.H. Hurley. 2014. The beginning of the end: how scaffolds nucleate autophagosome biogenesis. *Trends in Cell Biology*. 24:73-81.

Steck, A., N. Yuki, and F. Graus. 2013. Chapter 11 - Antibody testing in peripheral nerve disorders. *In* Handbook of Clinical Neurology. Vol. Volume 115. S. Gérard and K. Christian, editors. Elsevier. 189-212.

Steinert, J.R., S. Campesan, P. Richards, C.P. Kyriacou, I.D. Forsythe, and F. Giorgini. 2012. Rab11 rescues synaptic dysfunction and behavioural deficits in a *Drosophila* model of Huntington's disease. *Human Molecular Genetics*. 21:2912-2922.

Stepanenko, O.V., O.V. Stepanenko, D.M. Shcherbakova, I.M. Kuznetsova, K.K. Turoverov, and V.V. Verkhusha. 2011. Modern fluorescent proteins: from chromophore formation to novel intracellular applications. *BioTechniques*. 51:313-314, 316, 318 passim.

Stromhaug, P.E., and P.O. Seglen. 1993. Evidence for acidity of prelysosomal autophagic/endocytic vacuoles (amphisomes). *Biochemical Journal*. 291 (Pt 1):115-121.

Suetsugu, S., S. Kurisu, and T. Takenawa. 2014. Dynamic shaping of cellular membranes by phospholipids and membrane-deforming proteins. *Physiological Reviews*. 94:1219-1248.

Sun, Y., Y. Fang, M.S. Yoon, C. Zhang, M. Roccio, F.J. Zwartkruis, M. Armstrong, H.A. Brown, and J. Chen. 2008. Phospholipase D1 is an effector of Rheb in the mTOR pathway. *PNAS*. 105:82186-82691.

Suzuki, K., T. Kirisako, Y. Kamada, N. Mizushima, T. Noda, and Y. Ohsumi. 2001. The pre-autophagosomal structure organized by concerted functions of APG genes is essential for autophagosome formation. *The EMBO Journal*. 20:5971-5981.

Suzuki, K., Y. Kubota, T. Sekito, and Y. Ohsumi. 2007. Hierarchy of Atg proteins in pre-autophagosomal structure organization. *Genes to Cells*. 12:209-218.

Szatmari, Z., V. Kis, M. Lippai, K. Hegedus, T. Farago, P. Lorincz, T. Tanaka, G. Juhasz, and M. Sass. 2014. Rab11 facilitates cross-talk between autophagy and endosomal pathway through regulation of Hook localization. *Molecular Biology of the Cell*. 25:522-531.

Takahara, T., and T. Maeda. 2013. Evolutionarily conserved regulation of TOR signalling. *Journal of Biochemistry*. 154:1-10.

Takahashi, Y., C.L. Meyerkord, T. Hori, K. Runkle, T.E. Fox, M. Kester, T.P. Loughran, and H.G. Wang. 2011. Bif-1 regulates Atg9 trafficking by mediating the fission of Golgi membranes during autophagy. *Autophagy*. 7:61-73.

Takats, S., P. Nagy, A. Varga, K. Pircs, M. Karpati, K. Varga, A.L. Kovacs, K. Hegedus, and G. Juhasz. 2013. Autophagosomal Syntaxin17-dependent lysosomal degradation maintains neuronal function in *Drosophila*. *The Journal of Cell Biology*. 201:531-539.

Tamai, K., N. Tanaka, A. Nara, A. Yamamoto, I. Nakagawa, T. Yoshimori, Y. Ueno, T. Shimosegawa, and K. Sugamura. 2007. Role of Hrs in maturation

of autophagosomes in mammalian cells. *Biochemical and Biophysical Research Communications* . 360:721-727.

Tan, C.C., J.T. Yu, M.S. Tan, T. Jiang, X.C. Zhu, and L. Tan. 2014. Autophagy in aging and neurodegenerative diseases: implications for pathogenesis and therapy. *Neurobiology of Aging*. 35:941-957.

Tan, S.H., G. Shui, J. Zhou, J.J. Li, B.H. Bay, M.R. Wenk, and H.M. Shen. 2012. Induction of autophagy by palmitic acid via protein kinase C-mediated signaling pathway independent of mTOR (mammalian target of rapamycin). *The Journal of Biological Chemistry*. 287:14364-14376.

Tang, H.W., H.M. Liao, W.H. Peng, H.R. Lin, C.H. Chen, and G.C. Chen. 2013. Atg9 interacts with dTRAF2/TRAF6 to regulate oxidative stress-induced JNK activation and autophagy induction. *Developmental Cell*. 27:489-503.

Tang, H.W., Y.B. Wang, S.L. Wang, M.H. Wu, S.Y. Lin, and G.C. Chen. 2011. Atg1-mediated myosin II activation regulates autophagosome formation during starvation-induced autophagy. *The EMBO Journal*. 30:636-651.

Tauchi-Sato, K., S. Ozeki, T. Houjou, R. Taguchi, and T. Fujimoto. 2002. The surface of lipid droplets is a phospholipid monolayer with a unique fatty acid composition. *The Journal of Biological Chemistry*. 277:44507-44512.

Tee, A.R., J. Blenis, and C.G. Proud. 2005. Analysis of mTOR signaling by the small G-proteins, Rheb and RhebL1. FEBS Lett. 579:4763-4768.Thiam, A.R., R.V. Farese, and T.C. Walther. 2013. The biophysics and cell biology of lipid droplets. *Nature Reviews Molecular Cell Biology*. 14:775-786.

Thiele, C., and J. Spandl. 2008. Cell biology of lipid droplets. *Current Opinion in Cell Biology*. 20:378-385.

Thielemann, D.T., A.T. Wagner, E. Rosch, D.K. Kolmel, J.G. Heck, B. Rudat, M. Neumaier, C. Feldmann, U. Schepers, S. Brase, and P.W. Roesky. 2013. Luminescent cell-penetrating pentadecanuclear lanthanide clusters. *Journal of the American Chemical Society*. 135:7454-7457.

Thumm, M., R. Egner, B. Koch, M. Schlumpberger, M. Straub, M. Veenhuis, and D.H. Wolf. 1994. Isolation of autophagocytosis mutants of *Saccharomyces cerevisiae*. *FEBS Letters*. 349:275-280.

Tracy, K., and E.H. Baehrecke. 2013. The role of autophagy in Drosophila metamorphosis. *Current Topics in Developmental Biology*. 103:101-125.

Tsukada, M., and Y. Ohsumi. 1993. Isolation and characterization of autophagy-defective mutants of *Saccharomyces cerevisiae*. *FEBS Letters*. 333:169-174.

Vaccari, T., T.E. Rusten, L. Menut, I.P. Nezis, A. Brech, H. Stenmark, and D. Bilder. 2009. Comparative analysis of ESCRT-I, ESCRT-II and ESCRT-III function in Drosophila by efficient isolation of ESCRT mutants. *Journal of Cell Science*. 122:2413-2423.

van Meer, G. 2005. Cellular lipidomics. *The EMBO Journal*. 24:3159-3165.

van Weert, A.W., K.W. Dunn, H.J. Geuze, F.R. Maxfield, and W. Stoorvogel. 1995. Transport from late endosomes to lysosomes, but not sorting of integral membrane proteins in endosomes, depends on the vacuolar proton pump. *The Journal of Cell Biology*. 130:821-834.

van Zutphen, T., V. Todde, R. de Boer, M. Kreim, H.F. Hofbauer, H. Wolinski, M. Veenhuis, I.J. van der Klei, and S.D. Kohlwein. 2014. Lipid droplet autophagy in the yeast *Saccharomyces cerevisiae*. *Molecular Biology of the Cell*. 25:290-301.

Vanlandingham, P.A., and B.P. Ceresa. 2009. Rab7 regulates late endocytic trafficking downstream of multivesicular body biogenesis and cargo sequestration. *The Journal of Biological Chemistry*. 284:12110-12124.

Vaughan, J.G., B.L. Reid, S. Ramchandani, P.J. Wright, S. Muzzioli, B.W. Skelton, P. Raiteri, D.H. Brown, S. Stagni, and M. Massi. 2013. The photochemistry of rhenium(I) tricarbonyl N-heterocyclic carbene complexes. *Dalton Transactions*. 42:14100-14114.

Vázquez, C.L., and M.I. Colombo. 2009. Chapter 6 Assays to assess autophagy induction and fusion of autophagic vacuoles with a degradative compartment, using monodansylcadaverine (MDC) and DQ-BSA. *In* Methods in Enzymology. Vol. Volume 452. J.K. Daniel, editor. Academic Press. 85-95.

Viola-Villegas, N., A.E. Rabideau, J. Cesnavicious, J. Zubieta, and R.P. Doyle. 2008. Targeting the folate receptor (FR): imaging and cytotoxicity of ReI conjugates in FR-overexpressing cancer cells. *ChemMedChem*. 3:1387-1394.

Vlahakis, A., M. Graef, J. Nunnari, and T. Powers. 2014. TOR complex 2-Ypk1 signaling is an essential positive regulator of the general amino acid control response and autophagy. *Proceedings of the National Academy of Sciences of the United States of America*. 111:10586-10591.

Walton, J.W., A. Bourdolle, S.J. Butler, M. Soulie, M. Delbianco, B.K. McMahon, R. Pal, H. Puschmann, J.M. Zwier, L. Lamarque, O. Maury, C. Andraud, and D. Parker. 2013. Very bright europium complexes that stain cellular mitochondria. *Chemical Communications*. 49:1600-1602.

Wang, C., Z.H. Liu, and X. Huang. 2012. Rab32 is important for autophagy and lipid storage in *Drosophila*. *PLoS One*. 7.

Wang, J., S. Menon, A. Yamasaki, H.T. Chou, T. Walz, Y. Jiang, and S. Ferro-Novick. 2013. Ypt1 recruits the Atg1 kinase to the preautophagosomal structure. *Proceedings of the National Academy of Sciences of the United States of America*. 110:9800-9805.

Wang, S., S. Liu, H. Liu, J. Wang, S. Zhou, R.J. Jiang, W.G. Bendena, and S. Li. 2010. 20-hydroxyecdysone reduces insect food consumption resulting in fat body lipolysis during molting and pupation. *Journal of Molecular Cell Biology*. 2:128-138.

Wang, Z., W.A. Wilson, M.A. Fujino, and P.J. Roach. 2001. Antagonistic controls of autophagy and glycogen accumulation by Snf1p, the yeast homolog of

AMP-activated protein kinase, and the cyclin-dependent kinase Pho85p. *Molecular and Cellular Biology*. 21:5742-5752.

Webber, J.L., and S.A. Tooze. 2010. New insights into the function of Atg9. *FEBS Letters*. 584:1319-1326.

Weidberg, H., T. Shpilka, E. Shvets, A. Abada, F. Shimron, and Z. Elazar. 2011. LC3 and GATE-16 N termini mediate membrane fusion processes required for autophagosome biogenesis. *Developmental Cell*. 20:444-454.

Werrett, M.V., D. Chartrand, J.D. Gale, G.S. Hanan, J.G. MacLellan, M. Massi, S. Muzzioli, P. Raiteri, B.W. Skelton, M. Silberstein, and S. Stagni. 2011. Synthesis, structural, and photophysical investigation of diimine triscarbonyl Re(I) tetrazolato complexes. *Inorganic Chemistry*. 50:1229-1241.

Werrett, M.V., S. Muzzioli, P.J. Wright, A. Palazzi, P. Raiteri, S. Zacchini, M. Massi, and S. Stagni. 2013. Proton-induced reversible modulation of the luminescent output of Rhenium(I), Iridium(III), and Ruthenium(II) tetrazolate complexes. *Inorganic Chemistry*. 53:229-243.

Winslow, A.R., C.W. Chen, S. Corrochano, A. Acevedo-Arozena, D.E. Gordon, A.A. Peden, M. Lichtenberg, F.M. Menzies, B. Ravikumar, S. Imarisio, S. Brown, C.J. O'Kane, and D.C. Rubinsztein. 2010. alpha-Synuclein impairs macroautophagy: implications for Parkinson's disease. *Journal of Cell Biology*. 190:1023-1037.

Wirth, M., J. Joachim, and S.A. Tooze. 2013. Autophagosome formation--the role of ULK1 and Beclin1-PI3KC3 complexes in setting the stage. *Seminars in Cancer Biology*. 23:301-309.

Wolfe, D.M., J.H. Lee, A. Kumar, S. Lee, S.J. Orenstein, and R.A. Nixon. 2013. Autophagy failure in Alzheimer's disease and the role of defective lysosomal acidification. *The European Journal of Neuroscience*. 37:1949-1961.

Wollert, T., and J.H. Hurley. 2010. Molecular mechanism of multivesicular body biogenesis by ESCRT complexes. *Nature*. 464:864-869.

Wood, W.G., L. Li, W.E. Muller, and G.P. Eckert. 2014. Cholesterol as a causative factor in Alzheimer's disease: a debatable hypothesis. *Journal of Neurochemistry*. 129:559-572.

Wright, P.J., S. Muzzioli, M.V. Werrett, P. Raiteri, B.W. Skelton, D.S. Silvester, S. Stagni, and M. Massi. 2012. Synthesis, photophysical and electrochemical investigation of dinuclear tetrazolato-bridged Rhenium complexes. *Organometallics*. 31:7566-7578.

Wurpel, G.W., J.M. Schins, and M. Muller. 2002. Chemical specificity in three-dimensional imaging with multiplex coherent anti-Stokes Raman scattering microscopy. *Optics Letters*. 27:1093-1095.

Xu, K.D., Y. Yang, M. Yan, J.A. Zhan, X.A. Fu, and X.X. Zheng. 2010. Autophagy plays a protective role in free cholesterol overload-induced death of smooth muscle cells. *Journal of Lipid Research*. 51:2581-2590.

Yam, V.W.-W., and K.M.-C. Wong. 2011. Luminescent metal complexes of d6, d8 and d10 transition metal centres. *Chemical Communications*. 47:11579-11592.

Yamada, T., A.R. Carson, I. Caniggia, K. Umebayashi, T. Yoshimori, K. Nakabayashi, and S.W. Scherer. 2005. Endothelial nitric-oxide synthase antisense (NOS3AS) gene encodes an autophagy-related protein (APG9-like2) highly expressed in trophoblast. *The Journal of Biological Chemistry*. 280:18283-18290.

Yamamoto, H., S. Kakuta, T.M. Watanabe, A. Kitamura, T. Sekito, C. Kondo-Kakuta, R. Ichikawa, M. Kinjo, and Y. Ohsumi. 2012. Atg9 vesicles are an important membrane source during early steps of autophagosome formation. *The Journal of Cell Biology*. 198:219-233.

Yang, D.S., P. Stavrides, M. Saito, A. Kumar, J.A. Rodriguez-Navarro, M. Pawlik, C. Huo, S.U. Walkley, M. Saito, A.M. Cuervo, and R.A. Nixon. 2014. Defective macroautophagic turnover of brain lipids in the TgCRND8

Alzheimer mouse model: prevention by correcting lysosomal proteolytic deficits. *Brain: A Journal of Neurology*. 137:3300-3318.

Yang, H.J., C.L. Hsu, J.Y. Yang, and W.Y. Yang. 2012. Monodansylpentane as a blue-fluorescent lipid-droplet marker for multi-color live-cell imaging. *PLoS One*. 7:e32693.

Yen, W.L., T. Shintani, U. Nair, Y. Cao, B.C. Richardson, Z. Li, F.M. Hughson, M. Baba, and D.J. Klionsky. 2010. The conserved oligomeric Golgi complex is involved in double-membrane vesicle formation during autophagy. *The Journal of Cell Biology*. 188:101-114.

Yin Zhang, K., K. Ka-Shun Tso, M.-W. Louie, H.-W. Liu, and K. Kam-Wing Lo. 2013. A phosphorescent Rhenium(I) tricarbonyl polypyridine complex appended with a fructose pendant that exhibits photocytotoxicity and anhanced uptake by breast cancer cells. *Organometallics*. 32:5098-5102.

Yla-Anttila, P., H. Vihinen, E. Jokitalo, and E.L. Eskelinen. 2009. 3D tomography reveals connections between the phagophore and endoplasmic reticulum. *Autophagy*. 5:1180-1185.

Young, A.R., E.Y. Chan, X.W. Hu, R. Kochl, S.G. Crawshaw, S. High, D.W. Hailey, J. Lippincott-Schwartz, and S.A. Tooze. 2006. Starvation and ULK1-dependent cycling of mammalian Atg9 between the TGN and endosomes. *Journal of Cell Science*. 119:3888-3900.

Yu, L., C.K. McPhee, L. Zheng, G.A. Mardones, Y. Rong, J. Peng, N. Mi, Y. Zhao, Z. Liu, F. Wan, D.W. Hailey, V. Oorschot, J. Klumperman, E.H. Baehrecke, and M.J. Lenardo. 2010. Termination of autophagy and reformation of lysosomes regulated by mTOR. *Nature*. 465:942-946.

Yuan, H.X., Y. Xiong, and K.L. Guan. 2013. Nutrient sensing, metabolism, and cell growth control. *Molecular Cell*. 49:379-387.

Zhang, J., R.E. Campbell, A.Y. Ting, and R.Y. Tsien. 2002. Creating new fluorescent probes for cell biology. *Nature Reviews Molecular Cell Biology* 3:906-918.

Zhang, J., R. Xue, W.Y. Ong, and P. Chen. 2009a. Roles of cholesterol in vesicle fusion and motion.*Biophysical Journal*. 97:1371-1380.

Zhang, X.D., L. Qi, J.C. Wu, and Z.H. Qin. 2013. DRAM1 regulates autophagy flux through lysosomes. *PLoS One*. 8.

Zhang, Y.-Y., X. Li, S.-W. Qian, L. Guo, H.-Y. Huang, Q. He, Y. Liu, C.-G. Ma, and Q.-Q. Tang. 2011. Transcriptional activation of histone H4 by C/EBPβ during the mitotic clonal expansion of 3T3-L1 adipocyte differentiation. *Molecular Biology of the Cell*. 22:2165-2174.

Zhang, Y., S. Goldman, R. Baerga, Y. Zhao, M. Komatsu, and S. Jin. 2009b. Adipose-specific deletion of autophagy-related gene 7 (atg7) in mice reveals a role in adipogenesis. *Proceedings of the National Academy of Sciences of the United States of America*. 106:19860-19865.

Zhao, Q., C. Huang, and F. Li. 2011. Phosphorescent heavy-metal complexes for bioimaging. *Chemical Society reviews*. 40:2508-2524.

Zhou, W., R. Hoffmann, A. Franke, H. Yang, H. Kuhl, and P. Hanrath. 2002. Intravascular ultrasound evaluating coronary stents for patients with coronary artery disease: compared old with new multilink stents. *Chinese Medical Sciences Journal*. 17:95-100.

Zirin, J., and N. Perrimon. 2010. *Drosophila* as a model system to study autophagy. *Seminars in immunopathology*. 32:363-372.

Zoncu, R., L. Bar-Peled, A. Efeyan, S. Wang, Y. Sancak, and D.M. Sabatini. 2011. mTORC1 senses lysosomal amino acids through an inside-out mechanism that requires the vacuolar H(+)-ATPase. *Science*. 334:678-683.

Zou, T., C.T. Lum, S.S. Chui, and C.M. Che. 2013. Gold(III) complexes containing N-heterocyclic carbene ligands: thiol "switch-on" fluorescent probes and anti-cancer agents. *Angewandte Chemie International Edition*. 52:2930-2933.